

Particle Flow Promoted by External Forces in a Confined Space - Feed Frame Case

by

Daniel Mateo-Ortiz

Dissertation submitted in partial fulfillment of the requirements for the degree of

DOCTOR OF PHILOSOPHY
in
CHEMICAL ENGINEERING

UNIVERSITY OF PUERTO RICO
MAYAGUEZ CAMPUS

2014

Approved by:

Rafael Méndez, Ph.D.
President, Graduate Committee

Date

Nelson Cardona-Martínez, Ph.D.
Member, Graduate Committee

Date

Ubaldo Cordova, Ph.D.
Member, Graduate Committee

Date

Rodolfo Romañach, Ph.D.
Member, Graduate Committee

Date

Juan A. Ortíz
Graduate Studies Representative

Date

Aldo Acevedo, Ph.D.
Chairperson of the Department

Date

ABSTRACT

Pharmaceutical tablets are the most sold and preferred drug solid dosage form due to its many advantages. The feed frame was designed to transfer the powder from the hopper to the tablet press dies as the die disk rotates. The die filling process is complex and dynamic and entails different stages that present distinctive features. A proper understanding of the feed frame system is important to reduce or avoid possible problems during tablet manufacturing and to accomplish a successful tablet processing.

For these reasons, this dissertation aims to provide a fundamental and practical understanding of particle flow in a confined space while applying external forces. It also develops a fundamental mathematical model to describe the force exerted by the paddles. This is needed to optimize the operation of feed frames that are used to ensure uniform filling of tablet press dies.

To obtain an in-depth understanding of powder flow inside the feed frame, the Discrete Element Method (DEM) was used. The objective was to study the paddle wheel and die disk speed effect on particle size segregation inside the feed frame and dies. The results show that particle size segregation can occur during the die filling process. Paddle wheel speed was demonstrated to be the most important factor to control top to bottom segregation inside the feed frame.

Another study was developed to correlate powder attrition and overlubrication with experimental and numerical residence time distribution (RTD) data. A correlation between particle size and force applied to particles was developed using DEM. The results show that paddle wheel speed, die disk speed, exit contributions and outlet mass flowrate have an effect on RTD.

Near infrared spectroscopy (NIR) was used to monitor the powder flow and to complement its understanding during the die filling process. The different factors that could affect the prediction of the developed NIR calibration models were studied. The results show that NIR spectra can help in the understanding of powder flow inside the feed frame. It was demonstrated that the content uniformity can be assessed with high accuracy during the die filling process.

RESUMEN

Las tabletas son la forma de dosis de medicamentos preferida y más vendida debido a sus múltiples ventajas. El dispositivo de llenado de dados fue diseñado para transferir el polvo de la tolva a los dados de la compresora de tabletas mientras gira el disco. El proceso de llenado de dados es uno complejo y dinámico compuesto por diferentes etapas, cada una con características particulares. Para reducir y/o evitar los problemas que pueden surgir durante la manufactura de tabletas y lograr que el proceso sea exitoso es necesario tener un conocimiento fundamental acerca del dispositivo de llenado de dados.

Por tal razón, esta disertación tiene como objetivo proveer un conocimiento fundamental y práctico acerca del flujo de partículas promovido por fuerzas externas dentro de un espacio confinado. Además, desarrolla un modelo matemático fundamental que describe la fuerza ejercida por las aspas. Esto es necesario para optimizar el funcionamiento de los dispositivos de llenado utilizados con el propósito de obtener un llenado de dados uniforme.

Para obtener un entendimiento del flujo de polvos en un dispositivo de llenado de dados se simuló utilizando el Método de Elemento Discreto (DEM, por sus siglas en inglés). El objetivo fue estudiar el efecto de la velocidad de las aspas y del disco en la segregación por tamaño de partículas dentro del dispositivo de llenado y los dados. Los resultados muestran que la segregación por tamaño de partículas puede ocurrir durante el llenado de los dados. Se demostró que el factor que tiene más influencia sobre la segregación vertical es la velocidad de las aspas.

Otro estudio fue desarrollado para correlacionar el rompimiento y la sobre lubricación de partículas utilizando la distribución del tiempo de residencia (RTD, por sus siglas en inglés). Se desarrolló una correlación entre el tamaño de las partículas y la fuerza aplicada

sobre las mismas utilizando DEM. Los resultados muestran que la velocidad de las aspas, la velocidad del disco, las contribuciones de salida y el flujo másico de salida tienen efecto sobre la distribución de tiempo de residencia..

La espectroscopia de infrarrojo cercano (NIR, por sus siglas en inglés) fue utilizada para monitorear y complementar el entendimiento durante el proceso de llenado de dados. Se estudiaron los diferentes factores que pueden afectar las predicciones de los modelos de calibración de NIR que fueron desarrollados. Los resultados muestran que los espectros de NIR pueden ayudarnos a entender el flujo de partículas dentro del dispositivo de llenado. Se demostró que la uniformidad del contenido de ingrediente activo puede evaluarse con alta precisión durante el proceso de llenado.

© Copyright 2014
Daniel Mateo-Ortiz. All rights reserved.

*To God, my wife Paola Montes, my parents
Luz E. Ortiz, Luis A. Mateo and my siblings
Sarai Mateo, Gadiel Mateo and Carlos Mateo
for their unconditional love, support and for
all the special and unforgettable moments that
we lived together.*

ACKNOWLEDGEMENTS

I am deeply grateful to God for giving me the wisdom to complete this goal. Thank you because without You nothing would have been possible. I thank God for putting on my path my beautiful and beloved wife Paola Montes who has been my unconditional support and companion during this journey. I am thankful for your friendship, care and love. I want to acknowledge my parents Lucy Ortiz and Luis Mateo who gave me daily support and unconditional love and my siblings Sarai Mateo, Gadiel Mateo and Carlos Mateo for all the special and unforgettable moments that we lived together.

I want to express my gratitude to my advisor, Dr. Rafael Méndez for his advice, support and guidance, which contributed significantly to my professional development. I appreciate all the scientific discussions that we had which has helped me become a better researcher. I would like to thank my graduate committee members Dr. Ubaldo Córdova, Dr. Rodolfo Romañach and Dr. Nelson Cardona for their availability, comments and suggestions made during the follow-up meetings and for the corrections to this dissertation.

I would like to express my sincere gratitude to Dr. Carlos Velázquez and Dr. Nelson Cardona for their advice and guidance in the Pharmaceutical Engineering Education and Outreach Program that were a huge part of my development as a person and as a professional. Thank you for helping me develop my teaching and communication skills and for also being my friends. I admire your commitment and enthusiasm for education at all levels.

I want to thank the “Team Pharma”, my lab mates, David Mota, Sonia Avilés, Miguel Florián, Madeline Candelaria and Vladimir Villanueva for a beautiful relationship that grew into a strong friendship. I really learned a lot from each one of you. I want to thank also Mrs. Carmen Vanessa Santiago and Catherine Pérez, for their assistance in administrative matters of C-PEDaL and the ERC-SOPS. I want to acknowledge Yleana Colón for the great

collaboration and all the useful scientific conversation on the NIR studies.

I wish to acknowledge the University of Puerto Rico at Mayaguez campus, the Chemical Engineering Department, the Engineering Research Center for Structured Organic Particulate Systems (ERC- SOPS, Grant: EEC-0540855) and the Alfred P. Sloan Fellowship for their financial support during my PhD studies.

I also want to thank Merck & Co. and AbbVie for allowing me the opportunity to perform internships that were a significant part of my professional career development. I want to thank specifically Ryan Adorno and Luis Sierra from Merck and Brian Anderson from AbbVie for their trust, support and believing in my potential. I am very grateful of my great managers Kristin Ploeger from Merck and Courtney Morgret from AbbVie for all the lessons, guidance and for helping me develop my technical, planning and organizational skills.

I want to give special thanks to all my undergraduate students for their dedication and commitment to the development of the simulations and experiments: Lyan Ortiz, Pamela López, Valeria Semidei, José Oquendo, Leyda González, Nitza Guzman, Luis Nieves, Jean Caminero, Keishlyanne Díaz, Ketzya Ruiz, Ericka Reyes, Bernadette Nuñez, Jacklyn Martínez, Arnaldo López, and Emanuel Vélez.

I like to thank my friends: Camilo Mora, Christian Rivera, Stephany Herrera, Noelia Lasanta, Angélica Román, Ariangelis Ortíz, Keren Valentín, Edward Guerrero, Lorena and Paul Meza for their friendship. Thank you because without you this journey would have been much harder. Thank you all! I want to thank also my very special undergraduate friends, Yashira Zayas, Brenda Torres, Arisleida Sánchez and Alexandra Martínez for all the great moments and the many things we learned together. I am deeply grateful of my three wonderful friends, which are like my brothers, Emanuel Pedrosa, Josué Flores and Jonathan

López for their unconditional love and support.

Finally, I am very grateful of my church “Ministerio Cristiano Catacumba 5” for helping me in all matters of my life, specifically my spiritual growth and for teaching me how to be a better human being. I want to specially thank my youth pastor Rey F. Matos, Carlos Frontera and Emanuel Pedrosa for all the great conversations, advice and all the time we spent together. I learned many important things from you.

TABLE OF CONTENTS

| | | |
|----------|--|-----------|
| 1 | INTRODUCTION | 1 |
| 1.1 | Die Filling Process..... | 1 |
| 1.2 | Experimental Die Filling Studies..... | 2 |
| 1.3 | Computational Die Filling Studies | 3 |
| 1.4 | Particle Size Segregation | 4 |
| 1.5 | Residence Time Distribution in Solid Units operation..... | 5 |
| 1.6 | Particle Flow Promoted by Paddle Movement | 6 |
| 1.7 | Analysis of Powder Phenomena inside Feed Frames using In-line Near Infrared Spectroscopy (NIRS) | 8 |
| 1.8 | Dissertation Scope and Overview..... | 10 |
| 1.9 | References..... | 11 |
| 2 | PARTICLE SIZE SEGREGATION PROMOTED BY POWDER FLOW IN CONFINED SPACE: THE DIE FILLING PROCESS CASE | 17 |
| 2.1 | Summary | 17 |
| 2.2 | Methodology..... | 18 |
| 2.2.1 | Computational Study (DEM Simulations)..... | 18 |
| 2.2.2 | Experimental Study | 20 |
| 2.3 | Results and Discussion | 21 |
| 2.3.1 | Feed Frame Mass Hold-up..... | 21 |
| 2.3.2 | Exits Contribution to Die Filling and Die Weight Variability | 23 |
| 2.3.3 | Velocity Profile..... | 26 |
| 2.3.4 | DEM Particle Size Segregation | 26 |
| 2.3.5 | Experimental Results | 31 |
| 2.4 | Conclusion | 32 |
| 2.5 | References..... | 33 |
| 3 | RELATIONSHIP BETWEEN RESIDENCE TIME DISTRIBUTION AND FORCES APPLIED BY PADDLES ON POWDER ATTRITION DURING THE DIE FILLING PROCESS | 35 |
| 3.1 | Summary | 35 |
| 3.2 | Materials and Methods..... | 36 |
| 3.2.1 | Experimental Section..... | 36 |
| 3.2.1.1 | Pulse Injection Tracer Experiments | 36 |
| 3.2.1.2 | UV-Vis Spectroscopy | 37 |
| 3.2.1.3 | Strain Measurement..... | 37 |
| 3.2.2 | Computational Section..... | 37 |
| 3.3 | Results and Discussion | 39 |
| 3.3.1 | Experimental Results..... | 39 |
| 3.3.1.1 | RTD as function of Operating Conditions | 39 |
| 3.3.1.2 | Shear Strain as a function of System Parameters | 40 |
| 3.3.2 | Computational Results..... | 41 |
| 3.3.2.1 | Particle Trajectories..... | 41 |
| 3.3.2.2 | RTD as function of Operating Conditions | 42 |
| 3.3.2.3 | Residence time distribution as a function of particle size | 45 |
| 3.3.2.4 | Particles in the Vicinity of Feed Frame Paddles | 46 |
| 3.3.2.5 | DEM shear strain as a function of operating parameters | 50 |
| 3.4 | Conclusion | 51 |
| 3.5 | References..... | 52 |
| 4 | MICRODYNAMIC ANALYSIS OF PARTICLE FLOW IN A CONFINED SPACE: THE FEED FRAME CASE | 53 |
| 4.1 | Summary | 53 |

| | | |
|------------|---|-----------|
| 4.2 | Paddle Force Model Development | 54 |
| 4.3 | Materials and Methods..... | 56 |
| 4.4 | Results and Discussion | 60 |
| 4.4.1 | Feed Frame Mass Hold-up..... | 60 |
| 4.4.2 | Die Weight Variability | 61 |
| 4.4.3 | Velocity Profile..... | 63 |
| 4.4.4 | Powder Flow Behavior | 63 |
| 4.4.5 | Force Distribution..... | 65 |
| 4.4.6 | Velocity Vector Analysis..... | 67 |
| 4.5 | Conclusion | 69 |
| 4.6 | References..... | 70 |
| 5 | ANALYSIS OF POWDER PHENOMENA INSIDE A FETTE 3090 FEED FRAME USING IN-LINE NIR SPECTROSCOPY | 72 |
| 5.1 | Summary | 72 |
| 5.2 | Materials and Methods..... | 73 |
| 5.2.1 | Materials | 73 |
| 5.2.1.1 | Experimental Equipment..... | 73 |
| 5.2.1.2 | Materials | 74 |
| 5.2.2 | Experimental Set-up | 74 |
| 5.2.2.1 | Experimental Set-up for Preliminary Experiments | 74 |
| 5.2.2.2 | Preliminary Experiments..... | 75 |
| 5.2.2.3 | NIR Prediction as a Function of Probe Distance..... | 75 |
| 5.2.2.4 | Experimental Set-up for Experiments | 76 |
| 5.2.3 | Near Infrared Spectroscopy | 76 |
| 5.2.3.1 | Instrumentation..... | 76 |
| 5.2.3.2 | Software Data Processing..... | 76 |
| 5.2.3.3 | Off-line NIR Calibration Model..... | 77 |
| 5.2.3.4 | In-line NIR Calibration Model..... | 78 |
| 5.2.3.5 | Repeatability Study | 79 |
| 5.3 | Results and Discussion | 79 |
| 5.3.1 | Preliminary Results..... | 79 |
| 5.3.1.1 | Feed Frame Monitory Locations | 79 |
| 5.3.1.2 | Powder Wave Behavior inside the Feed Frame | 80 |
| 5.3.1.3 | Feed Frame Mass Hold-up Effect | 81 |
| 5.3.2 | Evaluation of Spectra Properties | 82 |
| 5.3.2.1 | Off-line Calibration Spectra | 83 |
| 5.3.2.2 | In-line Calibration Spectra | 84 |
| 5.3.3 | NIR Calibration Model Developments..... | 85 |
| 5.3.4 | Repeatability Study..... | 87 |
| 5.3.5 | Prediction as a Function of Probe Distance | 87 |
| 5.3.6 | In-line Spectra of Experiments | 88 |
| 5.3.7 | Summary NIR Prediction at Different Paddle Wheel Speeds | 91 |
| 5.4 | Conclusion | 93 |
| 5.5 | References..... | 94 |
| 6 | CONCLUDING REMARKS | 95 |
| 6.1 | General Conclusions | 95 |
| 6.2 | Recommendations and Future Perspectives | 97 |

LIST OF TABLES

| | |
|---|----|
| Table 2.1. DEM parameters..... | 19 |
| Table 2.2. Top–bottom D50 values at each sample location inside the feed frame. | 28 |
| Table 3.1. RTD as function of operating conditions..... | 40 |
| Table 3.2. Mean residence time for different particle diameters. | 45 |
| Table 4.1. Input parameters used to develop the simulations..... | 60 |
| Table 4.2. Feed frame mass hold-up, die weight variability and force results | 61 |
| Table 5.1. Summary parameters of the off-line and in-line NIR calibration models constructed and evaluated. | 87 |
| Table 5.2. Prediction as function of probe distance..... | 88 |
| Table 5.3. Prediction at different paddle wheel speeds. | 92 |

LIST OF FIGURES

| | |
|---|----|
| Figure 1.1. Diagram of a feed frame..... | 1 |
| Figure 1.2. 3-stage die filling process..... | 2 |
| Figure 1.3. Shoe delivery system..... | 3 |
| Figure 1.4. Diagrammatic representation of the flow of granular material over a blade..... | 8 |
| Figure 2.1. Tablet press feed frame simulated in EDEM. | 18 |
| Figure 2.2. Manesty Beta Press feed frame exits..... | 20 |
| Figure 2.3. Top–bottom feed frame sample locations. | 21 |
| Figure 2.4. Hopper (A), feed frame (B), exit 1 (C), exit 2 (D) and exit 3 (F). | 22 |
| Figure 2.5. Feed frame mass hold-up..... | 22 |
| Figure 2.6. Exit contributions A: 24 rpm paddle wheel & 29 rpm die disk speed. B: 72 rpm paddle wheel & 29 rpm die disk speed. C: 24 rpm paddle wheel & 57 rpm die disk speed. D: 72 rpm paddle wheel & 57 rpm die disk speed..... | 24 |
| Figure 2.7. Die weight variability at each operating parameter..... | 25 |
| Figure 2.8. Velocity profile at A: 24 rpm paddle wheel speed. B: 72 rpm paddle wheel speed. | 26 |
| Figure 2.9. A: Feed frame top view at 24 rpm paddle wheel speed. B: Feed Frame bottom view at 24 rpm paddle wheel speed. C: Feed frame top view at 72 rpm paddle wheel speed. D: Feed frame bottom view at 72 rpm paddle wheel speed..... | 27 |
| Figure 2.10. Feed frame front view. | 28 |
| Figure 2.11. Top and bottom selections of die..... | 30 |
| Figure 2.12. Example of top to bottom segregation in a die..... | 30 |
| Figure 2.13. Top to bottom particle segregation in the dies at each operating parameter. | 30 |
| Figure 2.14. Particle vectors at A: 24 rpm paddle wheel speed. B: 72 rpm paddle wheel speed. | 31 |
| Figure 3.1. Manesty Beta Press Feed Frame Exits and Zones..... | 36 |
| Figure 3.2. Manual Selection of Tracer. | 38 |
| Figure 3.3. E(t) distribution as function of operating conditions..... | 40 |
| Figure 3.4. Feed Frame trajectory of particles..... | 42 |
| Figure 3.5. E(t) distributions as function of operating conditions for DEM simulations. | 43 |
| Figure 3.6. CSTR model and Computational RTD profile..... | 44 |

| | |
|---|----|
| Figure 3.7. E(t) distributions as a function of particle size (24 rpm paddle Wheel-29 rpm die disk speed). | 46 |
| Figure 3.8. Compressive force zone 1 (front view). | 47 |
| Figure 3.9. Compressive force zone 2 (front view). | 48 |
| Figure 3.10. Compressive Force as function of particle diameter. | 49 |
| Figure 3.11. Tangential force as function of particle diameter..... | 50 |
| Figure 4.1. Section area of annulus..... | 55 |
| Figure 4.2. Differential volume element of an annulus section. | 56 |
| Figure 4.3. Feed Frame (a), die (b), particle between paddles (c). | 57 |
| Figure 4.4. Feed frame dimensions..... | 58 |
| Figure 4.5. Angle of repose..... | 59 |
| Figure 4.6. Feed Frame at (a) 60 rpm with 8 paddles 6.5 mm height, (b) 8 paddles 4.5 mm height, (c) 14 paddles 6.5 mm height..... | 62 |
| Figure 4.7. Velocity Profile (a) 20 rpm, (b) 60 rpm. | 63 |
| Figure 4.8. Particle flow behavior in Manesty Beta Press feed frame (a) paddle wheel zone 1 (b) paddle wheel zone 2. | 65 |
| Figure 4.9. Force distribution, (a) top view, (b) side view. | 66 |
| Figure 4.10. Average total force as function of angular distance for the simulations with different number of paddles. | 67 |
| Figure 4.11. Average total force as function of angular distance for the simulations with different paddle wheel speed. | 67 |
| Figure 4.12. Velocity vectors in the vicinity of the paddle..... | 68 |
| Figure 4.13. Particle Velocity for the Z direction..... | 69 |
| Figure 5.1. Fette 3090 feed frame..... | 73 |
| Figure 5.2. Experimental setup. | 75 |
| Figure 5.3. NIR probe position. | 75 |
| Figure 5.4. Tray sampling procedure..... | 78 |
| Figure 5.5. Stagnant powder observed at the right window location..... | 80 |
| Figure 5.6. Left window location where all measurements were obtained. | 80 |
| Figure 5.7. Powder wave behavior effect on NIR spectra baseline. | 81 |
| Figure 5.8. Mass hold-up effect on NIR spectra baseline..... | 82 |

| | |
|--|----|
| Figure 5.9. Spectra of the two main components in the formulation..... | 83 |
| Figure 5.10. PCA score plot of off-line NIR calibration model developed in the 1130–1380, 1697–2135 nm spectral region using SNV+ 1st deriv (17) pre-treatment..... | 84 |
| Figure 5.11. PCA score plot for in-line spectra. PCA performed with calibration sample set in the 1130–1380 nm, 1697–2135 nm spectral regions. | 85 |
| Figure 5.12. PCA score plot of in-line NIR calibration model developed in the 1130–1380, 1697–2135 nm spectral region using SNV+ 1st deriv (17) pre-treatment..... | 86 |
| Figure 5.13. Spectra baseline shift vs. Sample order. 16.5 (a), 33.0 (b), 49.5 rpm (c)..... | 89 |
| Figure 5.15. Spectra at 16.5, 33.0, 49.5 rpm..... | 91 |

CHAPTER 1

1 INTRODUCTION

1.1 Die Filling Process

Pharmaceutical tablets are the most sold, common and preferred drug solid dosage form worldwide due to its many advantages. Some of these advantages are: simplicity of manufacture, cost of manufacturing, convenience of administration and stability [1,2]. Tablets are produced in multi-station rotary tablet presses designed to produce thousands of tablets at a fast rate during each working day. The powder to produce tablets cannot enter directly from the tablet press hopper into the dies; therefore the feed frame (Fig. 1.1) was designed to transfer the powder from the hopper to the tablet press dies as the die disk rotates. After the dies are filled, the tablet is compressed with punches, decompressed, and finally ejected. The dies and punches help in defining the tablet size and shape.

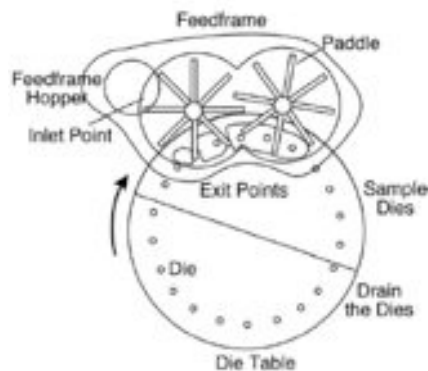


Figure 1.1. Diagram of a feed frame.

The die filling process is complex and dynamic and entails different stages that present distinctive features. The first stage is the powder flow from the hopper to the feed frame. The second stage is the powder flow through a confined space, which is the feed frame, forced by the paddle wheels to the die opening. The final stage is the tablet press die-filling step. This 3-stage die filling process (Fig. 1.2) is one of the key steps to control the

final properties of tablets since it affects their quality directly. This process used to be treated as a black box. Recent studies [3–7] have contributed to a better understanding of this important process during tablet manufacturing.

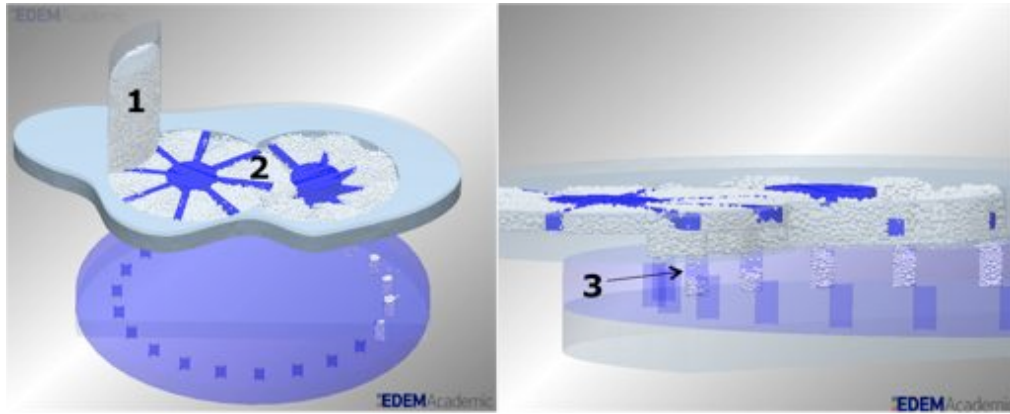


Figure 1.2. 3-stage die filling process.

Tablet properties are the result of powder properties and powder behavior during all of the previous stages. Therefore, a proper understanding of the feed frame system and powder behavior through the previous stages is important to reduce or avoid the possible problems during tablet manufacturing and to accomplish a successful tablet processing [8]. Some tablet manufacturing problems are due to poor die filling, such as: inhomogeneous density distributions [9] and tablet die weight variability. Weight variation between tablets with respect to dose and weight must be reduced to a minimum to offer people the best quality product. Uniformity of weight can be controlled from the die filling stage, which therefore ensures consistency of dosage units during the later stages of compression, decompression and ejection.

1.2 Experimental Die Filling Studies

According to our literature review, there have been few publications dedicated to powder behavior inside the feed frames. Most of the knowledge resides with the equipment

manufacturers and it is not readily available. Nevertheless, the die filling step has been studied extensively. However, the system used in previous publications to study this process is simple and does not take into account significant and complex features of a real tablet press-feeding device (feed frame). These studies used a simple shoe delivery system that consists of a rectangular cross-sectioned box with a constant velocity over the die and a high-speed video system to determine powder flow behavior during the die filling process [8,10–14] (Fig 1.3). High shoe speed can result in a lower filling rate and in some cases, incomplete filling [11]. Other experiments have been done with a circular cross-sectioned feed shoe in order to investigate uniformity and pressure distribution inside dies [12]. Increasing shoe speed has a positive impact on pressure uniformity and symmetry index [13].

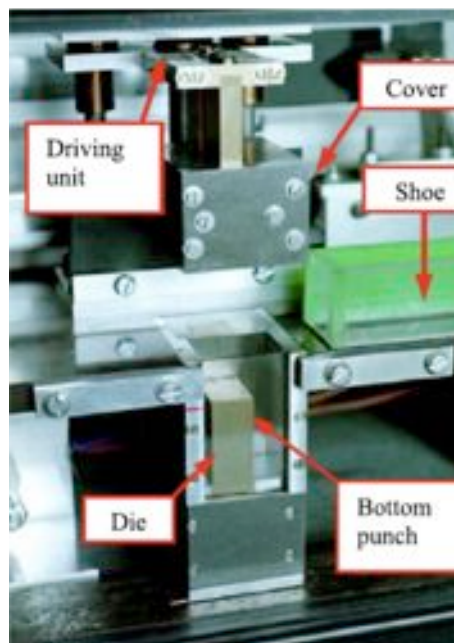


Figure 1.3. Shoe delivery system.

1.3 Computational Die Filling Studies

Experimental measurements of particle flow are often problematic or expensive to make. Some locations and particle properties are difficult and challenging to investigate experimentally. DEM models can be used to overcome these difficulties, reduce the number

of experiments, and optimize design and operating conditions. DEM models the behavior of each particle and the overall system performance is the result of all the individual interactions. The number of particles that DEM can simulate is limited to the computational power because of the extensive calculations that this method entails. DEM has been widely used to simulate pharmaceutical processes and powder phenomena such as milling [14], sieving [10], particle flow behavior [15], size segregation [16] and other pharmaceutical operations.

DEM is a common technique to study particle flow and specially die filling [9,17–21]. It has been demonstrated that DEM can capture major features of the die filling process [17]. Powder trend and behavior is consistent experimentally and numerically during this process [22]. Different particle shapes and pressure build-up have been studied in terms of powder flowability and critical velocity [22]. This process could provide a non-homogeneous density distribution during powder transfer but it has a small effect on the final density distribution of the compacted component. It was demonstrated that the non-homogeneous density distribution is mainly influenced by the combination of cavity geometry and feeding shoe velocity [8,9,17]. Cohesive materials slow down the die filling process and also affect negatively the die weight variability and the force required for compression [23]. All the previous mentioned systems do not appear to model the feed frame system to a significant degree.

1.4 Particle Size Segregation

Particulate materials may segregate upon processing and handling based on differences in particle properties such as size, density, or shape. This is important for the pharmaceutical industry to optimize the operation of feed frames to avoid segregation problems. Particle size segregation was evaluated during die filling in the presence of air using a coupled discrete element method (DEM) and computational fluid dynamics (CFD)

[20,21]. The filling process was studied with a stationary and a moving shoe [20,21]. Reducing particle density ratios and promoting bulk flow by increasing shoe speed can provide less segregation during the die filling process [24]. Vertical size segregation occurs during die filling since fine particles can percolate through the coarse particles [25]. Air can reduce this segregation since the air drag effect can suppress the percolation of small particles [25]. The powder flow rate in presence of air is less than in vacuum because of the resistance of air. The air effect is negligible when nose flow is predominant because air can escape from the die cavity [25]. The percolation velocity is affected mostly by particle size and particle density, restitution and friction coefficients between particles, and void fraction of packing [26]. It also increases with reducing restitution coefficient and particle size and is related to the number of collisions and the intensity of those collisions between particles [26].

1.5 Residence Time Distribution in Solid Units operation

The Residence Time Distribution (RTD) is defined as the probability distribution of time that solid or fluid materials spend inside one or more units in a continuous flow system [27]. It is important to have an understanding of the material flow profile in every unit operation in order to characterize mixing and flow within the unit operation. It is also useful to develop models, design equipment and troubleshooting. RTD studies are commonly used in many industrial processes, such as pharmaceutical products and continuous manufacturing of chemicals, plastics and food. There are many RTD applications in solid processes such as continuous mixers [28–30], extruders [31,32], rotary drums [33], fluidized beds [34] and centrifugal mills [35].

As paddles pass through the powder bed inside the feed frame, shear is applied to the particles. It has been demonstrated that this shear can cause powder attrition and therefore modify the particle size distribution (PSD) of the material [5]. The shear applied to the

lubricated material was also demonstrated to affect powder overlubrication and therefore, dissolution rate of tablets, tablet hardness and powder flowability increased [4]. Therefore, it is important to establish a relationship between RTD, powder breakage and powder over lubrication. The RTD analysis is also important to understand some particle phenomena inside the feed frame such as particle size segregation. There are two common ways to do RTD measurement, pulse injection and step change of a tracer at the inlet of a continuous system. Previous work [3] on analyzing the RTD during the die filling process has used the step change measurement. To our knowledge none have used the pulse injection measurement for feed frames which is the method used in this work.

DEM has been used to study pharmaceutical processes such as feeding [36], particle mixing [29,37], granulation [38], and coating [39]. DEM can also be used to study RTD in particle processes. One advantage of measuring RTD using DEM is that this method does not introduce the problem of tracer disturbance since a group of all particles in the system is tracked. It also provides the capability of measuring the RTD of particles by size ranges. In order to achieve reliable conclusions a correlation with computational data (DEM) and experimental data should be established.

1.6 Particle Flow Promoted by Paddle Movement

The effect of feed frame and paddle wheel design and operating conditions on particle flow is not fully understood. Feed frames have different numbers of interconnected compartments and therefore different numbers of paddle wheels, which spread the powder over an area for the dies to be filled. Most feed frames have two or more compartments, which complicate the powder flow and makes it difficult to understand powder phenomena inside feed frames. The proper understanding of this process can be used to avoid some problems such as high tablet weight variability. Performance optimization of the tablet press

feed frames is an issue of great significance in the pharmaceutical industry. Inadequate die filling in the tablet compressing step can result in rejection of the finished product because of poor quality. Thus, by gaining knowledge of how the equipment design and operating conditions can affect the die weight variability, tablet quality can be improved. Therefore, optimization of the feed frame design plays a vital role in die filling and tablet compressing applications.

Particle flow promoted by moving blades or paddles have been studied extensively for years [40–49]. However, the main focus of these studies has been on mixers and not tablet press feed frames. Bridgwater studied the particle flow over a long flat blade. Figure 1.4 depicts the analysis in which the blade width is b and the material is shown moving from left to right with an approach velocity s . The blade face is inclined at an angle α to the rearward horizontal, this is known as the rake angle. The projected height of the blade is B and the vertical distance from the undisturbed free surface to the lower horizontal edge is Z , this being termed the blade immersion. The horizontal force on the blade H of length L may be expressed in a dimensionless relationship:

$$\frac{H}{\gamma B^2 L} = f\left(\frac{Z}{B}, \frac{L}{B}, \frac{W}{B}, \delta_f, \delta, \alpha, \frac{s^2}{gB}, \phi, \varepsilon\right) \quad (1.1)$$

where γ is the specific weight of the bed, g is gravity, δ the dynamic external angle of friction between the blade and the material, ϕ is the static angle of friction of the material, and ε is the void fraction of the bed. W is the distance from the bottom of the bed to the lower edge of the blade, and δ_f the dynamic external angle of friction between the granular material and the floor. Although the studies of Bagster and Bridgwater [46,48] provide information on particle movement in a horizontal powder bed, this work examines the rotational powder movement promoted by the feed frame paddle wheels.

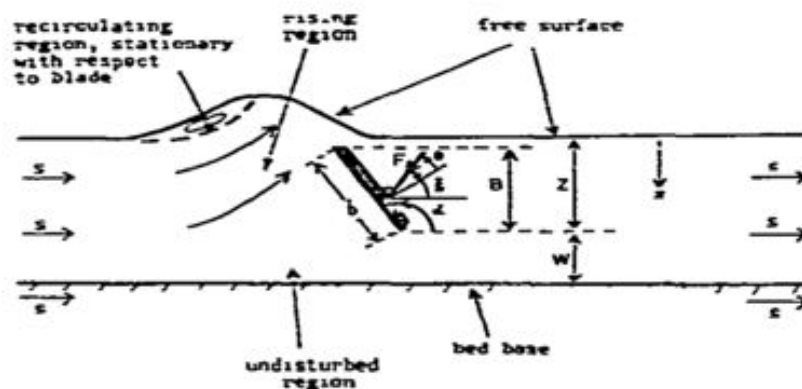


Figure 1.4. Diagrammatic representation of the flow of granular material over a blade.

Particle flow can be divided into two categories: confined and unconfined flow. Confined flow is the flow in which boundaries are confined such as direct shear and annular cell test [50]. Unconfined flow can be described as particle flow in which one side is unconfined such as surface and vibrating flow [50]. The amount of material in the system can also determine if the flow is confined or unconfined. Since a tablet press feed frame is a continuous system and a confined space, it can be described as a continuous confined flow. Bagster and Bridgwater described the powder behavior promoted by blade or paddle movement [46–48]. As a blade moves in a horizontal direction, a heap of material is produced. Bridgwater studies are for unconfined flow (Fig. 1.4); therefore in the case of the flow inside the feed frame, the level of confinement inside the feed frame limits the formation of the heap.

1.7 Analysis of Powder Phenomena inside Feed Frames using In-line Near Infrared Spectroscopy (NIRS)

New analytical methods are needed to understand and optimize the processes by which tablets are produced. There are few published studies describing the use of NIRS in real time analysis of powders in feed frames, and additional process understanding is necessary [51–54]. NIRS was chosen to study drug concentration and powder flow inside the feed frame

because it is a non-invasive and a non-destructive method. It also has the capability of identifying a formulation and quantifying the amount of drug in the formulation [55]. Because of these advantages, NIRS is frequently used within the process analytical technology (PAT) framework.

NIRS has been used as a technique for blend uniformity determination [56–59] and other pharmaceutical operations such as crystallization [60], granulation [61,62], fluid bed drying [63], tableting process [64,65] and coating [66,67]. In addition, NIRS calibration models have been successfully developed to monitor powder flow properties [68] and post-blending segregation [69], among others. Even though the powder flow in some pharmaceutical operations such as mixing is chaotic, the place in which the probe is located is not in the operation itself. There are some examples in which the probe is located in a chute [59] or a conveyor belt [70] where the powder presents less physical changes. If the probe is placed where the powder behavior is chaotic, it will cause significant physical changes, non-consistent sample presentation and therefore, a challenge for in-line monitoring.

An NIR spectrometer installed on top of the feed frame windows has the potential of improving the product quality by providing continuous real-time quality assurance and provide a better understanding of the powder flow behavior inside the feed frame. Since the die filling process is the step just before the tablet compression (final product), the NIR monitoring at this stage would be more representative for the final product. In addition, it enables the opportunity to do discrete process control. The powder flow through the feed frame creates a complex behavior, which implies the problems with chaotic flow, and could be a challenge for the in-line analytical application.

1.8 Dissertation Scope and Overview

This dissertation is aimed at providing a fundamental and practical understanding of particle flow in a confined space while applying external forces. It also presents a detailed study of the micro/macro dynamics of the particle flow inside the feed frame. Chapter 2 and 3 mainly focus on the macro dynamics and chapter 4 focuses on the micro dynamics. This is needed to optimize the operation of force-feeding devices (feed frames) used to ensure uniform filling of tablet press dies. Specifically, the main contributions of this work are: the study of particle size segregation promoted by powder flow in confined space, a relationship between residence time distribution and forces applied by paddles on powder attrition during the die filling process, microdynamic analysis of particle flow in a confined space and the analysis of powder phenomena inside a Fette 3090 feed frame using in-line NIR spectroscopy.

Chapter 2 describes the segregation phenomena using DEM simulations inside a tablet press feed frame, compares the results experimentally and describes the phenomena due to differences in particle size. This chapter is also focused on the feed frame processing and characterization, die filling stage, understanding of powder behavior during die filling and possible effects on tablets.

Chapter 3 presents a correlation of powder attrition and powder hydrophobicity with experimental and numerical RTD data. An analysis with computational data (DEM) and experimental data was performed.

Chapter 4 provides a fundamental and practical understanding of particle microdynamics in a confined space while external forces are applied. A fundamental mathematical model of the force applied by the feed frame paddles as function of paddle wheel designs and operating conditions is presented.

Chapter 5 describes the use of near infrared spectroscopy (NIR) to understand and monitor the die filling process. The different factors that could affect the prediction of the

developed NIR calibration models are also discussed in detail in this chapter. The results presented here show that NIR spectra can help in the understanding of powder flow inside the feed frame. This chapter also closely examines the powder behavior at different paddle wheel speeds and their impact on NIR spectra and therefore on NIR prediction. It details the development of the different calibration models used to predict the API concentration. The final remarks of the dissertation are summarized in Chapter 6.

1.9 References

- [1] S.V. Sastry, J.R. Nyshadham, J.A. Fix, Recent technological advances in oral drug delivery – a review, *Pharm. Sci. Technol. Today*. 3 (2000) 138–145.
- [2] M. Jivraj, L.G. Martini, C.M. Thomson, An overview of the different excipients useful for the direct compression of tablets, *Pharm. Sci. Technol. Today*. 3 (2000) 58–63.
- [3] R. Mendez, F. Muzzio, C. Velazquez, Study of the effects of feed frames on powder blend properties during the filling of tablet press dies, *Powder Technol.* 200 (2010)
- [4] R. Mendez, F.J. Muzzio, C. Velazquez, Powder hydrophobicity and flow properties: Effect of feed frame design and operating parameters, *AIChE J.* 58 (2012) 697–706.
- [5] R. Mendez, C. Velazquez, F.J. Muzzio, Effect of feed frame design and operating parameters on powder attrition, particle breakage, and powder properties, *Powder Technol.* 229 (2012) 253–260.
- [6] D. Mateo-Ortiz, F.J. Muzzio, R. Méndez, Particle size segregation promoted by powder flow in confined space: The die filling process case, *Powder Technol.* (2014).
- [7] D. Mateo-Ortiz, Y. Colon, R.J. Romañach, R. Méndez, Analysis of powder phenomena inside a Fette 3090 feed frame using in-line NIR spectroscopy, *J. Pharm. Biomed. Anal.* 100 (2014) 40–49.
- [8] O. Coube, A.C.F. Cocks, C.-Y. Wu, Experimental and numerical study of die filling, powder transfer and die compaction, *Powder Metall.* 48 (2005) 68–76.
- [9] C. Bierwisch, T. Kraft, H. Riedel, M. Moseler, Die filling optimization using three-dimensional discrete element modeling, *Powder Technol.* 196 (2009) 169–179.
- [10] C.-Y. Wu, A.C.F. Cocks, Flow behaviour of powders during die filling, *Powder Metall.* 47 (2004) 127–136.

- [11] I.C. Sinka, L.C.R. Schneider, a C.F. Cocks, Measurement of the flow properties of powders with special reference to die fill., *Int. J. Pharm.* 280 (2004) 27–38.
- [12] L.C.. Schneider, I.C. Sinka, A.C.F. Cocks, Characterisation of the flow behaviour of pharmaceutical powders using a model die–shoe filling system, *Powder Technol.* 173 (2007) 59–71.
- [13] S. Jackson, I.C. Sinka, A.C.F. Cocks, The effect of suction during die fill on a rotary tablet press., *Eur. J. Pharm. Biopharm.* 65 (2007) 253–6.
- [14] I.C. Sinka, F. Motazedian, a. C.F. Cocks, K.G. Pitt, The effect of processing parameters on pharmaceutical tablet properties, *Powder Technol.* 189 (2009) 276–284.
- [15] S.S. Roudsari, V.M. Puri, Uniformity Differentiation Analysis. Part 1: Powder Deposition Characteristics in Rectangular Shallow Die Using Feed Shoe with Circular Cross Section, *Part. Sci. Technol.* 28 (2010) 161–172.
- [16] S.S. Roudsari, V.M. Puri, Uniformity Differentiation Analysis. Part 2: Powder Deposition Characteristics in Circular Shallow Die Using Feed Shoe with Circular Cross Section, *Part. Sci. Technol.* 28 (2010) 173–182.
- [17] a. Mehrotra, B. Chaudhuri, A. Faqih, M.S. Tomassone, F.J. Muzzio, A modeling approach for understanding effects of powder flow properties on tablet weight variability, *Powder Technol.* 188 (2009) 295–300.
- [18] Y. Guo, C.-Y. Wu, C. Thornton, The effects of air and particle density difference on segregation of powder mixtures during die filling, *Chem. Eng. Sci.* 66 (2011) 661–673.
- [19] Y. Guo, C.-Y. Wu, K.D. Kafui, C. Thornton, 3D DEM/CFD analysis of size-induced segregation during die filling, *Powder Technol.* 206 (2011) 177–188.
- [20] C.-Y. Wu, A.C.F. Cocks, Numerical and experimental investigations of the flow of powder into a confined space, *Mech. Mater.* 38 (2006) 304–324.
- [21] M. Rahman, H. Zhu, A. Yu, J. Bridgwater, DEM simulation of particle percolation in a packed bed, *Particuology.* 6 (2008) 475–482.
- [22] M. Marigo, D.L. Cairns, M. Davies, a. Ingram, E.H. Stitt, A numerical comparison of mixing efficiencies of solids in a cylindrical vessel subject to a range of motions, *Powder Technol.* 217 (2012) 540–547.
- [23] D. Suzzi, G. Toschkoff, S. Radl, D. Machold, S.D. Fraser, B.J. Glasser, et al., DEM simulation of continuous tablet coating: Effects of tablet shape and fill level on inter-tablet coating variability, *Chem. Eng. Sci.* 69 (2012) 107–121.
- [24] C.C. Kwan, H. Mio, Y. Qi Chen, Y. Long Ding, F. Saito, D.G. Papadopoulos, et al., Analysis of the milling rate of pharmaceutical powders using the Distinct Element Method (DEM), *Chem. Eng. Sci.* 60 (2005) 1441–1448.

- [25] J. Li, C. Webb, S.S. Pandiella, G.M. Campbell, Discrete particle motion on sieves—a numerical study using the DEM simulation, *Powder Technol.* 133 (2003) 190–202.
- [26] S. Luding, *Particulate solids modeling with discrete element methods*, (2006).
- [27] Y. Gao, F.J. Muzzio, M.G. Ierapetritou, A review of the Residence Time Distribution (RTD) applications in solid unit operations, *Powder Technol.* 228 (2012) 416–423.
- [28] Y. Gao, A. Vanarase, F. Muzzio, M. Ierapetritou, Characterizing continuous powder mixing using residence time distribution, *Chem. Eng. Sci.* 66 (2011) 417–425.
- [29] A. Sarkar, C.R. Wassgren, Simulation of a continuous granular mixer: Effect of operating conditions on flow and mixing, *Chem. Eng. Sci.* 64 (2009) 2672–2682.
- [30] K. Marikh, H. Berthiaux, V. Mizonov, E. Barantseva, D. Ponomarev, Flow Analysis and Markov Chain Modelling to Quantify the Agitation Effect in a Continuous Powder Mixer, *Chem. Eng. Res. Des.* 84 (2006) 1059–1074.
- [31] C. Bi, B. Jiang, Study of residence time distribution in a reciprocating single-screw pin-barrel extruder, *J. Mater. Process. Technol.* 209 (2009) 4147–4153.
- [32] H. Fang, F. Mighri, A. Aji, P. Cassagnau, S. Elkoun, Flow behavior in a corotating twin-screw extruder of pure polymers and blends: Characterization by fluorescence monitoring technique, *J. Appl. Polym. Sci.* 120 (2011) 2304–2312.
- [33] R.G. Sherritt, J. Chaouki, A.K. Mehrotra, L. a. Behie, Axial dispersion in the three-dimensional mixing of particles in a rotating drum reactor, *Chem. Eng. Sci.* 58 (2003) 401–415.
- [34] A.T. Harris, R.B. Thorpe, J.F. Davidson, Stochastic modelling of the particle residence time distribution in circulating uidised bed risers, 57 (2002) 4779–4796.
- [35] H.C. Cho, K.H. Kim, H. Lee, D.J. Kim, Study of residence time distribution and mill hold-up for a continuous centrifugal mill with various G/D ratios in a dry-grinding environment, *Miner. Eng.* 24 (2011) 77–81.
- [36] Q.F. Hou, K.J. Dong, A.B. Yu, DEM study of the flow of cohesive particles in a screw feeder, *Powder Technol.* 256 (2014) 529–539.
- [37] M. Florian, C. Velázquez, R. Méndez, New continuous tumble mixer characterization, *Powder Technol.* 256 (2014) 188–195.
- [38] R.M. Dhenge, K. Washino, J.J. Cartwright, M.J. Hounslow, A.D. Salman, Twin screw granulation using conveying screws: Effects of viscosity of granulation liquids and flow of powders, *Powder Technol.* 238 (2013) 77–90.
- [39] J.E. Hilton, D.Y. Ying, P.W. Cleary, Modelling spray coating using a combined CFD–DEM and spherical harmonic formulation, *Chem. Eng. Sci.* 99 (2013) 141–160.

- [40] H.P. Kuo, P.C. Knight, D.J. Parker, A.S. Burbidge, M.J. Adams, J.P.K. Seville, Non-equilibrium particle motion in the vicinity of a single blade, *Powder Technol.* 132 (2003) 1–9.
- [41] Y.C. Zhou, A.B. Yu, R.L. Stewart, J. Bridgwater, Microdynamic analysis of the particle flow in a cylindrical bladed mixer, *Chem. Eng. Sci.* 59 (2004) 1343–1364.
- [42] R.L. Stewart, J. Bridgwater, D.J. Parker, Granular flow over a flat-bladed stirrer, *Chem. Eng. Sci.* 56 (2001) 4257–4271.
- [43] S.L. Conway, A. Lekhal, J.G. Khinast, B.J. Glasser, Granular flow and segregation in a four-bladed mixer, *Chem. Eng. Sci.* 60 (2005) 7091–7107.
- [44] G.R. Chandratilleke, A.B. Yu, R.L. Stewart, J. Bridgwater, Effects of blade rake angle and gap on particle mixing in a cylindrical mixer, *Powder Technol.* 193 (2009) 303–311.
- [45] G.R. Chandratilleke, A.B. Yu, J. Bridgwater, A DEM study of the mixing of particles induced by a flat blade, *Chem. Eng. Sci.* 79 (2012) 54–74.
- [46] D.F. Bagster, J. Bridgwater, The flow of granular material over a moving blade, *Powder Technol.* 3 (1969) 323–338.
- [47] D.F. Bagster, The prediction of the force needed to move blades through a bed of cohesionless granules, *Powder Technol.* 3 (1969) 153–162.
- [48] D.F. Bagster, J. Bridgwater, The measurement of the force needed to move blades through a bed of cohesionless granules, *Powder Technol.* 1 (1967) 189–198.
- [49] K. Malhotra, A.S. Mujumdar, H. Imakoma, M. Okazaki, Fundamental particle mixing studies in an agitated bed of granular materials in a cylindrical vessel, *Powder Technol.* 55 (1988) 107–114.
- [50] H.P. Zhu, Z.Y. Zhou, R.Y. Yang, a B. Yu, Discrete particle simulation of particulate systems: A review of major applications and findings, *Chem. Eng. Sci.* 63 (2008) 5728–5770.
- [51] P.R. Wahl, G. Fruhmann, S. Sacher, G. Straka, S. Sowinski, J.G. Khinast, PAT for tableting: Inline monitoring of API and excipients via NIR spectroscopy., *Eur. J. Pharm. Biopharm.* (2014).
- [52] H.W. Ward, D.O. Blackwood, M. Polizzi, H. Clarke, Monitoring blend potency in a tablet press feed frame using near infrared spectroscopy., *J. Pharm. Biomed. Anal.* 80 (2013) 18–23.
- [53] K. Muteki, D.O. Blackwood, B. Maranzano, Y. Zhou, Y.A. Liu, K.R. Leeman, et al., Mixture Component Prediction Using Iterative Optimization Technology (Calibration-Free/Minimum Approach), *Ind. Eng. Chem. Res.* 52 (2013) 12258–12268.

- [54] Y. Liu, D. Blackwood, Sample Presentation in Rotary Tablet Press Feed Frame Monitoring by Near Infrared Spectroscopy, *Am. Pharm. Rev.* (2012) 1–9.
- [55] M. Blanco, M. Alcalá, M. Bautista, Pharmaceutical gel analysis by NIR spectroscopy. Determination of the active principle and low concentration of preservatives., *Eur. J. Pharm. Sci.* 33 (2008) 409–14.
- [56] Z. Shi, R.P. Cogdill, S.M. Short, C. a Anderson, Process characterization of powder blending by near-infrared spectroscopy: blend end-points and beyond., *J. Pharm. Biomed. Anal.* 47 (2008) 738–45.
- [57] I. Storme-Paris, I. Clarot, S. Esposito, J.C. Chaumeil, a Nicolas, F. Brion, et al., Near InfraRed Spectroscopy homogeneity evaluation of complex powder blends in a small-scale pharmaceutical preformulation process, a real-life application., *Eur. J. Pharm. Biopharm.* 72 (2009) 189–98.
- [58] L. Martínez, A. Peinado, L. Liesum, G. Betz, Use of near-infrared spectroscopy to quantify drug content on a continuous blending process: influence of mass flow and rotation speed variations., *Eur. J. Pharm. Biopharm.* 84 (2013) 606–15.
- [59] A.U. Vanarase, M. Alcalà, J.I. Jerez Rozo, F.J. Muzzio, R.J. Romañach, Real-time monitoring of drug concentration in a continuous powder mixing process using NIR spectroscopy, *Chem. Eng. Sci.* 65 (2010) 5728–5733.
- [60] G.X. Zhou, L. Crocker, J. Xu, J. Tabora, Z. Ge, In-Line Measurement of a Drug Substance via Near Infrared Spectroscopy to Ensure a Robust Crystallization Process, 95 (2006) 2337–2347.
- [61] M. Alcalà, M. Blanco, M. Bautista, J.M. González, On-line monitoring of a granulation process by NIR spectroscopy., *J. Pharm. Sci.* 99 (2010) 336–345.
- [62] P. Luukkonen, M. Fransson, I.N. Björn, J. Hautala, B. Lagerholm, S. Folestad, Real-Time assessment of granule and tablet properties using in-line data from a high-shear granulation process., *J. Pharm. Sci.* 97 (2008) 950–959.
- [63] R.L. Green, G. Thureau, N.C. Pixley, A. Mateos, R. a Reed, J.P. Higgins, In-line monitoring of moisture content in fluid bed dryers using near-IR spectroscopy with consideration of sampling effects on method accuracy., *Anal. Chem.* 77 (2005) 4515–22.
- [64] A.D. Karande, P.W.S. Heng, C.V. Liew, In-line quantification of micronized drug and excipients in tablets by near infrared (NIR) spectroscopy: Real time monitoring of tableting process., *Int. J. Pharm.* 396 (2010) 63–74.
- [65] K. Järvinen, W. Hoehe, M. Järvinen, S. Poutiainen, M. Juuti, S. Borchert, In-line monitoring of the drug content of powder mixtures and tablets by near-infrared spectroscopy during the continuous direct compression tableting process., *Eur. J. Pharm. Sci.* 48 (2013) 680–8.

- [66] M. Andersson, S. Folestad, J. Gottfries, M.O. Johansson, M. Josefson, K.G. Wahlund, Quantitative analysis of film coating in a fluidized bed process by in-line NIR spectrometry and multivariate batch calibration., *Anal. Chem.* 72 (2000) 2099–108.
- [67] M. Andersson, M. Josefson, F.W. Langkilde, K.G. Wahlund, Monitoring of a film coating process for tablets using near infrared reflectance spectrometry., *J. Pharm. Biomed. Anal.* 20 (1999) 27–37.
- [68] J. Roperó, L. Beach, M. Alcalà, R. Rentas, R. Davé, R. Romañach, Near-infrared Spectroscopy for the In-line Characterization of Powder Voiding Part I: Development of the Methodology, *J. Pharm. Innov.* 4 (2009) 187–197.
- [69] M.J. Barajas, A.R. Cassiani, W. Vargas, C. Conde, J. Roperó, J. Figueroa, et al., Near-Infrared Spectroscopic Method for Real-Time Monitoring of Pharmaceutical Powders During Voiding, *Appl. Spectrosc.* 61 (2007) 490–496.
- [70] Y. Colón, M. Florian, D. Acevedo, R. Méndez, R. Romañach, Near Infrared Method Development for a Continuous Manufacturing Blending Process, *J. Pharm. Innov.* (2014) 1–11.

CHAPTER 2

2 PARTICLE SIZE SEGREGATION PROMOTED BY POWDER FLOW IN CONFINED SPACE: THE DIE FILLING PROCESS CASE¹

2.1 Summary

Tablet compression has great significance in the pharmaceutical industry since most of the drugs are in the tablet dosage form. The tablet press feed frame is used to fill powder into the empty dies. Die filling is one of the key steps to control final properties of tablets. Using the Discrete Element Method (DEM), a standard feed frame taken from a Manesty Betapress was simulated as a representation of the tableting process without the compression stage. DEM was used to understand the micro-macro dynamics of the particles inside the feed frame. Segregation behavior of a single material with a particle size distribution was investigated using this method. The DEM simulation components included 2 paddle wheel speeds (24 and 72 rpm) and 2 die disk speeds (29 and 57 rpm). The results obtained highlight the effect of feed frames on the powder properties. The DEM results show size segregation inside the feed frame and during the die filling stage. Velocity profiles and particle vectors show that the percolation phenomenon is the most significant segregation mechanism. Paddle wheel speed was demonstrated to be the most important factor to control particle size segregation inside the feed frame.

¹ This chapter is based on the publication: D. Mateo-Ortiz, F.J. Muzzio, R. Méndez, Particle size segregation promoted by powder flow in confined space: The die filling process case, Powder Technol. (2014).

2.2 Methodology

2.2.1 Computational Study (DEM Simulations)

During the tablet press operation, powder flows through a feed frame, enters a die, and then is compressed into tablets. This makes it impossible to determine powder properties as it is entering the die. To determine the properties and behavior of the powder inside the feed frame and dies, two main methods were used. The first method was to use a discrete element method (DEM) to answer the uncertainties of flow behavior and segregation within the feed frame and dies. The second method was experimental and relied on decoupling the feed frame from the tablet press with a custom made die disc without the compression step. This method was also used to validate the DEM simulations. The apparatus is a standard feed frame taken from a Manesty Betapress and a simulated die disc, which represents die-filling process without the compression step. The feed frame has two paddle wheels. One of them rotates counter-clockwise and the other one rotates clockwise, while the die disk rotates clockwise (Fig 2.1.). A previous publication [1] explains in more detail the description of the Manesty Betapress feed frame. EDEM software was used to perform all the simulations. The system simulated was first build in AutoCAD® and then the drawing was imported to EDEM (DEM Solutions). The simulated feed frame system is shown in Fig. 2.1.

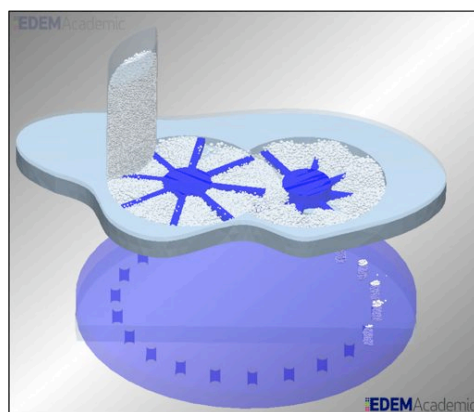


Figure 2.1. Tablet press feed frame simulated in EDEM.

The parameters used in the simulations are presented in Table 2.1, where the particle properties are similar to those used in the literature [2-9]. Our computational capabilities were also taken into consideration for the selection of the particle size. These simulation parameters values describe the particle properties affecting significantly the results. The cohesion model used for the simulations modifies the Hertz-Mindlin model by adding a normal cohesion force. This force takes the form: $F = kA$, where A is the contact area and k is a cohesion energy density with units Jm^3 . The value of k for the simulations was 500.

Table 2.1. DEM parameters.

| Parameter | Value | Reference value |
|--|-----------------|------------------------|
| Average particle diameter (mm) | 1.5 | 1.0–4.55 [2,3–5] |
| Particle standard deviation (mm) | 0.75 | – |
| Particle Poisson's ratio | 0.5 | 0.3–0.4 [2,4,8,9] |
| Particle shear modulus (Pa) | 1×10^8 | 2×10^6 [2,4] |
| Particle density (g/cm^3) | 1.4 | 1.1–1.7 [7] |
| Geometry Poisson's ratio | 0.3 | 0.3–0.35 [2,4–6] |
| Geometry shear modulus (Pa) | 3×10^9 | 3×10^9 [2,4] |
| Geometry density (g/cm^3) | 1.2 | 1.2 [2,4] |
| Particle–particle restitution coefficient | 0.5 | 0.40–0.73 [2,4,6,7] |
| Particle–particle coefficient static friction | 0.5 | 0.50 [2,4,8] |
| Particle–particle coefficient rolling friction | 0.005 | 0.01 [2,4,7] |
| Particle–geometry restitution coefficient | 0.5 | 0.40–0.73 [2,4,7] |
| Particle–geometry coefficient static friction | 0.8 | 0.35–0.6 [2,4,9] |
| Particle–geometry coefficient rolling friction | 0.005 | 0.01–0.005 [2,4,7] |

In order to analyze the data from the simulations, selections were created at different locations of the feed frame. The selections allow data to be extracted from a particular area in the domain. Also, it helps to monitor any particle through a particular area. The data can be exported based on these selections. All the simulations were evaluated using the same Manesty Beta Press feed frame design. The design of experiment components includes 2 paddle wheel speeds (24 and 72 rpm) and 2 die disk speeds (29 and 57 rpm). These operating

values were selected based on typical tablet press operation speeds used in the pharmaceutical industry.

2.2.2 Experimental Study

A Manesty Beta Press feed frame was used to validate the DEM simulations. The feed frame has three exits with different sizes and shapes (Fig. 2.2). The materials used in the experimental study were Monohydrate Lactose (Tabletose 70 Agglomerated, Ph. EUR/USP-NF/JP, Malkerei Meggle Wasserburg GmbH & Co.) with 125 μm median particle size, 1% Magnesium Stearate (Ligamed MF-2-K, Peter Greven) with median particle size < 10 μm and a granulation made with Lactose, Anhydrous NF Direct Tableting (Kerry Bio-Science) with a 12.5% Povidone USP, Plasdone K-29/32 (ISP Technologies Inc.) solution as the binder. After the material was granulated, it was sieved to obtain particles between 425 – 710 μm .

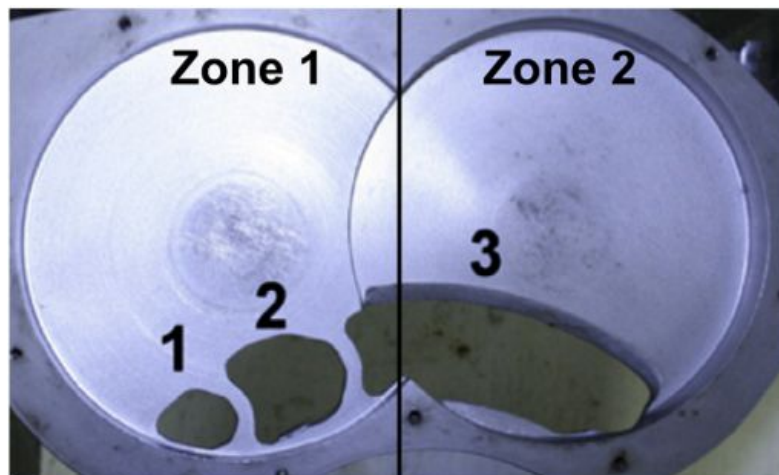


Figure 2.2. Manesty Beta Press feed frame exits.

The experimental setup equipment consists of two loss in weight feeders to feed the lactose (Schenck Accurate, model Modpharma 2007) and the granulation (Gericke, model 153) at a controlled rate, a continuous tumble mixer and finally the Manesty Beta Press feed

frame. In the simulations, the particles enter the feed frame mixed, therefore, a continuous tumble mixer was used for the monohydrate lactose and the granulation before the feed frame stage. The objective of the mixture between the monohydrate lactose and the granulation was to obtain particles with greater size than the monohydrate lactose 70 in order to obtain a wider particle size distribution (PSD). The feed frame was operated for two minutes before taking samples. This time period represents approximately eight times the time it takes for the system to reach steady state in the simulations. Samples were taken at the entrance of the feed frame every 5 seconds and at the exit of the dies every 3 seconds. At the end of the experiment the feed frame was opened and samples were carefully taken at different locations (Fig. 2.3) from the top and bottom layers of the material left inside the feed frame. In order to characterize the particles size distribution of each sample, a laser diffraction method (Insittec T Malvern Inc.) was used.

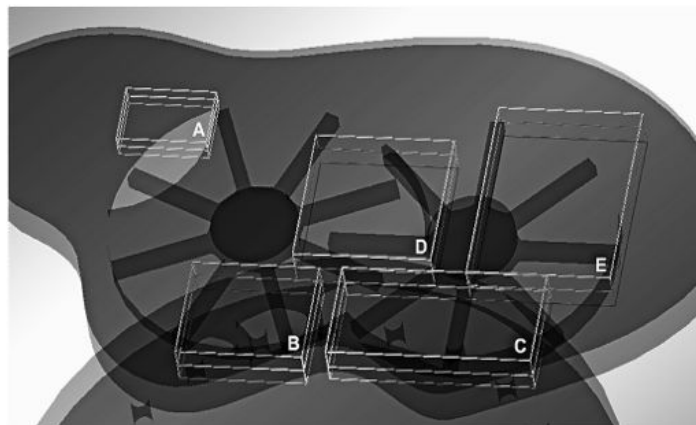


Figure 2.3. Top–bottom feed frame sample locations.

2.3 Results and Discussion

2.3.1 Feed Frame Mass Hold-up

The total mass inside the feed frame (feed frame mass hold-up) was obtained analyzing a rectangular selection with the dimensions equal to the feed frame. More details

about the selection can be seen in Fig. 2.4B. The mass inside the feed frame was analyzed every 0.5 seconds. The mass hold up inside the feed frame was mainly influenced by the die disk speed factor because it controlled the outlet flowrate, therefore changing the accumulation inside the feed frame. The higher the die disk speed, the lower the mass hold-up inside the feed frame. For all the simulations the hold-up reached mass steady state after approximately 15 seconds. It was observed that the velocity to reach steady state is affected by the paddle wheel speed. The simulations at 72 rpm paddle wheel speed reached mass steady state approximately 5 seconds faster (Fig. 2.5).

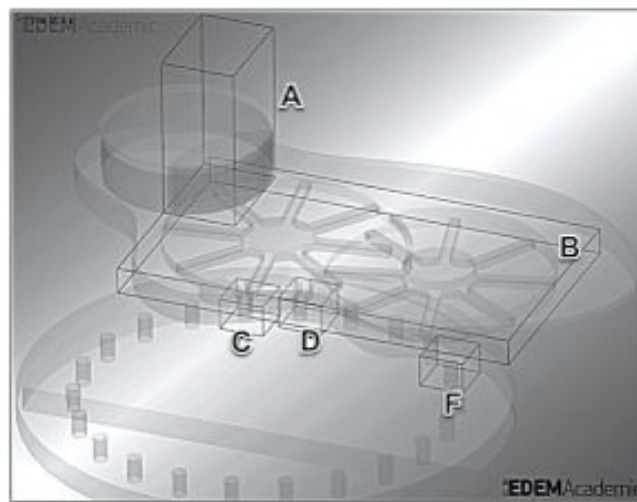


Figure 2.4. Hopper (A), feed frame (B), exit 1 (C), exit 2 (D) and exit 3 (F).

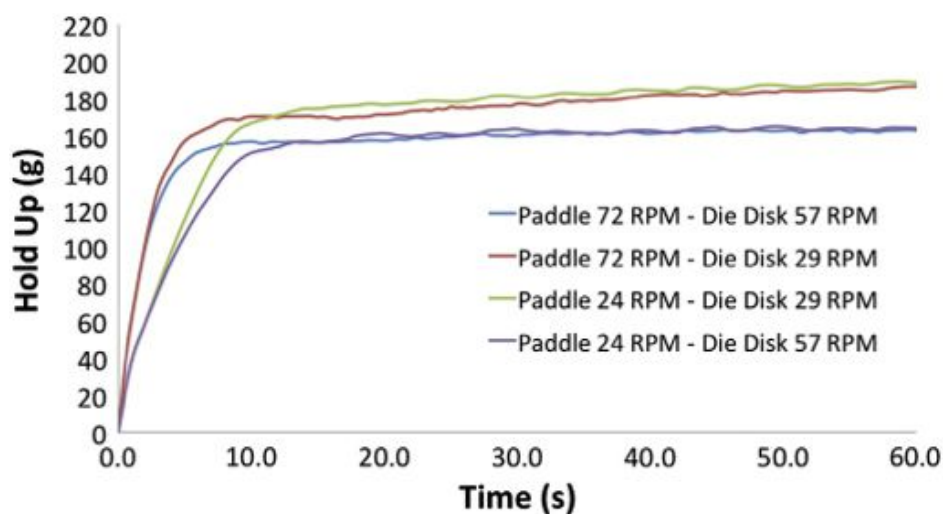


Figure 2.5. Feed frame mass hold-up.

The particles used in this simulation can be considered free flowing based on the particle parameters selected. If the particles were more cohesive, the paddle wheel speed factor would change significantly the mass hold-up inside the feed frame, therefore, the powder confinement could increase and segregation could decrease [10].

2.3.2 Exits Contribution to Die Filling and Die Weight Variability

The Manesty Beta Press feed frame has three exits, two in the first stage (zone 1) and one in the second stage (zone 2) with different shapes and sizes (Fig. 2.2). Previous results demonstrated that the properties of the material leaving the feed frame are affected by exit positions and operating conditions [11]. Three selections just below each exit were created to capture the data of each of the three exits (Fig. 2.4C, 2.4D, 2.4F). Using these selections, the mass weight contribution from each exit to the dies was determined. A die was analyzed approximately every second after the simulation reached mass steady state. Each die was followed from exit 1 to exit 3 to measure the die weight contribution of each exit. Figure 2.6 describes the average exits contribution to the amount of mass in the dies. Even though the two exits from stage one are small, for lower die disc speed (Fig. 2.6A and Fig. 2.6B) more than 80% of the particles entering the feed frame were forced to leave through zone 1. The paddle wheel speed decreased the amount of particles leaving the first stage. As the die disk speed was doubled to 57 rpm (Fig. 2.6C and Fig. 2.6D), most of the powder left the feed frame through exit 3 (zone 2). Previous results demonstrated that powder leaving zone 2 was submitted to higher shear and attrition, increasing the possibility of powder stratification in the die for granular material sensitive to total shear applied [11]. The exit contribution mass variability increased as paddle wheel speed increased. This can be observed when comparing Fig. 2.6C with Fig. 2.6D in which both simulations were performed using the same die disk

speed but different paddle wheel speeds.

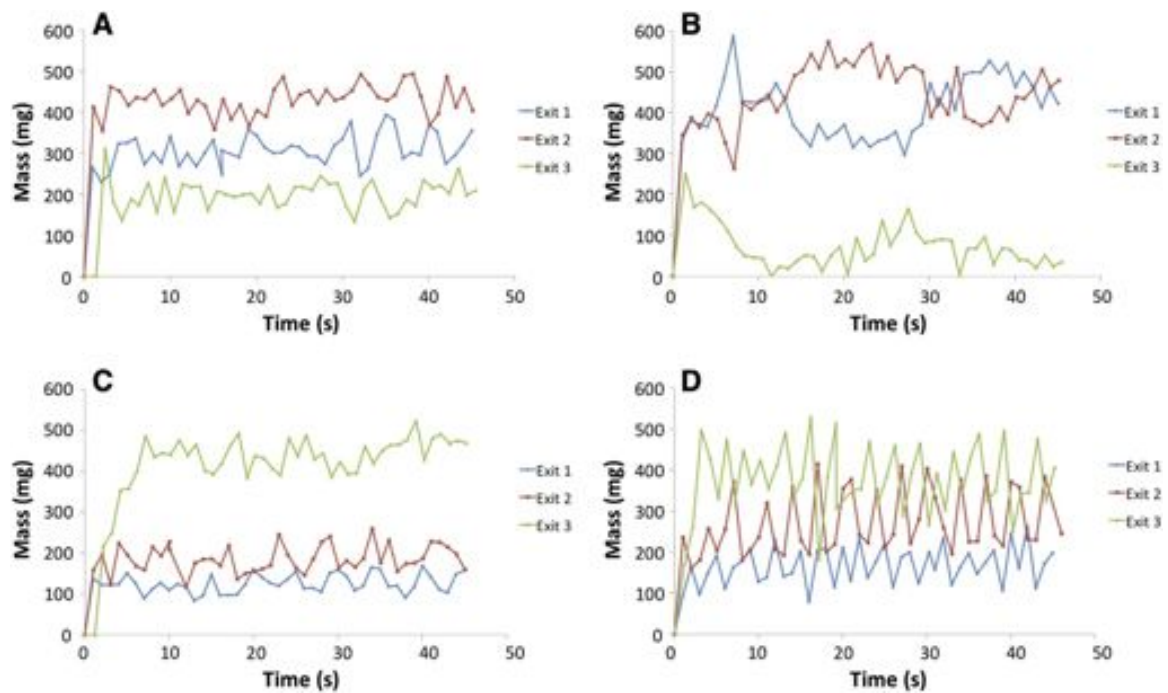


Figure 2.6. Exit contributions **A:** 24 rpm paddle wheel & 29 rpm die disk speed. **B:** 72 rpm paddle wheel & 29 rpm die disk speed. **C:** 24 rpm paddle wheel & 57 rpm die disk speed. **D:** 72 rpm paddle wheel & 57 rpm die disk speed.

It was found that the lower the die disk speed, the lower the relative standard deviation (RSD) of the die weight (Fig. 2.7). The average residence time of dies passing under the exits at die disk speed of 29 rpm is 0.51 seconds and for die disk speed at 57 rpm the average residence time is 0.26 seconds. This demonstrated that the residence time of the dies in the filling area affects significantly the weight variability and the average die weight. The maximum mass that can fit in a die is approximately 950 mg but at high die disk speed the dies are filled with less than 900 mg. These results can be compared to the die filling process with a shoe in which high shoe speed can be related to die disk speed and as the die disk speed and shoe speed increases there is an incomplete filling [12].

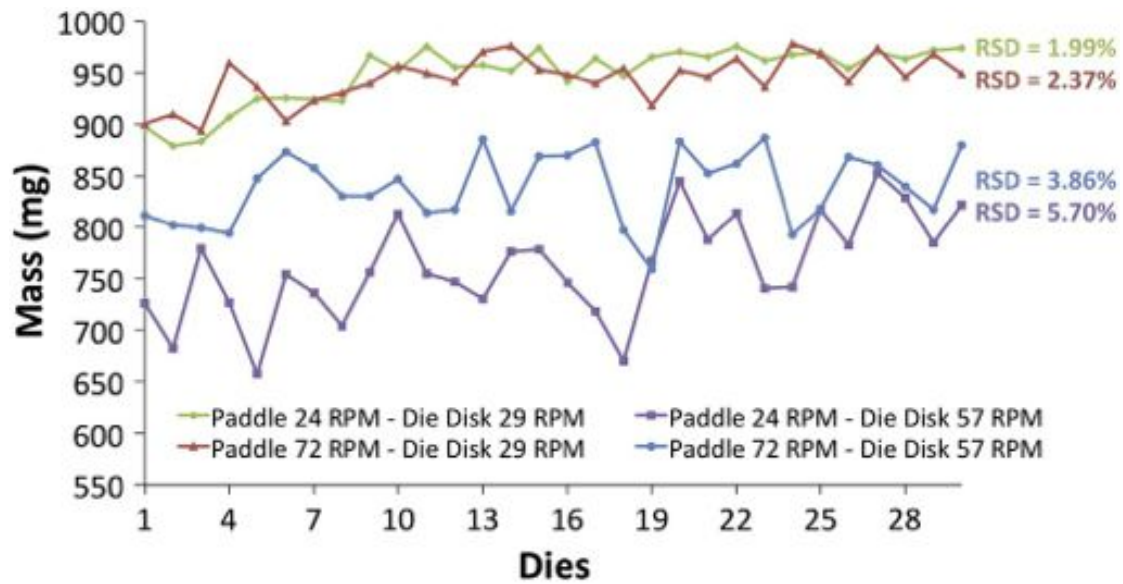


Figure 2.7. Die weight variability at each operating parameter.

The average mass hold-up at paddle wheel speed of 24 rpm and die disk speed of 29 rpm was 187.5 g and the average mass hold-up at paddle wheel speed of 72 rpm and die disk speed of 29 rpm is 185.5 g. This difference can be attributed to a relationship between feed frame mass hold-up and die weight variability. The RSD of the die weight variability of the simulation at blade speed of 24 rpm and die disk speed of 29 rpm was 1.99% compared to 2.37% of the simulation at blade speed of 72 rpm and die disk speed of 29 rpm, meaning that at low paddle wheel speed more mass is going out at a more constant rate explaining the slight difference between the two average mass hold-ups of each simulation. Even though the exit contribution mass variability increases as paddle wheel speed increases, when comparing the two simulations at die disk speed of 57 rpm, the RSD of the die weight variability decreases as the paddle wheel speed increases. This is mainly because at a die disk speed of 57 rpm, the outlet mass rate increase and a faster paddle wheel speed (72 rpm) helps in distributing particles through the two stages of the feed frame at a faster and more constant rate and therefore the RSD of the die weight variability decreases.

2.3.3 Velocity Profile

The velocity profiles at each paddle wheel speed, 24 rpm and 72 rpm, can be seen in Figure 2.8A and Figure 2.8B where colors indicate the particle speed: blue particles ranging from 0.00 to 16.67 cm/s, green particles from 16.67 to 33.33 cm/s and red particles from 33.33 to 50.00 cm/s. In general, at 24 rpm paddle wheel speed the particles are moving slower with respect to 72 rpm blade speed and have more time for particle rearrangement, hence smaller particles reach the bottom of the feed frame and dies easily.

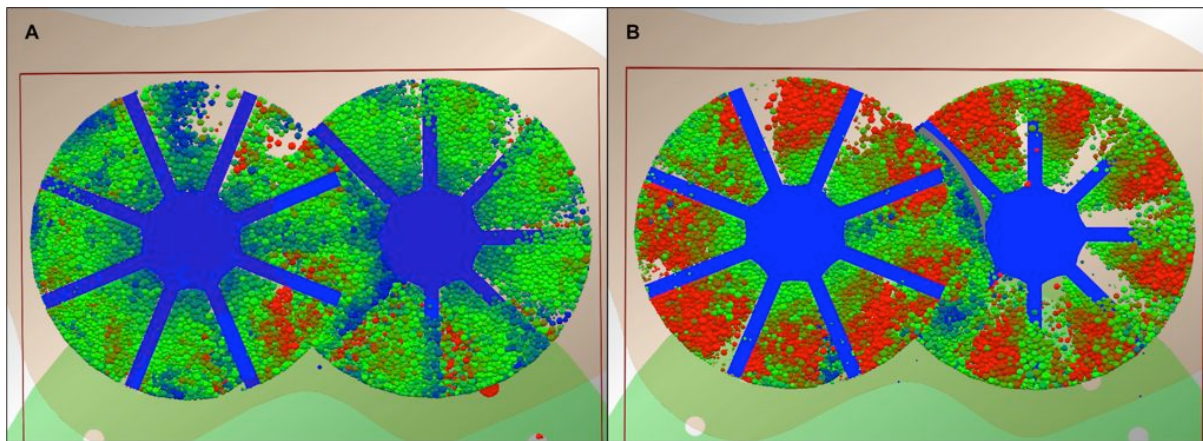


Figure 2.8. Velocity profile at **A:** 24 rpm paddle wheel speed. **B:** 72 rpm paddle wheel speed.

All particles rotate at the same angular velocity, but particles farther from the axis of rotation move at a higher tangential velocity than particles closer to it. This suggests that increasing the diameter of the center of the paddle wheel could decrease the die weight variability. This would reduce the velocity gradient between particles closer to the axis of rotation to the ones that are far from it, creating a more homogenous die filling.

2.3.4 DEM Particle Size Segregation

Another important parameter to describe powder phenomena inside the feed frame is

the effect of the paddle wheel speed and die disk speed on particle size segregation inside the feed frame and in the dies. Figure 2.9 shows a top and bottom view of the feed frame in which colors indicate the particle diameter: blue particles ranging from 349.7 to 988.6 μm , green particles ranging from 988.6 to 1627.4 μm and red particles ranging from 1627.4 to 2266.3 μm . Comparing Fig. 2.9A with Fig. 2.9B and Fig. 2.9C with Fig. 2.9D, segregation was observed inside the feed frame based on the top part of the feed frame versus the bottom part. The results show bigger particles at the top of the feed frame relative to the bottom for both paddle wheel speeds. Figure 2.10 shows a snapshot of the simulation at low paddle wheel speed and low die disk speed after the system reached mass steady state and the smaller particles can be observed at the bottom of the feed frame.

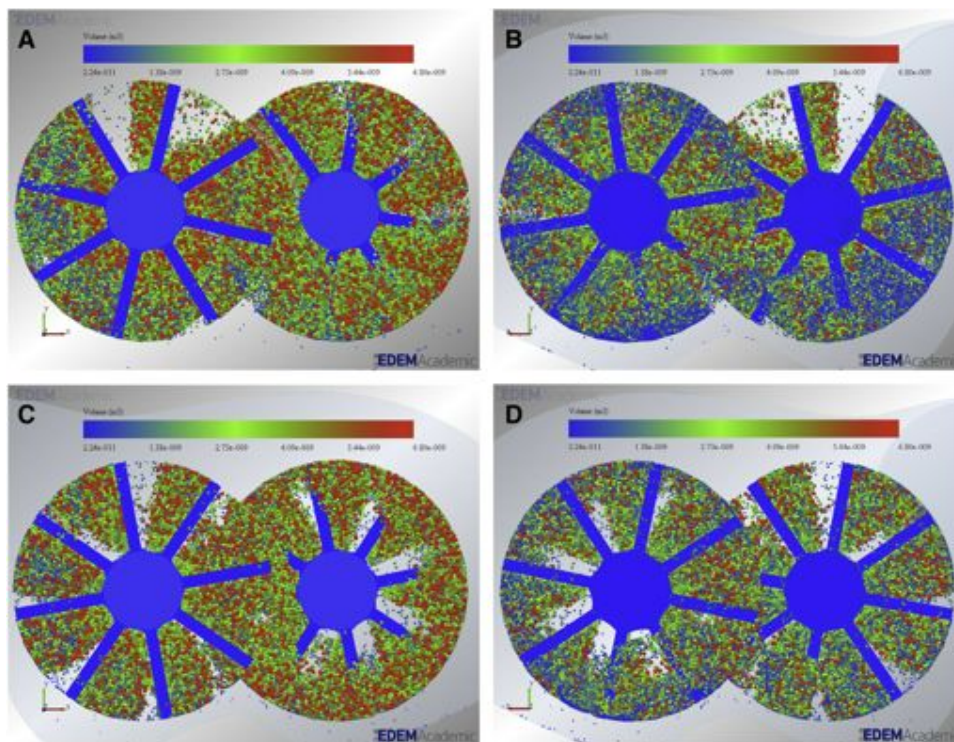


Figure 2.9. **A:** Feed frame top view at 24 rpm paddle wheel speed. **B:** Feed Frame bottom view at 24 rpm paddle wheel speed. **C:** Feed frame top view at 72 rpm paddle wheel speed. **D:** Feed frame bottom view at 72 rpm paddle wheel speed.

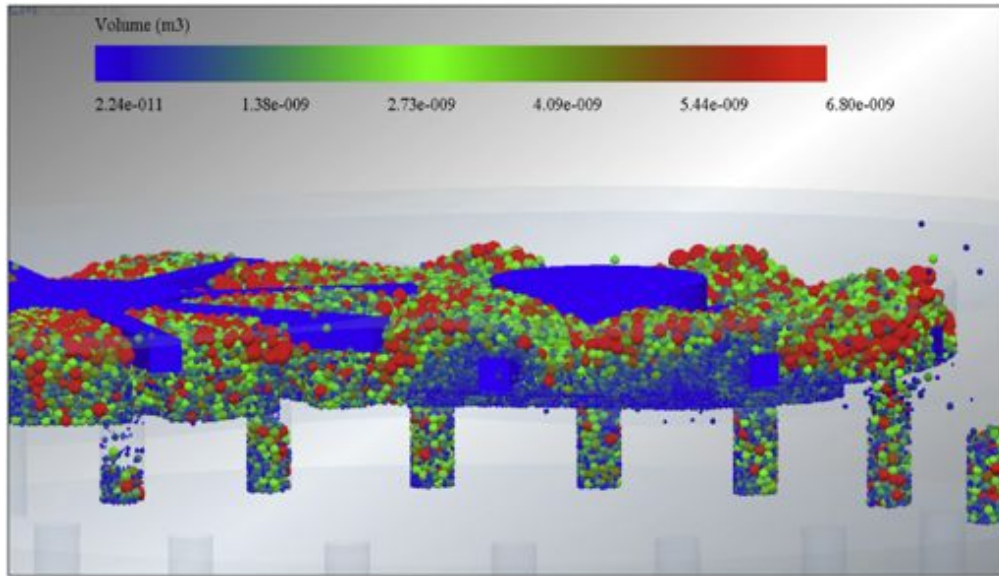


Figure 2.10. Feed frame front view.

To qualitatively measure the segregation inside the feed frame, selections were created at different locations (Fig. 2.3). Table 2.2 shows the mean particle size (D50) at each selection and the difference between the top and bottom particles diameters of each location. Based on the DEM results, the D50 of the top and bottom entrance locations are similar with a difference of 17 μ m. This demonstrates that the material is not getting segregated at the entrance and that the hopper has a small effect on segregation. When analyzing the top and bottom D50 values taken at other locations (Table 2.2), larger particles are observed at the top compared to the bottom and a significant difference between the values. These DEM results demonstrated particle size segregation inside the feed frame.

Table 2.2. Top–bottom D50 values at each sample location inside the feed frame.

| Sample Location | Experimental | | DEM Simulation | |
|--------------------------|----------------|-----------------------|----------------|-----------------------|
| | D50 (μ m) | Difference (μ m) | D50 (μ m) | Difference (μ m) |
| Top Entrance (Zone 1) | 605.69 | 38.92 | 1343.62 | 17.07 |
| Bottom Entrance (Zone 1) | 566.77 | | 1326.55 | |
| Top Exits 1 & 2 | 620.98 | 206.59 | 1471.50 | 235.79 |
| Bottom Exits 1 & 2 | 414.39 | | 1235.71 | |

| | | | | |
|---------------------------|--------|--------|---------|--------|
| Top Exit 3 | 593.67 | | 1767.25 | |
| Bottom Exit 3 | 472.45 | 121.22 | 1497.41 | 269.84 |
| Top Between Zone 1 & 2 | 572.45 | | 1860.13 | |
| Bottom Between Zone 1 & 2 | 490.26 | 82.19 | 1742.45 | 117.68 |
| Top sample Zone 2 | 637.48 | | 1878.35 | |
| Bottom sample Zone 2 | 516.94 | 120.54 | 1710.41 | 167.94 |

To evaluate segregation in the dies, the previous selection at exit 3 was divided into two new selections, the top half die selection and the bottom half die selection (Fig. 2.11). Fifty dies were analyzed for 50 seconds (1 die per second) after mass steady state was achieved for each simulation. The particle count and average particle diameter at each half of the die was analyzed (Fig. 2.12). The diameter of the blue particles range from 349.7 to 1017.5 μm , the green particles range from 1017.5 to 1685.2 μm and the red particles range from 1685.2 to 2352.9 μm . An average of the average particle diameters was calculated to evaluate the vertical segregation (Fig. 13). It was observed that at low paddle wheel speed, the difference in average particle size from the top to the bottom increases and the difference decreases as the paddle wheel speed increases. Due to segregation, there are smaller particles on the bottom of the feed frame as well as in the bottom half of dies. The results showed (Fig. 2.13) that particle size segregation is most significant in the dies when paddle wheel speeds are low (24 rpm), but at high paddle speeds (72 rpm) there was less segregation. Thus, size segregation is demonstrated inside the feed frame and dies.

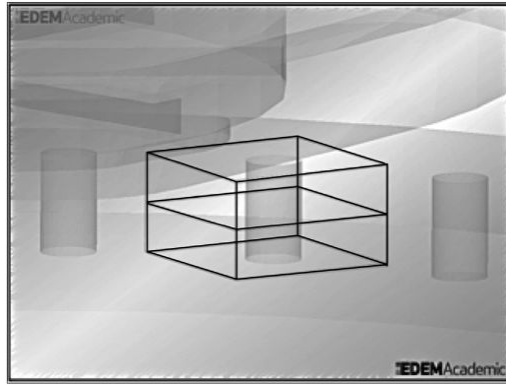


Figure 2.11. Top and bottom selections of die.

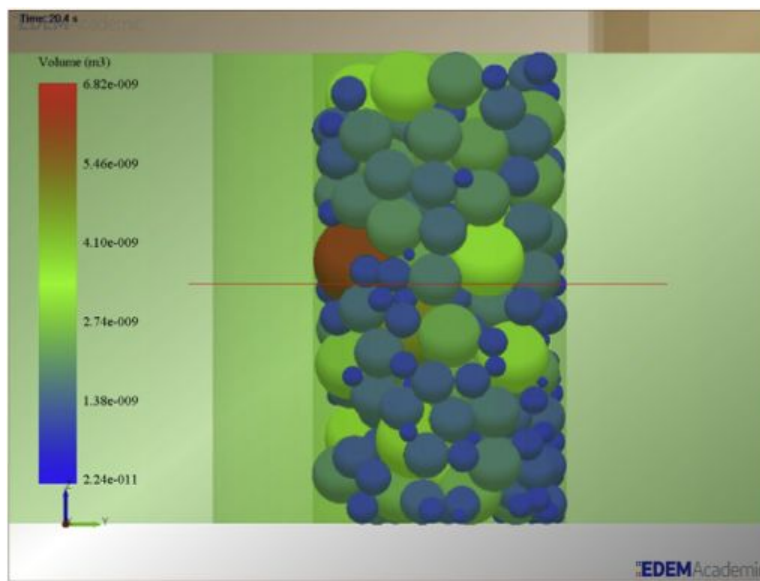


Figure 2.12. Example of top to bottom segregation in a die.

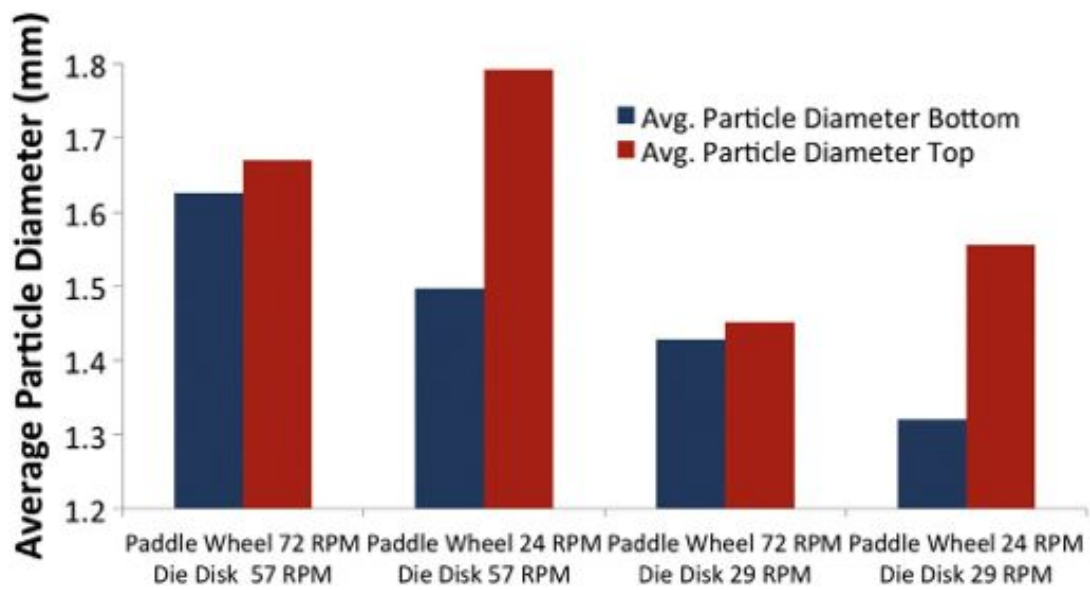


Figure 2.13. Top to bottom particle segregation in the dies at each operating parameter.

To explain the percolation segregation phenomena, Figures 2.14A and 2.14B represent the particle velocity vectors as a function of size. The diameter of the blue particles range from 349.7 to 988.6 μm , the green particles range from 988.6 to 1627.4 μm and the red particles range from 1627.4 to 2266.3 μm . At a paddle wheel speed of 24 rpm, it can be observed (Fig. 2.14A) that particles are moving relatively slow and therefore the gravity force dominates the force exerted by the paddles. Therefore, the particles have more time for rearrangement and for moving downward rather than horizontally. Figure 2.14B shows that the force exerted on the particles dominates, preventing particles going downward and therefore preventing the percolation phenomena. Velocity profiles and the particle vectors show that the percolation phenomenon is the most significant segregation factor.

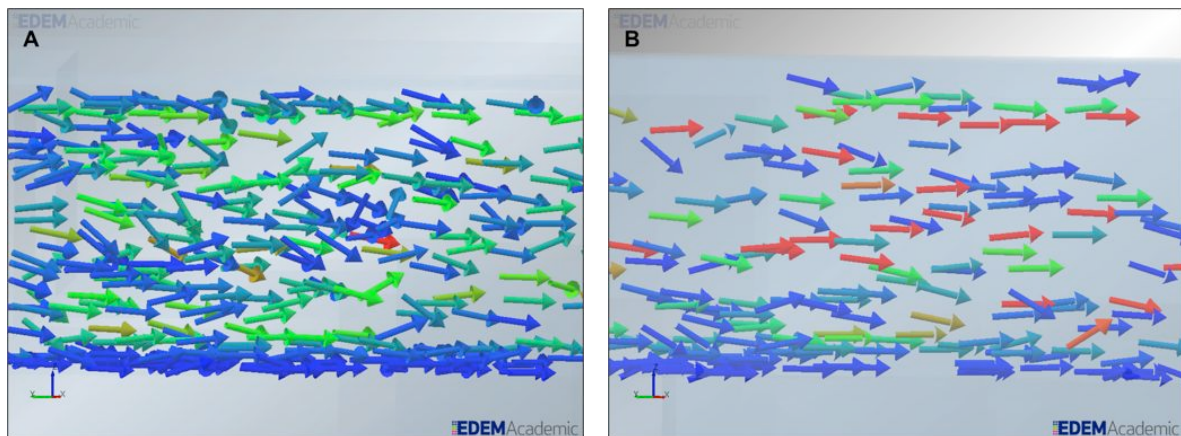


Figure 2.14. Particle vectors at **A:** 24 rpm paddle wheel speed. **B:** 72 rpm paddle wheel speed.

2.3.5 Experimental Results

An experiment was performed at 24 rpm paddle wheel speed and 29 rpm die disk speed because at those conditions a higher segregation level was observed with the DEM simulations. The lactose and the granulated material went through the feeders, then were

mixed in a tumble mixer and samples were taken every 5 seconds just before entering the feed frame and every 3 seconds after the material went through the feed frame and die disk for 100 seconds. The D50 of the average PSD at the entrance was 488.8 μm with a standard deviation of 82.7 and the D50 of the average PSD is 457.9 μm at the exit with a standard deviation of 63.1. Table 2.2 shows the D50 of the top and bottom samples taken at the different locations inside the feed frame (Fig. 3). Even though grab sampling was performed, the segregation signal was significant, therefore, these phenomena can be mainly attributed to the feed frame processing parameters. The D50 of the top and bottom samples taken at the entrance are similar which shows that the material is not segregated at the entrance. However, when analyzing the top and bottom samples taken in the other locations, larger particles were observed at the top half compared to the bottom half with a significant difference between the D50 values. These results confirmed that segregation occurs inside the feed frame and validates what was observed in the DEM simulations. Therefore, a tendency can be established between the DEM simulations and the experiments. Roudsari and Puri demonstrated that particle segregation might promote non uniform die filling [13]. Therefore, nonsymmetrical pressure distribution could occur and it has been determined to cause different physical tablet problems (i.e., low strength, cracking, and shrinkage) [13].

2.4 Conclusion

The results obtained highlighted the effect of feed frames over the resulting powder properties. The DEM results show particle size segregation inside the feed frame and during the die filling stage. The velocity profiles and particle vectors show that the percolation phenomenon is the most significant segregation mechanism. Although the top and bottom of the dies were not experimentally analyzed because of the experimental complexity, it was shown in the simulations that the material segregates inside the feed frame at low paddle

wheel speeds and therefore the material is segregated when it enters the dies. The paddle wheel speed was demonstrated to be the most important factor to control top to bottom segregation inside the feed frame. Previous work on feed frames [11-14] demonstrated that particle attrition occurs at high paddle wheel speed and over lubrication of the material, therefore, the optimum paddle wheel speed depends on the particle properties.

2.5 References

- [1] R. Mendez, F. Muzzio, and C. Velazquez, Study of the effects of feed frames on powder blend properties during the filling of tablet press dies, *Powder Technology* 200 (3) (2010) 105–116.
- [2] M. Marigo, D.L. Cairns, M. Davies, a. Ingram, E.H. Stitt, A numerical comparison of mixing efficiencies of solids in a cylindrical vessel subject to a range of motions, *Powder Technol.* 217 (2012) 540–547.
- [3] Y. Yu and H. Saxén, Experimental and DEM study of segregation of ternary size particles in a blast furnace top bunker model, *Chemical Engineering Science* 65 (18) (2010) 5237–5250.
- [4] M. Marigo, D. L. Cairns, M. Davies, a. Ingram, and E. H. Stitt, Developing mechanistic understanding of granular behaviour in complex moving geometry using the Discrete Element Method, *Powder Technology* 212 (1) (2011) 17–24.
- [5] A. P. Grima and P. W. Wypych, Investigation into calibration of discrete element model parameters for scale-up and validation of particle–structure interactions under impact conditions, *Powder Technology* 212 (1) (2011) 198–209.
- [6] S. Rosenkranz, S. Breitung-Faes, and a. Kwade, Experimental investigations and modelling of the ball motion in planetary ball mills, *Powder Technology* 212 (1) (2011) 224–230.
- [7] J. Wiącek, M. Molenda, J. Horabik, and J. Y. Ooi, Influence of grain shape and intergranular friction on material behavior in uniaxial compression: Experimental and DEM modeling, *Powder Technology* 217 (2012) 435–442.
- [8] P. R. Santhanam and E. L. Dreizin, Predicting conditions for scaled-up manufacturing of materials prepared by ball milling, *Powder Technology* 221 (2012) 403–411.
- [9] I. Keppler, L. Kocsis, I. Oldal, I. Farkas, and A. Csatar, Grain velocity distribution in a mixed flow dryer, *Advanced Powder Technology* 23 (6) (2012) 824–832.

- [10] M. Rahman, H. Zhu, A. Yu, and J. Bridgwater, DEM simulation of particle percolation in a packed bed, *Particuology* 6 (6) (2008) 475–482.
- [11] R. Mendez, C. Velazquez, and F. J. Muzzio, Effect of feed frame design and operating parameters on powder attrition, particle breakage, and powder properties, *Powder Technology* 229 (2012) 253–260.
- [12] C.-Y. Wu and a. C. F. Cocks, Flow behaviour of powders during die filling, *Powder Metallurgy* 47 (2) (2004) 127–136.
- [13] S. S. Roudsari and V. M. Puri, Uniformity Differentiation Analysis. Part 2: Powder Deposition Characteristics in Circular Shallow Die Using Feed Shoe with Circular Cross Section, *Particulate Science and Technology* 28 (2) (2010) 173–182.
- [14] R. Mendez, C. Velazquez, and F. J. Muzzio, Powder Hydrophobicity and Flow Properties: Effect of Feed Frame Design and Operating Parameters, *AIChE J.* 58 (3)

CHAPTER 3

3 RELATIONSHIP BETWEEN RESIDENCE TIME DISTRIBUTION AND FORCES APPLIED BY PADDLES ON POWDER ATTRITION DURING THE DIE FILLING PROCESS

3.1 Summary

The die filling process, which happens prior to the compaction step, affects directly the quality of the final product (tablets). As paddles pass through the powder bed inside the feed frame, shear is applied to the particles. Therefore, it is important to establish a relationship between residence time distribution (RTD) and the forces applied by the feed frame paddles on powder attrition during the die filling process. The pulse injection method was used to study the RTD in the feed frame. The Discrete Element Method (DEM) was also used to measure the RTD of particles by size ranges and the mean residence time (MRT) inside the feed frame. The experimental and DEM simulation design of experiments included 2 paddle wheel speeds (24 and 72 rpm) and 2 die disk speeds (29 and 57 rpm). Experimental results show that higher paddle wheel speeds lead to lower mean residence times, narrower RTD profiles and larger number of paddle passes. The simulations RTD profiles are similar to an ideal continuous stirred tank reactor (CSTR) profile with a sharp peak and a tail. The operating conditions, feed frame exit contributions and outlet mass flowrate affect the MRT. The RTD analysis by particle size shows that particle size segregation occurs where the smaller particles are leaving the feed frame faster. The level of powder confinement inside the feed frames can have a significant effect on powder attrition. As the particle size increases, the compressive and tangential force applied to it increases. The tangential force data shows that the level of attrition is also affected by the paddle wheel speed. This study explains in detail different factors that can affect the residence time distribution and the force applied to particles that can ultimately cause particle breakage and powder hydrophobicity.

3.2 Materials and Methods

3.2.1 Experimental Section

3.2.1.1 Pulse Injection Tracer Experiments

The materials used in the experimental study were Tablettose 70 Agglomerated Monohydrate Lactose Ph. EUR/USP-NF/JP (Malkerei Meggle Wasserburg GmbH & Co.) with 125 μ m median particle size and Naproxen sodium (Zhejiang Tianxin Pharmaceutical Co.) with a median particle size of 28 μ m as the tracer. The equipment used in this study consists of a loss in weight feeder (Gericke, model 153) to feed the lactose at a controlled rate, and the Manesty Beta Press feed frame. The feed frame has three exits with different sizes and shapes (Fig. 3.1).

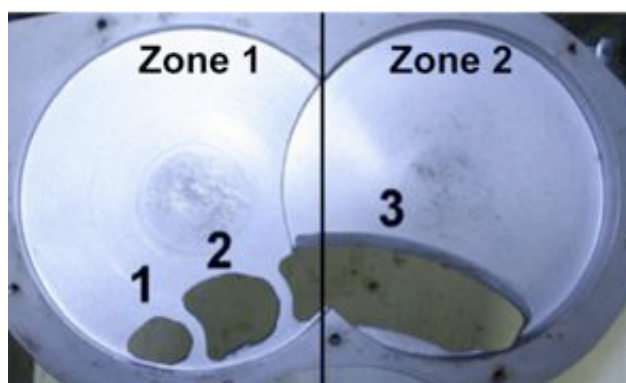


Figure 3.1. Manesty Beta Press Feed Frame Exits and Zones.

The design of experiment (DOE) components includes 2 paddle wheel speeds (24 and 72 rpm) and 2 die disk speeds (29 and 57 rpm). These operating conditions were selected based on typical tablet press operation speeds used in the pharmaceutical industry. The lactose went through the feeder and entered the feed frame at a feed rate of around 410g/min. The feed frame was operated for 2 minutes before taking samples. This period represent

approximately eight times the time it takes for the system to reach mass steady state in the DEM simulations. After this preliminary period, 5 grams of Naproxen were added to serve as the tracer. Samples were taken at the exit of the dies every 2 seconds for the first 30 seconds, every 5 seconds until the 2 minutes mark and every 10 seconds until the 3 minutes mark.

3.2.1.2 *UV-Vis Spectroscopy*

UV-Vis spectroscopy was used to measure the concentration of Naproxen in each sample and then determine the residence time distribution. The calibration curve for the concentration of Naproxen was obtained using a Genesys 10S UV-Vis Spectrophotometer at 318 nm to determine the residence time distribution (RTD). Subsequent dilutions that ranged from 0% to 50% were prepared from a stock solution, and their absorbance was measured. Validation samples were obtained to verify the calibration curve, and the maximum error percent obtained was 2.36%.

3.2.1.3 *Strain Measurement*

To estimate the amount of strain the powder received inside the feed frame, the number of paddle passes was calculated as a function of paddle wheel rotational speed, number of paddles and mean residence time (eq.1) [1].

$$Paddle\ passes = Paddle\ wheel\ speed\ (rpm) \times number\ of\ paddles \times \frac{MRT(s)}{60} \quad (3.1)$$

3.2.2 Computational Section

To obtain a better understanding of the die filling process, the Discrete Element Method (DEM) was used. DEM can provide information such as forces applied to individual

particles at a micro scale. A manual selection allows tracking a group of particles. This type of selection was used to define 1000 mg of particles as the tracer (Fig. 3.2). The RTD analysis was done in order to determine the mean residence time those particles spend in the system (feed frame) and to study the force applied to the particles. The simulations were run at the same operating conditions of the four experiments developed in the design of experiments.

The first step for RTD measurements using DEM was to determine the $F(t)$ function which was defined as the ratio of the mass of the tracer that has left the system at certain time t and the initial mass of the tracer inside the system at time t_0 . Then, this quantity was plotted against time (seconds) to obtain cumulative distribution $F(t)$ versus time. Finally, a plot of $1-F(t)$ versus time was constructed, and the area under the curve of this graph was determined to obtain the mean residence time. The RTD of particles by size ranges was also measured using this methodology.

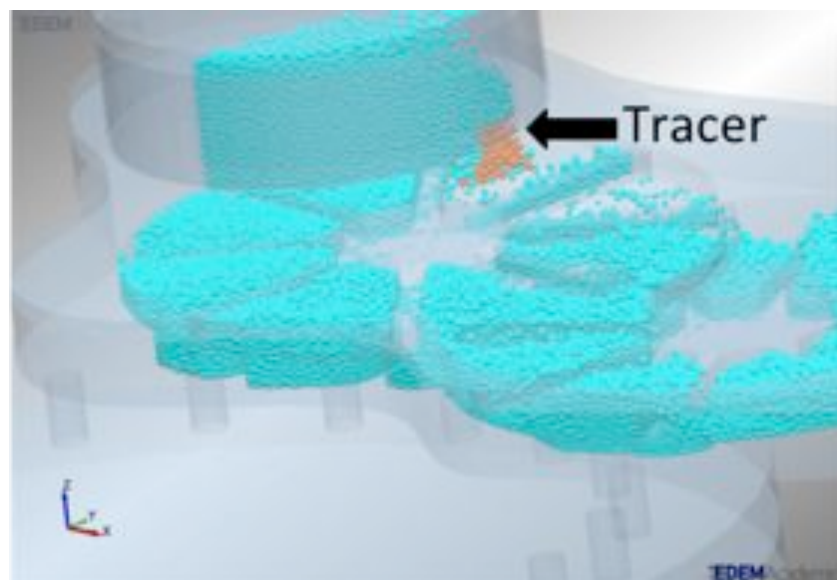


Figure 3.2. Manual Selection of Tracer.

3.3 Results and Discussion

3.3.1 Experimental Results

3.3.1.1 *RTD as function of Operating Conditions*

For clarity purposes the following nomenclature was used: operating conditions 1 was at 72 rpm paddle wheel speed and 57 rpm die disc speed, operating conditions 2 was at 24 rpm paddle wheel speed and 57 rpm die disc speed, operating conditions 3 was at 72 rpm paddle wheel speed and 29 rpm die disc speed and operating conditions 4 was at 24 rpm paddle wheel speed and 29 rpm die disc speed.

Figure 3.3 illustrates the influence of feed frame operating conditions on RTD characteristics, as obtained experimentally. The mean residence time (MRT) for each operating condition is listed in Table 3.1. For the experiment at lower paddle wheel speed (24 rpm) and lower die disk speed (29 rpm), the mean RTD was the highest of all experiments. The lower MRT was observed in the experiment at higher paddle wheel speed (72 rpm) and lower die disk speed (57 rpm). In general, higher paddle wheel speeds lead to lower mean residence time and narrower RTD profiles. When the paddle wheel speed decreases from 72 to 24 rpm, the RTD profiles are wider and the MRT increases.

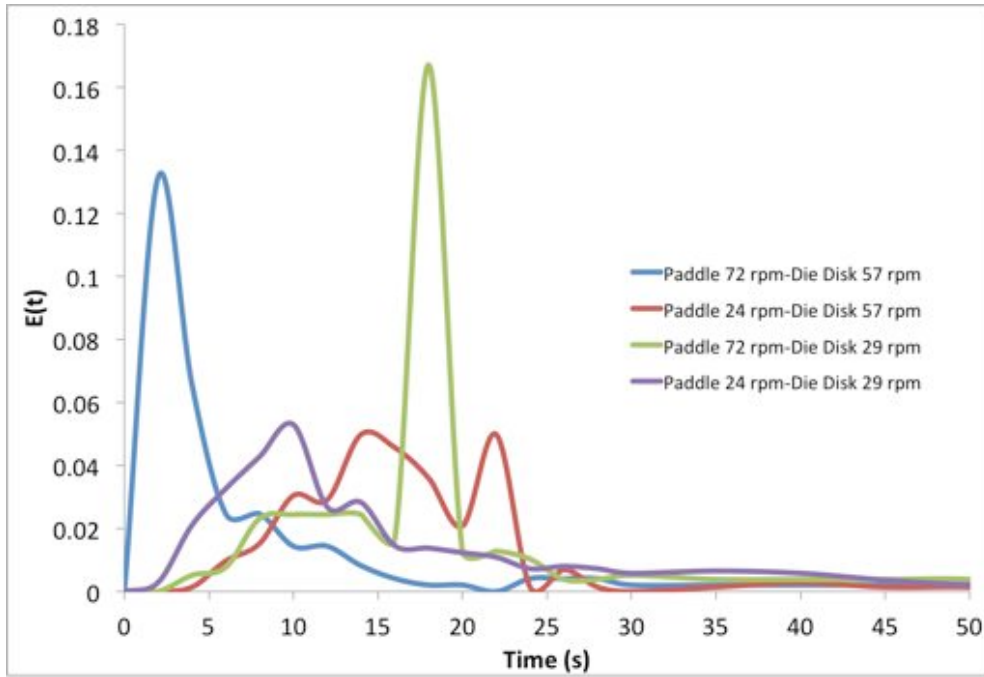


Figure 3.3. E(t) distribution as function of operating conditions.

Table 3.1. RTD as function of operating conditions.

| Operating conditions | | Experimental | | Computational (DEM) | | | |
|----------------------|----------------------------------|--------------|-------------------------|---------------------|---------------|------------------------|-------------------------|
| | | Mean RTD (s) | Number of paddle passes | Mean RTD (s) | Dead Time (s) | Avg. mass in dies (mg) | Number of paddle passes |
| 1 | Paddle 72 rpm Die disk 57 rpm | 29.8 | 348 | 8.05 | 0.55 | 845 | 58 |
| 2 | Paddle 24 rpm Die disk 57 rpm | 48.5 | 155 | 8.54 | 1.17 | 772 | 26 |
| 3 | Paddle 72 rpm Die disk 29 rpm | 33.0 | 317 | 5.92 | 0.39 | 944 | 43 |
| 4 | Paddle 24 rpm Die disk 29 rpm | 51.9 | 166 | 7.50 | 1.28 | 956 | 26 |

3.3.1.2 Shear Strain as a function of System Parameters

The number of paddle passes for each experiment is listed in table 1. It was found that the larger number of paddle passes in the experiments is at higher paddle wheel speed (72 rpm). Even though there are differences in the MRT at the different operating conditions, the paddle wheel speed factor has the greatest effect on the total strain applied to the powder. It is

important to have an estimate of the total strain applied to the particles since it may affect the powder properties (PSD, bulk density) and powder hydrophobicity. There are other factors related to the total strain applied to particles, which are discussed in the computational (DEM) section.

3.3.2 Computational Results

DEM was used to study in detail all the factors that can affect the residence time distribution and the force applied to particles that can ultimately cause particle attrition and powder hydrophobicity.

3.3.2.1 *Particle Trajectories*

A preliminary study was performed using DEM to analyze the trajectories of particles with diameters of 1.5-2.0 mm and 0.1-0.5 mm inside the feed frame to have a better understanding of the RTD. Five big (1.5-2.0 mm) and five small (0.1-0.5 mm) particles were tracked and it was observed that the small particles exit the feed frame faster through zone 1 while big particles stay recirculating around the feed frame for longer (Fig. 3.4). A combination of two factors could affect this phenomenon: particle size segregation (Chapter 2) [2] and the particle size used in the simulations. Since the particles were scaled up and the die diameter was kept equal to the real die disk dimensions, the powder flow of big particles into the die could be limited.

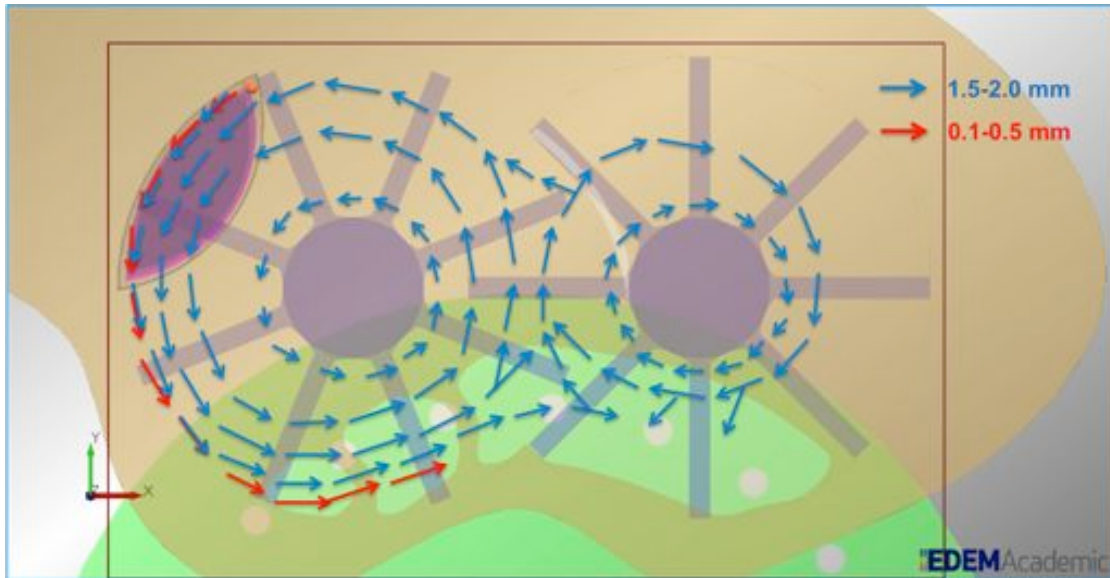


Figure 3.4. Feed Frame trajectory of particles.

3.3.2.2 RTD as function of Operating Conditions

Figure 3.5 shows the DEM simulations RTD profiles at different operating conditions. When comparing the DEM simulations RTD profiles with the experimental RTD profiles, a difference in profile shape can be observed. This is mainly due to the DEM particle shape (spheres), the sampling time step used and the particle properties selected. The sampling time step interval in the experiments went from 2 to 10 seconds while the DEM simulations time step was 0.01 seconds. As the paddle wheel speed increases, the simulations RTD profiles get closer to an ideal CSTR profile with a sharp peak and a tail (Fig. 3.6). The CSTR RTD profile was developed based on the equation of ideal CSTR (eq. 3.2).

$$E(t) = \frac{e^{-t/\tau}}{\tau} \quad (3.2)$$

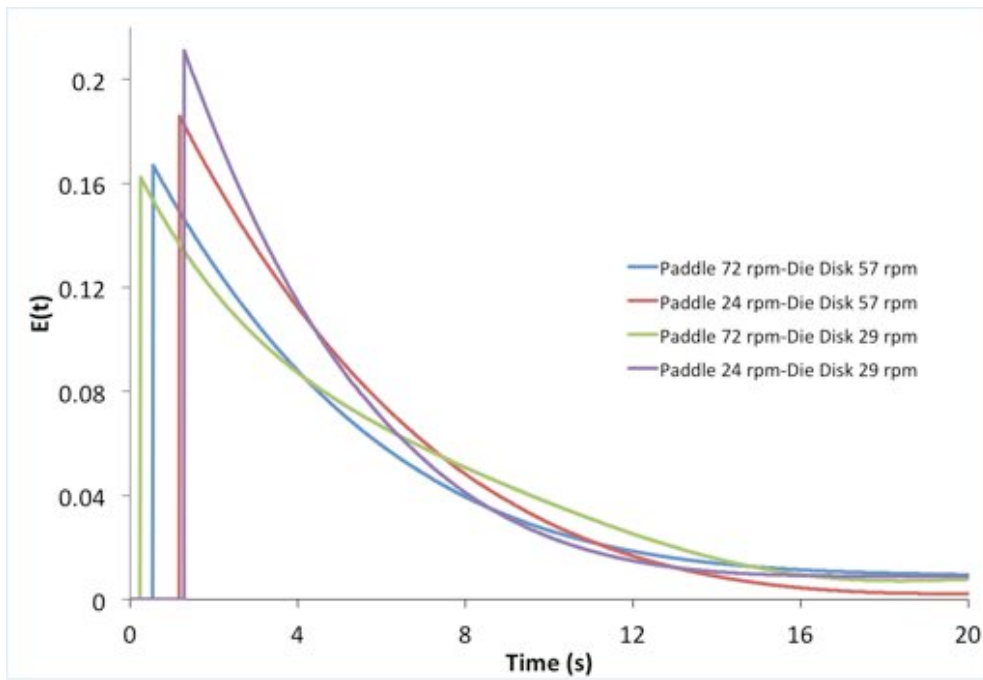


Figure 3.5. $E(t)$ distributions as function of operating conditions for DEM simulations.

The DEM mean residence time (MRT) for each operating condition is listed in Table 3.1. Based on the particle parameters used in the simulations and the particle shape (spheres) used to model the powder, the particles have a higher flowability when compared to the lactose used in the experiments. The tracer size used in the experiments was bigger (5g) than the tracer size used in the simulations (1g). For these reasons the computational (DEM) MRTs are lower in general. Based on the DEM data, the lower MRT was observed in the simulation at higher paddle wheel speed (72 rpm) and lower die disk speed (29 rpm).

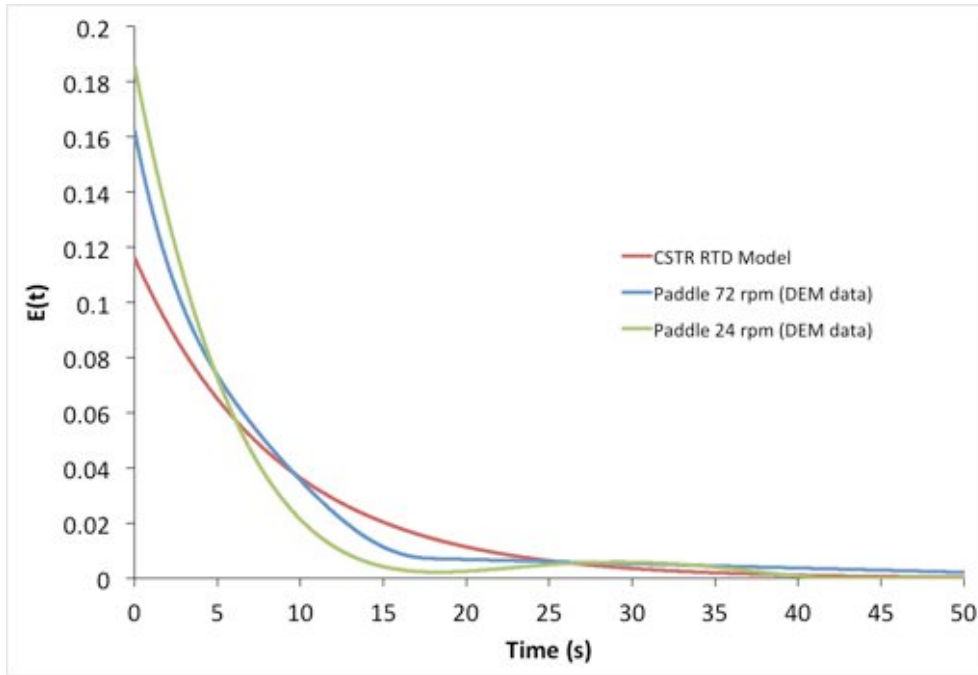


Figure 3.6. CSTR model and Computational RTD profile.

The Manesty Beta Press feed frame has three exits with different sizes and shapes (Fig. 1) [2]. For the simulations at a low die disk speed (29 rpm), dies are almost filled completely in the first two exits (zone 1). The majority of the die weight contribution comes from exit 3 (zone 2) at 57 rpm die disk speed (Chapter 2) [2]. The exit contributions analysis shows that at 57 rpm die disk speed the particle path length of most particles is longer than at 29 rpm, therefore increasing the MRT. In addition, when the die disk speed is increased from 29 to 57 rpm the outlet mass flowrate increases but does not double. The average mass in each die decreases as the die disk speed increases as shown in table 3.1. Even though the average mass that leaves the feed frame at die disk speed of 57 rpm is higher, the MRT increases. Based on the DEM data, this means that the exit contribution factor has a more significant effect on the MRT than the outlet mass flow rate and paddle wheel speed since the lower MRTs are at the lower die disk speed. This effect is mainly due to the DEM particle properties used in the simulations. Therefore, the MRT is not only affected by the operating conditions but also by the feed frame exit contributions (feed frame zones) and the average

mass in the dies for each simulation (outlet mass flowrate).

The time that the first particle takes to leave the feed frame was considered the dead time. The shortest dead time was observed at higher paddle wheel speed. The paddle wheel speed factor has a greater effect on dead time since the simulations at 24 rpm paddle wheel speed are approximately 2 or 3 times the dead time of the simulations at 72 rpm paddle wheel speed.

3.3.2.3 Residence time distribution as a function of particle size

To have a better understanding of the effect of particle size on the RTD, the same tracer used for the simulations was divided into 5 particle size ranges based on approximately the same quantity of particles in each range. The PSD of each tracer was similar with a D50 of 1.40 to 1.55 mm. The D50 of the particles inside the feed frame is 1.50 mm, which is similar to the D50 of the tracers. The RTD was measured for each range. The DEM mean residence time for each simulation and each size range is listed in Table 3.2. In general, it can be observed that bigger particles tend to spend more time in the system than smaller particles. Figure 3.7 shows the DEM simulations RTD profiles of each particle size range for the simulation at 24 rpm paddle wheel speed and 29 rpm die disk speed. The particle size range RTD profiles are also similar to an ideal CSTR profile.

Table 3.2. Mean residence time for different particle diameters.

| Simulation | Particle Diameter Range (mm) | | | | |
|------------|------------------------------|-------------|-------------|-------------|-------------|
| | 0.10 – 1.00 | 1.00 – 1.30 | 1.30 – 1.60 | 1.60 – 2.00 | 2.00 – 2.45 |
| | Mean Residence time (s) | | | | |
| 1 | 4.145 | 4.459 | 6.168 | 7.598 | 11.307 |
| 2 | 7.892 | 7.998 | 7.890 | 8.196 | 12.440 |
| 3 | 2.519 | 4.144 | 4.177 | 5.216 | 8.488 |
| 4 | 5.172 | 7.162 | 6.766 | 10.278 | 10.717 |

A separation between the $E(t)$ curves was observed (Fig. 3.7). This demonstrates segregation by particle size. In chapter 2, a top to bottom particle size segregation inside the feed frame was demonstrated [2]. Table 2 shows another type of segregation in which the smaller particles are leaving the feed frame faster. Although the system is in mass steady state, there is an accumulation of bigger particles inside the feed frame for the first 60 seconds, which is the total time for each simulation. There could be oscillatory particle size segregation, meaning that different particle sizes exit in an alternate manner.

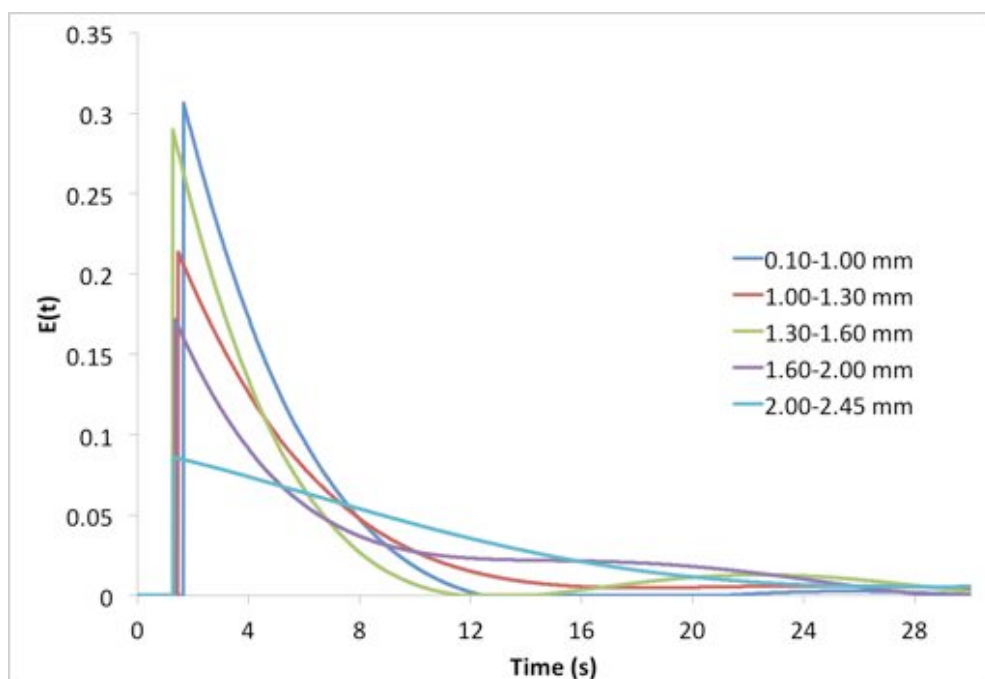


Figure 3.7. $E(t)$ distributions as a function of particle size (24 rpm paddle Wheel-29 rpm die disk speed).

3.3.2.4 Particles in the Vicinity of Feed Frame Paddles

The shear applied by the feed frame paddles can cause powder attrition and powder overlubrication that can modify the powder properties, affecting the final product quality. Therefore, a detailed study of the particles in the vicinity of the feed frame paddles was performed. Particle attrition can be related to the sum of the normal (compressive) and

tangential forces applied to particles. A compressive force analysis was performed in zones 1 and 2 of the feed frame (Fig. 3.1). Figures 3.8 and 3.9 show which particles received a higher compressive force (red ones) and which ones received a lower compressive force (blue ones). Particles receive the majority of the compressive force on the top and bottom of the paddles in zone 1 and only on the bottom in zone 2. This is mainly due to the level of particle confinement in each zone. Particles in zone 1 are more confined since the gap between the top of the paddle and the top of the feed frame is 1 mm while the gap in zone 2 is 7.5 mm. Therefore, particles in zone 2 receive less normal force than particles in zone 1. This means that the level of powder confinement or the gap size between the paddles and the feed frames can have a significant effect on powder attrition.

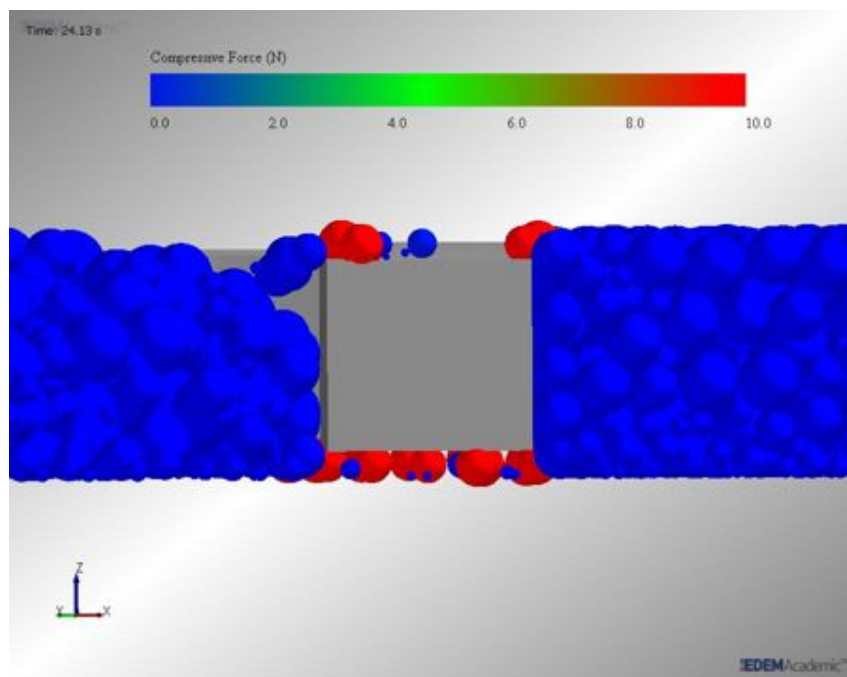


Figure 3.8. Compressive force zone 1 (front view).

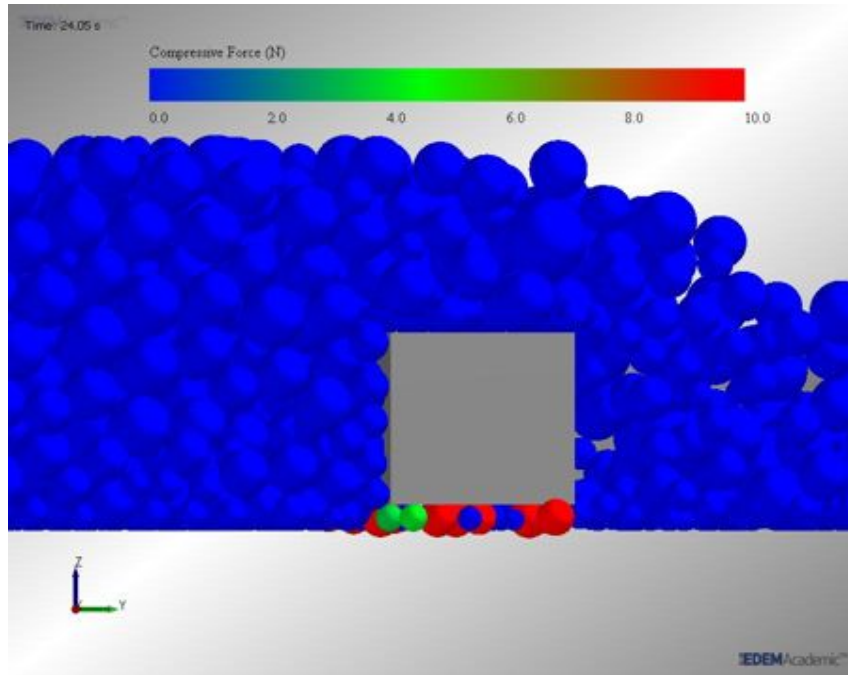


Figure 3.9. Compressive force zone 2 (front view).

A compressive force versus particle diameter analysis was performed in zone 1 for each simulation. As the particle size increases, the greater the compressive force applied to it (Fig. 3.10). The compressive force analysis shows the same behavior for all the operating conditions evaluated (Fig. 3.10). It is important to notice that the particles that receive a significant compressive force are those greater than 1 mm, which is the size of the gap between the top of the paddles and the top of the feed frame. In these simulations, particles were modeled as soft-spheres and not breakable, but in reality the force exerted by the paddles can have an effect on the final particle size distribution. This means that the level of attrition would also depend on the initial particle size distribution: the greater the inlet PSD, the greater the tendency of the particles to break. This corroborates the effect that was observed in a previous investigation [3].

In reality, not many pharmaceutical particles are bigger than 1 mm. Pharmaceutical powders have irregular particle shapes and particles can have a stronger interaction between each other since the number of contacts increases when compared to spheres. Particles could

be on top of each other, creating a group of particles that could have an overall particle size bigger than 1 mm. All these factors can cause particles smaller than 1 mm to receive a significant force that could break them.

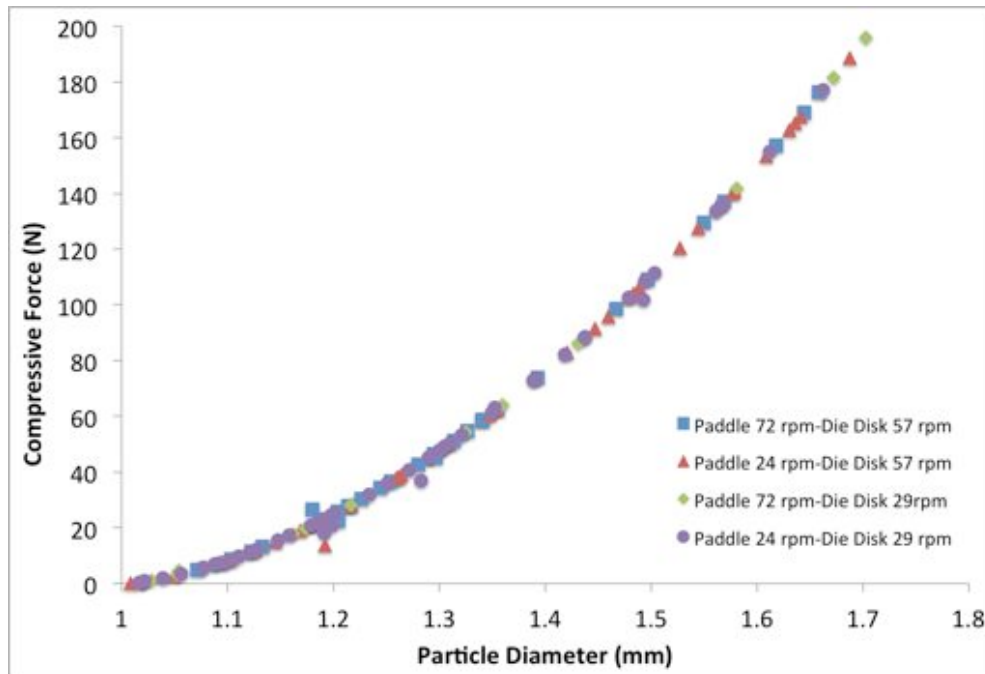


Figure 3.10. Compressive Force as function of particle diameter.

A tangential force versus particle diameter analysis was also performed in zone 1 for each simulation (Fig. 3.11). As the particle size increases, the greater the tangential force applied to it. It can be observed that the slope of the tangential force applied to the particles does change with different paddle wheel speeds. As the paddle wheel speed increases, more tangential force is applied to the particles. However, the tangential force is approximately two orders of magnitude less than the compressive force. Based on the tangential force data, the level of attrition is also affected by the paddle wheel rotational speed. This confirms the effect that was already observed in a previous work [3].

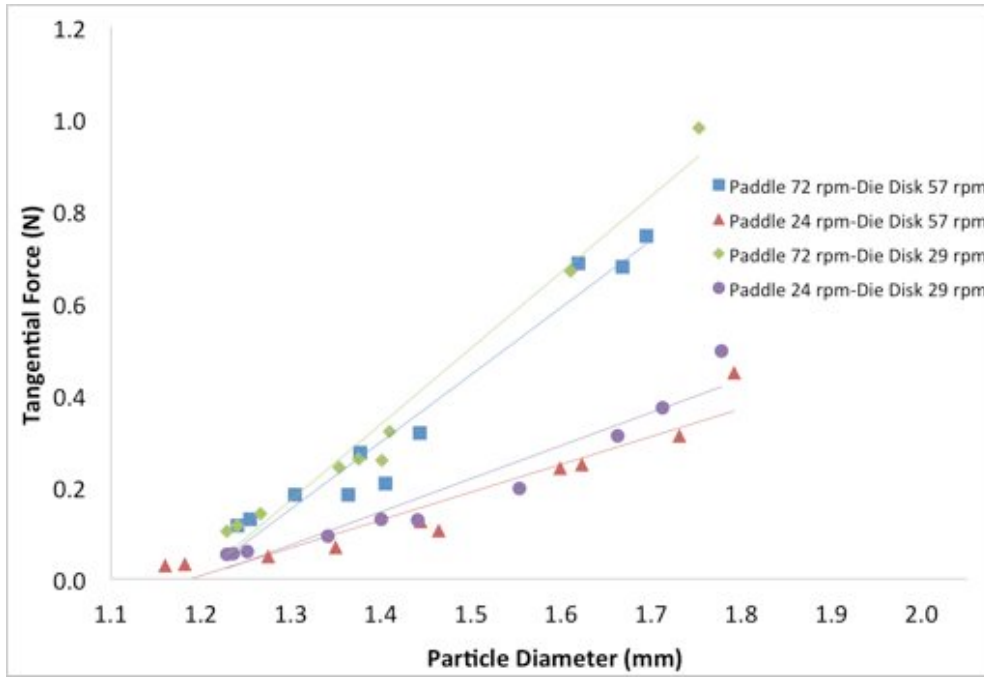


Figure 3.11. Tangential force as function of particle diameter.

3.3.2.5 DEM shear strain as a function of operating parameters

For the DEM data, the number of paddle passes that particles receive inside the feed frame is equal to the paddle wheel rotational speed multiplied by the number of paddles and mean residence time of the particles that receive a significant compressive and tangential force (1-2 mm). This equation (3.1) also means that a particle could receive a significant compressive and tangential force many times due to the number of paddles and MRT. The number of paddle passes for each simulation is listed in table 3.1. It was found that the larger number of paddle passes in the experiments is at higher paddle wheel speed (72 rpm). Similar to the experimental data, the paddle wheel speed factor has the greatest effect on the number of paddle passes.

3.4 Conclusion

In this study, a relationship between residence time distribution (RTD) and forces applied by the feed frame paddles on powder attrition was developed. An analysis with computational data (DEM) and experimental data was performed. The experimental results indicate that higher paddle wheel speeds lead to lower mean residence times, narrower RTD profiles and larger number of paddle passes. The computational (DEM) results show that as the paddle wheel speed increases, the simulations RTD profiles get closer to an ideal CSTR profile with a sharp peak and a tail. The difference between the simulations and experimental RTD profiles and MRTs values was mainly due to the DEM particle shape (spheres), the sampling time step used and the DEM particle properties selected. It was found that operating conditions, feed frame exit contributions and outlet mass flowrate affect the MRT. A DEM residence time distribution analysis by particle size shows that size induced segregation occurs in the system studied where the smaller particles are leaving the feed frame faster.

A detailed study of the particles in the vicinity of the feed frame paddles and the forces applied by it was performed. It was demonstrated using DEM that the level of powder confinement inside the feed frame can have a significant effect on powder attrition. As particle size increases, the compressive and tangential force applied to it increase. The tangential force data shows that the level of attrition is also affected by the paddle wheel speed. This study demonstrated using experimental and numerical data the different factors that can affect the residence time distribution and the force applied to particles that can ultimately cause particle breakage and powder hydrophobicity.

3.5 References

- [1] A.U. Vanarase, F.J. Muzzio, Effect of operating conditions and design parameters in a continuous powder mixer, *Powder Technol.* 208 (2011) 26–36.
- [2] D. Mateo-Ortiz, F.J. Muzzio, R. Méndez, Particle size segregation promoted by powder flow in confined space: The die filling process case, *Powder Technol.* (2014).
- [3] R. Mendez, C. Velazquez, F.J. Muzzio, Effect of feed frame design and operating parameters on powder attrition, particle breakage, and powder properties, *Powder Technol.* 229 (2012) 253–260.

CHAPTER 4

4 MICRODYNAMIC ANALYSIS OF PARTICLE FLOW IN A CONFINED SPACE: THE FEED FRAME CASE

4.1 Summary

The effect of feed frame and paddle wheel design and operating conditions on particle flow is not fully understood. Performance optimization of the tablet press feed frames is an issue of great significance in the pharmaceutical industry. Inadequate die filling in the tablet compressing step can result in rejection of the finished product because of poor quality. Particle flow promoted by the rotating feed frame paddles was investigated using the Discrete Element Method (DEM). Most feed frames have two or more compartments, which complicate powder flow and makes it difficult to understand powder phenomena inside feed frames. Therefore, a new feed frame was built in AutoCAD® based on a single paddle wheel (single compartment) to simplify and to have a better understanding of particle flow inside feed frames. A factorial design was developed, which involves 3 factors, each at 2 levels, for a total of 8 simulations. The factors were the paddle wheel rotational speed (20 and 60 rpm), the number of paddles (6 and 14 paddles) and the paddle height (4.5 and 6.5 mm). A single material with monosized spherical particles was investigated. Results show that the faster the paddle wheel speed, the lower the relative standard deviation (RSD) of the die weight. The number of paddles was also demonstrated to be an important factor on decreasing the die weight variability. It was found that the further the particles are from the paddle, the less the force acting on particles. The paddle force model was able to predict the total force applied to particles based on the feed frame design (number of paddles and paddle height) and particle bed density. Besides the force of gravity, the force applied by the paddles also induces powder flow into the dies. These findings can lead to changes in feed frame design (number

of paddles, paddle height, level of confinement and operating conditions) to avoid high die weight variability and improve tablet quality.

4.2 Paddle Force Model Development

The force exerted by the paddle to the powder bed is the driver for this dynamic system. Therefore, to define and better understand the force applied on powders by paddles, a force integration approach was used. For the purpose of modeling the powder bed is treated as a horizontal annulus section. Another assumption is that the powder acts mostly as a continuum. This means that the model does not take into account particle-particle forces. The force applied by the paddles can be calculated using Newton's second law:

$$F_{paddle} = ma = \rho Va \quad (4.1)$$

Since the powder bed is rotating, the centripetal acceleration was used:

$$a = r\omega^2 \quad (4.2)$$

Therefore:

$$F_{paddle} = \rho Vr\omega^2 \quad (4.3)$$

In equation 4.1, F_{paddle} is the force acting on the powder, the mass of the volume element is m , centripetal acceleration is a , the density of the powder bed is ρ , the volume of the element is V , the radius is r , and the angular velocity is ω . The volume of the element is based on the annulus area times the powder bed height (Fig. 4.1).

$$\text{section area of annulus} = A = \frac{\theta}{2}(R^2 + r^2) \quad (4.4)$$

$$\text{powder bed volume} = V = \frac{\theta}{2}(R^2 + r^2)h \quad (4.5)$$

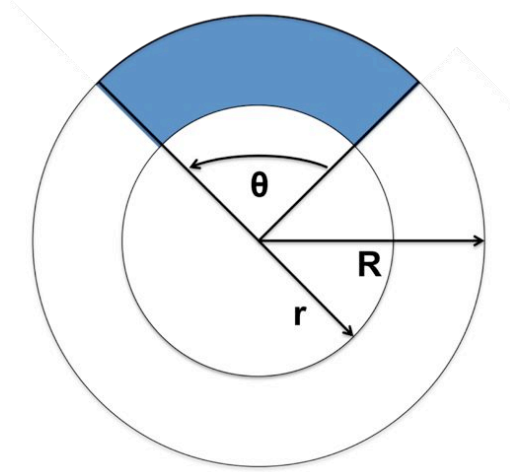


Figure 4.1. Section area of annulus.

and using a mean radius:

$$\bar{r} = \frac{R+r}{2} \quad (4.6)$$

The powder density at θ_{\min} is greater than the density at θ_{\max} since the forces at that point are higher creating a more compacted environment. That density could be close to the tap density. The density at θ_{\max} could also be related to the bulk density since the forces at that point are at the lowest. This means that the powder density is function of the angular distance.

Therefore the powder bed density can be computed as:

$$\bar{\rho} = \frac{\rho_{\theta_{\max}} + \rho_{\theta_{\min}}}{2} \quad (4.7)$$

Therefore:

$$F_{paddle} = \bar{\rho} \frac{\theta}{2} (R^2 + r^2) h \bar{r} \omega^2 \quad (4.8)$$

The force applied by the paddles in a cross section area can be computed as (Fig. 4.2):

$$dF_{paddle} = \frac{\bar{\rho}h\bar{r}\omega^2}{2}(R^2 + r^2)d\theta \quad (4.9)$$

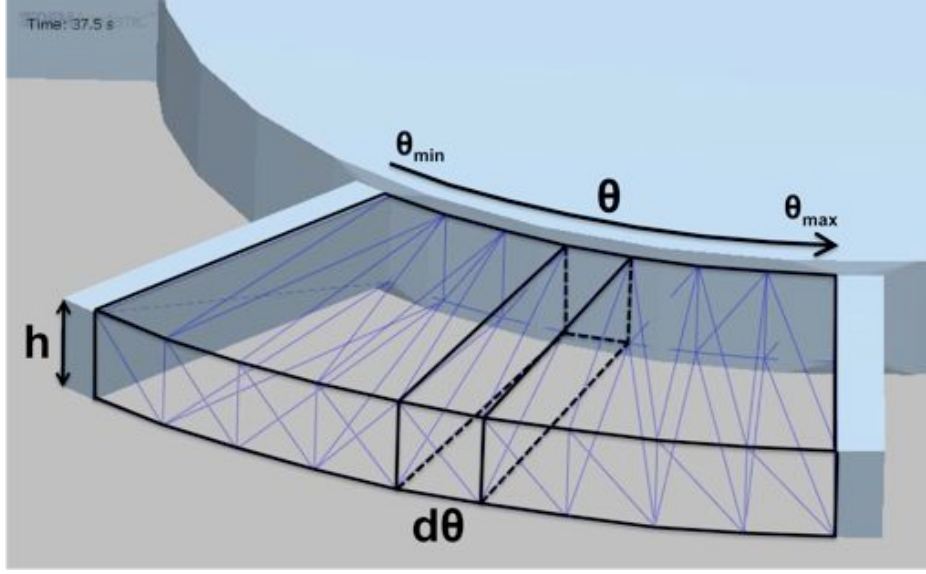


Figure 4.2. Differential volume element of an annulus section.

Integrating these forces from F_{max} to F_{min} :

$$\int_{F_{min}}^{F_{max}} dF_{paddle} = \int_{\theta_{max}}^{\theta_{min}} \frac{\bar{\rho}h\bar{r}\omega^2}{2}(R^2 + r^2)d\theta \quad (4.10)$$

Therefore, a model, which describes the force exerted by the feed frame paddles, is proposed as follow:

$$F_{paddle} = \frac{\bar{\rho}h\bar{r}\omega^2}{2}(R^2 + r^2)(\theta_{min} - \theta_{max}) \quad (4.11)$$

The difference between θ_{min} and θ_{max} changes with the number of paddles.

4.3 Materials and Methods

The discrete element method (DEM) was used to have a better understanding of the particle flow inside the feed frame. DEM offers advantages such as information at a particle

diameter length scale (e.g. inter particle forces, particle orientation). The EDEM software was used to perform all the simulations. The Hertz-Mindlin (no slip) contact model was used to describe how elements (particles, geometries) behave when they come into contact with each other. This is the default model used in EDEM due to its accurate and efficient force calculation. A cohesion model was used for all the simulations. This model modifies the Hertz-Mindlin model by adding a normal cohesion force. This force takes the form: $F = kA$, where A is the contact area and k is a cohesion energy density with units Jm^3 .

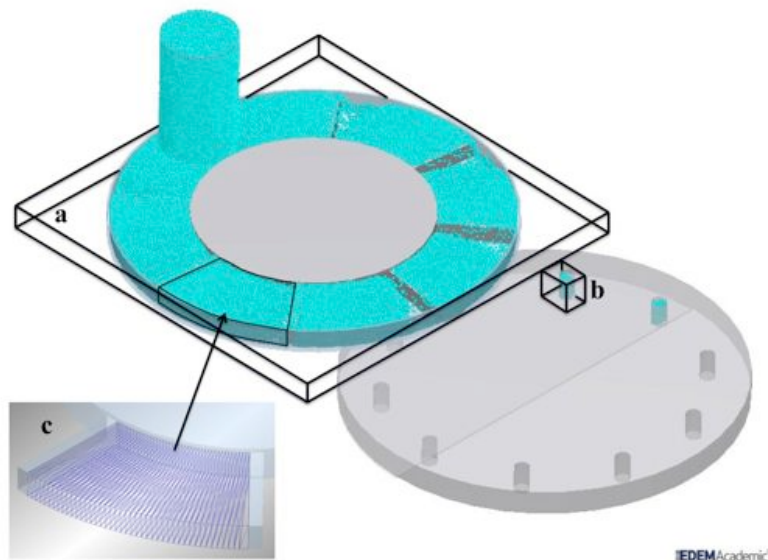


Figure 4.3. Feed Frame (a), die (b), particle between paddles (c).

The simulated system was first built in AutoCAD®. Then, the drawing was imported to EDEM (Fig. 4.3). The feed frame has one paddle wheel, which rotates counter-clockwise while the die disk rotates clockwise. A diagram with the feed frame dimensions is depicted in figure 4.4. The feed frame hopper is cylindrical with a diameter and height of 30 mm and 50 mm, respectively. The paddles are 6.5 and 4.5 mm in height with a thickness of 3.25 mm. Between the bottom of the paddles and the lower part of the feed frame, the gap is 1 mm (Fig.

4.5). The die disk consists of 10 dies and the diameter and thickness are 6 mm and 20 mm respectively, as illustrated in Fig. 4.4. The die disk moves below the feed frame and each die passes across one exit. Below the rotating disk, a lid closes the holes for half of their rotation to provide time for the dies to be filled.

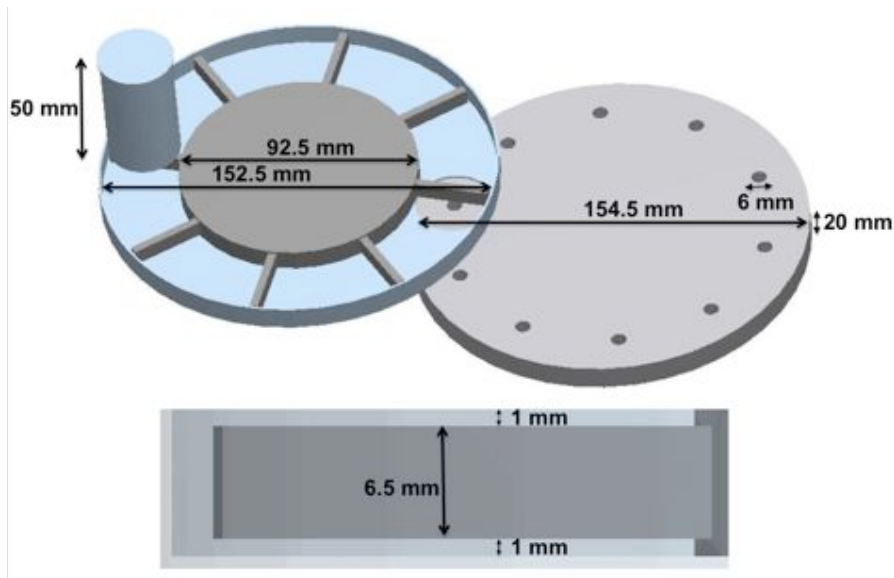


Figure 4.4. Feed frame dimensions.

There are various simple techniques used to select the simulation parameters such as: inclination [1,2], swing-arm [1,2] and angle of repose [1–5] tests. These are used to select the input parameters values of the particle-particle and particle-wall interactions in the simulations. For pharmaceutical powders, the angle of repose test is one of the most common techniques used for parameter calibration since it is a simple way to see the level of flowability of the material. Recommendations from the EDEM technical support team were also used for the initial parameters values for the angle of repose test. An angle of 32° was achieved (fig. 4.5), which is similar to a typical angle of repose for lactose (31-34 degrees). Therefore, the particles used in this study have flowability similar to lactose. In most cases, spherical systems are unstable and tend to produce a small angle of repose. This could lead to overestimation of the capacity of the material to flow. However, high friction values were

used to achieve an angle of repose similar to lactose. The parameters used in the simulations are presented in Table 4.1. Our computational power and the gap size between the paddles and the feed frame were also taken into consideration for the selection of the particle shape and size. These simulation parameters values describe the particle properties affecting significantly the results.

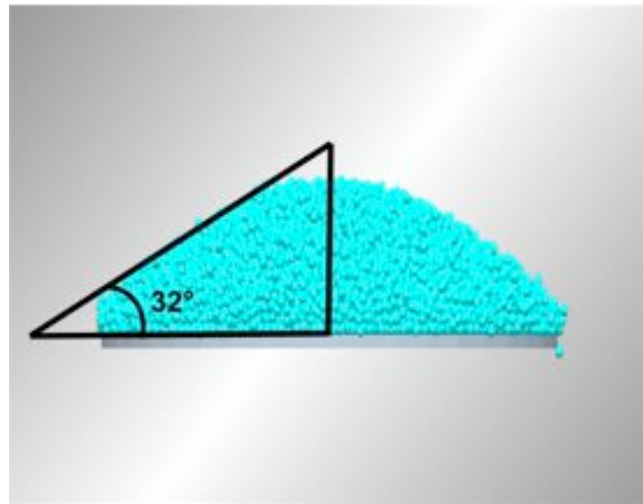


Figure 4.5. Angle of repose.

A factorial design was developed, which involves 3 factors, each at 2 levels, for a total of 8 simulations. The factors were the paddle wheel rotational speed (20 and 60 rpm), the number of paddles (6 and 14 paddles) and the paddle height (4.5 and 6.5 mm). These operating and design values were selected based on typical tablet press operation speeds and feed frame designs used in the pharmaceutical industry. Three more simulations were developed to have a better understanding of the number of paddles (6, 11 and 16 paddles). A single material with monosized spherical particles was investigated.

Selections were created at different locations of the feed frame to allow data to be extracted from a particular area in the domain. The particle mass inside the feed frame (mass hold-up) was obtained analyzing a rectangular selection shown in figure 4.3a. The mass was

analyzed every 0.3 s to verify when the system reached a mass steady state. The mass inside each die was obtained analyzing the selection shown in figure 4.3b. A die was analyzed approximately every half second after the simulation reached mass steady state. The relative standard deviation of the die weight was calculated for each simulation.

Table 4.1. Input parameters used to develop the simulations.

| Parameter | Value | Reference |
|---|----------------------|----------------------|
| Average particle diameter (mm) | 0.96 | - |
| Particle Poisson's ratio | 0.25 | lactose |
| Particle shear modulus (Pa) | 1×10^6 | lactose |
| Particle density (g/cm ³) | 1.54 | lactose |
| Geometry Poisson's ratio | 0.27 | stainless steel |
| Geometry shear modulus (Pa) | 7.8×10^{10} | stainless steel |
| Geometry density (g/cm ³) | 8 | stainless steel |
| Particle–particle restitution coefficient | 0.1 | angle of repose test |
| Particle–particle coefficient static friction | 1.2 | angle of repose test |
| Particle–particle coefficient rolling friction | 0.2 | angle of repose test |
| Particle–geometry restitution coefficient | 0.1 | angle of repose test |
| Particle–geometry coefficient static friction | 1 | angle of repose test |
| Particle–geometry coefficient rolling friction | 0.15 | angle of repose test |
| Cohesion particle-particle (Jm ³) | 5000 | angle of repose test |
| Cohesion particle-paddles (Jm ³) | 2500 | angle of repose test |
| Cohesion particle-Feed Frame walls (Jm ³) | 2500 | angle of repose test |

4.4 Results and Discussion

4.4.1 Feed Frame Mass Hold-up

The time when the feed frame reaches a mass steady state for each simulation is shown in table 4.2. For all the simulations, the mass hold-up reached mass steady state after approximately 35 s. The simulations at a higher paddle wheel speed (60 rpm) reached a steady state faster, demonstrating that the paddle wheel speed factor has a significant effect. However, the paddle height and the number of paddles do not have a significant effect on the time to reach steady state. The simulations at 60 rpm paddle wheel speed reached mass

steady state approximately 4 seconds faster than the simulations at 20 rpm. It was demonstrated in a previous work [6] that the mass hold-up inside the feed frame is mainly influenced by the die disk speed factor because it controlled the outlet flowrate. Since the die disk speed was constant for all simulations, the mass hold-up for each simulation was approximately the same, changing only due to the space that the number of paddles takes.

Table 4.2. Feed frame mass hold-up, die weight variability and force results

| Simulation | Time for Steady State (s) | Die weight Variability (RSD) | Die Weight Average (mg) | Paddle Force Model (N) | DEM Force (N) |
|-------------------------------------|---------------------------|------------------------------|-------------------------|------------------------|---------------|
| 6 Paddles_6.5 Paddle height_20 RPM | 35.5 | 21.3 | 178 | 0.0167 | 0.0197 |
| 8 Paddles_4.5 Paddle height_20 RPM | 35.0 | 15.1 | 177 | 0.0096 | 0.0083 |
| 8 Paddles_4.5 Paddle height_60 RPM | 30.0 | 10.5 | 202 | 0.0762 | 0.0129 |
| 8 Paddles_6.5 Paddle height_20 RPM | 33.3 | 20.9 | 173 | 0.0137 | 0.0124 |
| 8 Paddles_6.5 Paddle height_60 RPM | 29.0 | 12.0 | 209 | 0.0965 | 0.0169 |
| 11 Paddles_6.5 Paddle height_20 RPM | 33.5 | 13.4 | 170 | 0.0106 | 0.0079 |
| 14 Paddles_4.5 Paddle height_20 RPM | 34.0 | 8.7 | 171 | 0.0057 | 0.0051 |
| 14 Paddles_4.5 Paddle height_60 RPM | 30.3 | 3.1 | 206 | 0.0446 | 0.0051 |
| 14 Paddles_6.5 Paddle height_20 RPM | 34.5 | 9.8 | 160 | 0.0081 | 0.0062 |
| 14 Paddles_6.5 Paddle height_60 RPM | 29.5 | 4.6 | 207 | 0.0655 | 0.0055 |
| 16 Paddles_6.5 Paddle height_20 RPM | 33.5 | 8.1 | 169 | 0.0069 | 0.0048 |

4.4.2 Die Weight Variability

It is important to have an understanding of how to reduce the die weight variability to offer people the best quality product. The die weight variability (RSD) for each simulation is shown in table 4.2. It was found that the faster the paddle wheel speed, the lower the relative standard deviation (RSD) of the die weight. This is mainly due to the fact that as the paddle wheel speed increases, the material on top of the feed frame exit gets refilled faster. When more material is on top of the feed frame exit, the powder weight facilitates the die fill.

It was also demonstrated that the feed frames with a paddle height of 6.5 mm have higher RSD values than the ones at paddle height of 4.5 mm. Figure 4.6a shows a feed frame of 8

paddles with 6.5 mm height in which an empty space can be observed right behind the moving paddle. For clarity purposes, the powder between paddles is called a zone. The particle flow from zone to zone is limited by the paddle height and the space between the top of the paddle and the top of the feed frame, creating an empty or low quantity of particles region compared to the rest of the powder bed behind the moving paddle. This phenomenon affects negatively the die weight variability. The empty space is more noticeable at 60 rpm than at 20 rpm. Particle movement from zone to zone can also produce a back mixing effect. When paddle height is decreased from 6.5 to 4.5 mm the particle flow from zone to zone increases, refilling more the empty space behind the moving paddle (Fig. 4.6b). This explains the lower RSD of the die weight for the simulations with paddles of 4.5 mm height.

The number of paddles also affects significantly the die weight variability. As the number of paddles increases, the die weight variability decreases (table 4.2). Decreasing the number of paddles, increases the distance between paddles; therefore the empty space behind the moving blade increases. With 14 paddles the empty space was no longer noticed (Fig. 4.6c). Additional explanation of the number of paddles effect on die weight variability will be given in the following sections.

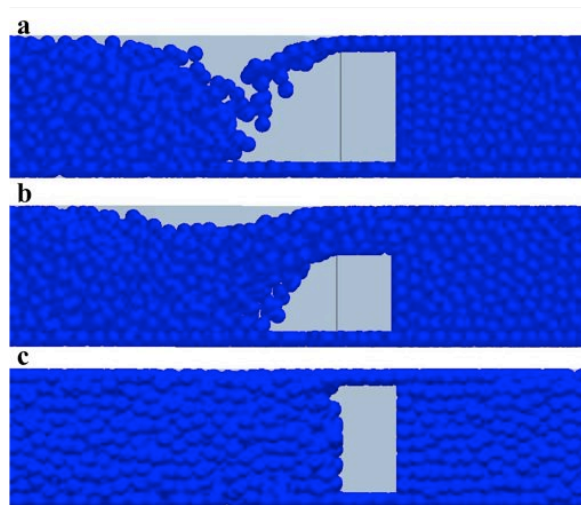


Figure 4.6. Feed Frame at (a) 60 rpm with 8 paddles 6.5 mm height, (b) 8 paddles 4.5 mm height, (c) 14 paddles 6.5 mm height.

4.4.3 Velocity Profile

The new feed frame design developed for the simulations has a larger paddle wheel diameter than the Manesty Beta Press [6], mainly to reduce the velocity difference between particles closer to the axis of rotation and the ones that are farther. The velocity profiles at each paddle wheel speed, 20 rpm and 60 rpm are depicted in figures 4.7a and 4.7b respectively, where colors indicate the particle speed: blue particles ranging from 0.00 to 16.67 cm/s, green particles from 16.67 to 33.33 cm/s and red particles from 33.33 to 50.00 cm/s. In general, at 20 rpm paddle wheel speed the particles are moving slower with respect to 60 rpm. Particles farther from the axis of rotation move at a higher tangential velocity than particles closer to it.

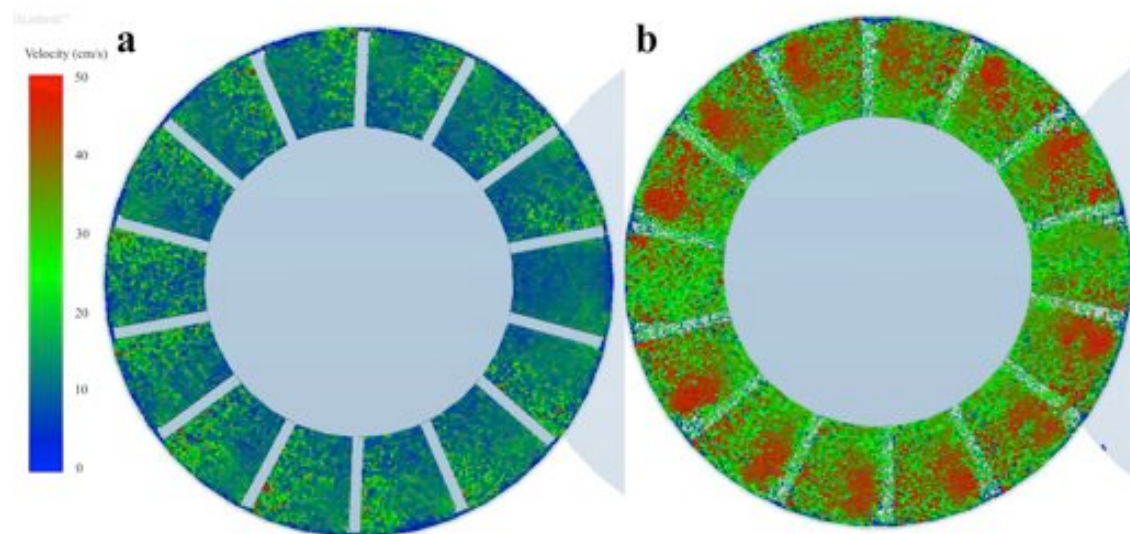


Figure 4.7. Velocity Profile (a) 20 rpm, (b) 60 rpm.

4.4.4 Powder Flow Behavior

Bridgwater [7] has demonstrated that particles rise to form a heap on top of a blade. This

pattern has been well described by Stewart and Bridgwater [8]. Figure 4.6 shows that this heap does not form due to the feed frame confinement.

Changes in paddle height can be related to the depth of immersion previously described by Bagster and Bridgwater [7,8]. The height of the blade is B and the vertical distance from the undisturbed free surface to the lower horizontal edge is Z , a dimensionless group is then defined as Z/B . Bagster and Bridgwater observed differences in flow pattern for different immersion values. Some differences were observed due to changes in the immersion (Z/B) cases considered in this work. The 6.5 mm and 4.5 mm paddles have immersion values (Z/B) of 1.15 and 1.67 respectively. When analyzing a different feed frame described in a previous work [6], greater changes in flow pattern were observed due to a deeper immersion. The Manesty feed frame paddles have the same height (6.5 mm) but the values of Z are 1.15 for the paddles in zone 1 and 2.15 for the paddles in zone 2. Significant differences in particle flow can be observed when comparing particle flow in zone 1 (Fig. 4.8a) and in zone 2 due to differences in immersion values (Fig. 4.8b).

In a previous study [9] a powder wave behavior was observed experimentally inside the feed frame. This behavior was demonstrated to have a significant effect on NIR spectra and prediction. The paddle movement also promotes this behavior. An analysis inside the feed frame designed for this study revealed that the powder wave behavior was only observed in two simulations: 8 paddles, 60 rpm, 6.5 mm paddle height and 8 paddles, 60 rpm, 4.5 mm paddle height (Fig. 4.6a and 4.6b). A more significant wave is observed in figure 4.6b because the particle flow from zone to zone is limited by the paddle height. This means that the paddle wheel rotational speed and the number of paddles also have a significant effect on this behavior. The powder wave behavior can be observed in the Manesty Beta Press Feed Frame but only in zone 2 (Fig. 4.8b). This behavior is also related to the paddle immersion:

greater immersion values tend to produce powder waves.

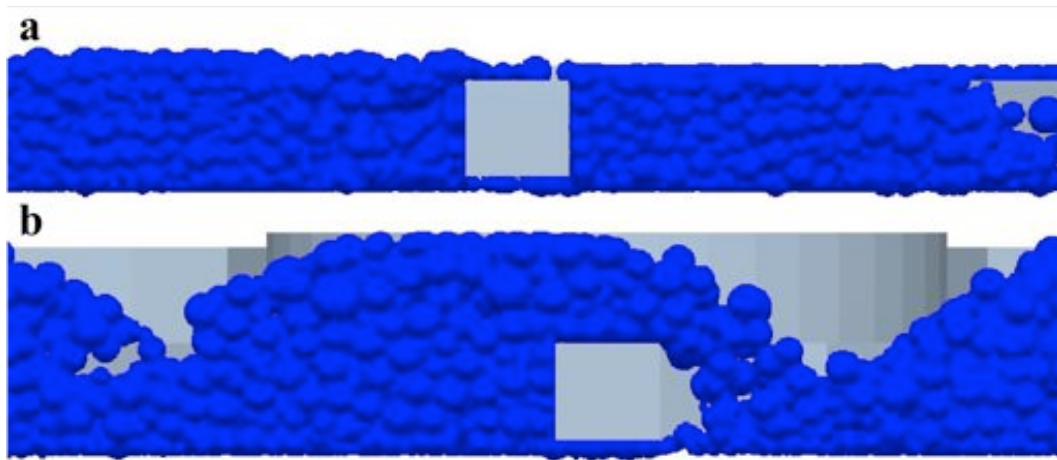


Figure 4.8. Particle flow behavior in Manesty Beta Press feed frame (a) paddle wheel zone 1 (b) paddle wheel zone 2.

4.4.5 Force Distribution

Figures 4.9a and 4.9b show a top and side view of the total force distribution, respectively. The total force is the vectorial summation of the contact forces (normal and tangential forces) acting on the particles per time step (resultant unbalanced force). Gravity also affects the particle motion. The further the particles are from the paddle, the less the force acting on particles (Fig. 4.9b). The energy provided by the paddles is dissipated with distance due to particle collisions, particle-particle and particle-wall frictions. As explained in section 4.4.3, particles farther from the axis of rotation move at a higher tangential velocity than particles closer to it. Therefore, as the radial distance increases, the force also increases (Fig. 4.9a).

Another work [10] demonstrated that particles on the top of the paddle have minimum contact forces. However, due to the confined flow, there is particle-wall friction not only at the bottom but also at the top of the feed frame. Figure 4.9b was divided into three layers to analyze the vertical force distribution. The higher total force occurs at the bottom layer mainly due to gravity and it decreases gradually from the bottom to the top. There is a

decrease of approximately 4% in the middle layer and a decrease of 6% in the top layer.

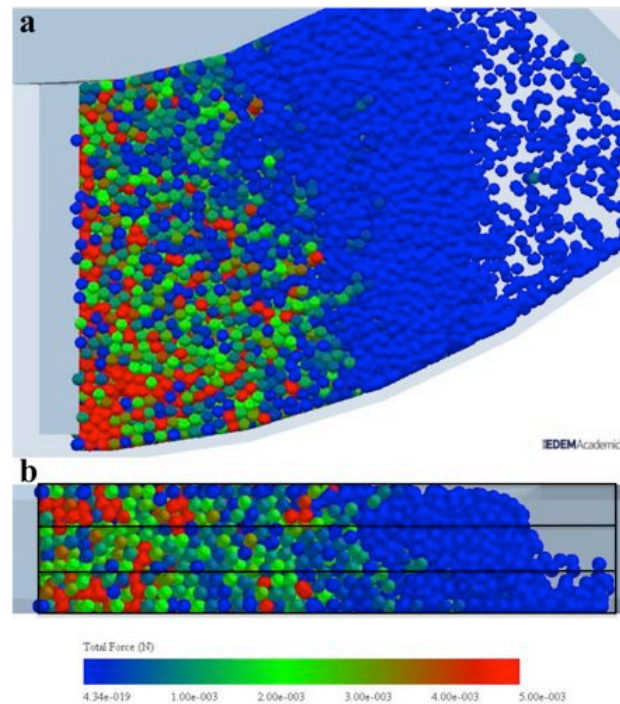


Figure 4.9. Force distribution, (a) top view, (b) side view.

The total force as function of angular distance (radians) was obtained by analyzing the selection shown in figure 4.3c. Each differential element is in cylindrical coordinates and is constant for all simulations, which is equal to 1 degree or 0.017 radians. Figure 4.10 shows the average total force as function of radians for different number of paddles. It can be observed that as the number of paddles is decreased, the initial force is higher, and as the angular distance increases, the force decreases approximately at the same rate until achieving an almost zero force. Figure 4.11 shows the average total force as a function of paddle wheel speed (rpm) for the simulations with 8 paddles. At 60 rpm the initial force is greater than at 20 rpm but it decreases faster than at 20 rpm. A similar behavior was observed for the simulations with 14 paddles.

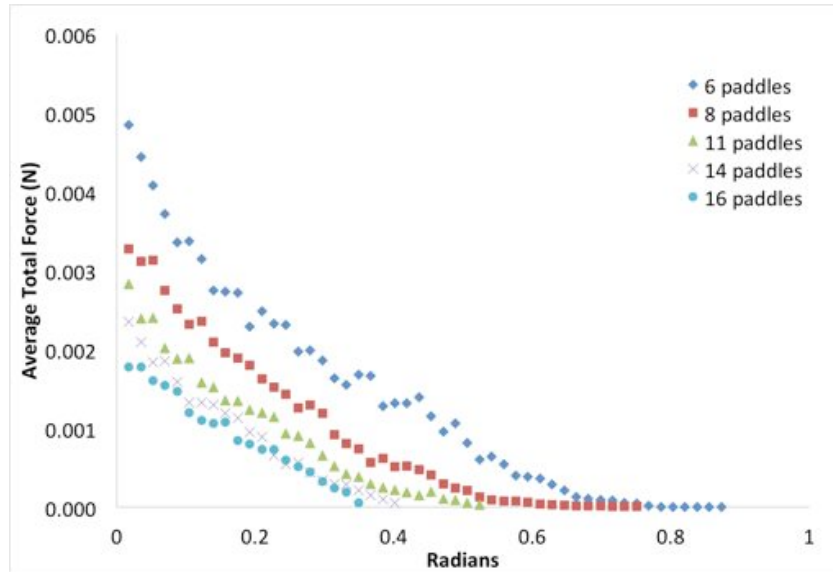


Figure 4.10. Average total force as function of angular distance for the simulations with different number of paddles.

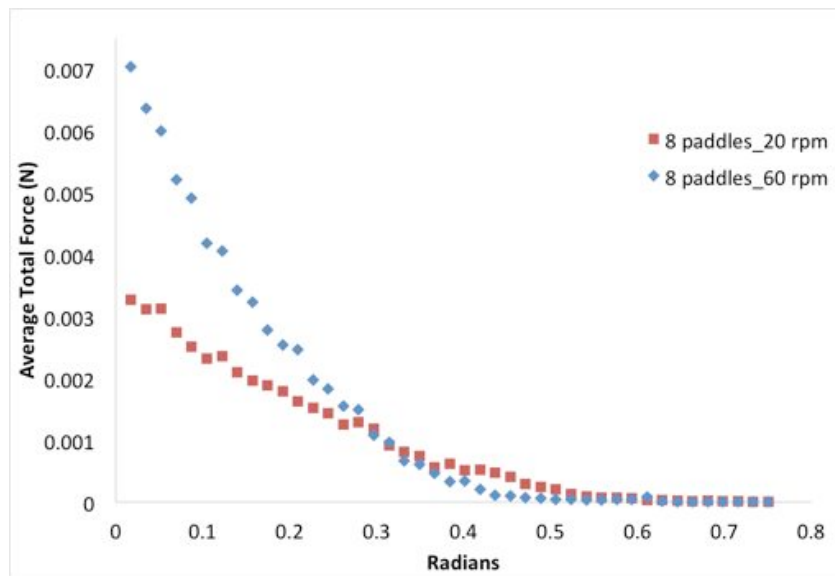


Figure 4.11. Average total force as function of angular distance for the simulations with different paddle wheel speed.

4.4.6 Velocity Vector Analysis

When the paddles apply force to the powder, it expands (powder dilation), thereby causing movement of the powder. This can be explained using the particle velocity vectors shown in figure 4.12 where the colors represent the total force magnitude, similar to figure

4.9b. When higher forces are applied, turbulent particle flow is observed near the paddle (segment a) and it decreases as the particles are farther from the paddle and energy is dissipated (segments b and c).

Figure 4.12 shows that at the end of segment c, particles have mostly a downward direction. This is because particles farther from the paddle receive less force and gravity starts having a greater effect on their direction. When the number of paddles is increased (reduction in space between paddles), this effect is no longer observed. The further the particles are from the paddle, the less confined they are. Therefore, the particle packing or particle bed density is greater closer to the paddle. Figure 4.12 also explains this phenomenon since the particle quantity decreases from segment a to segment c.

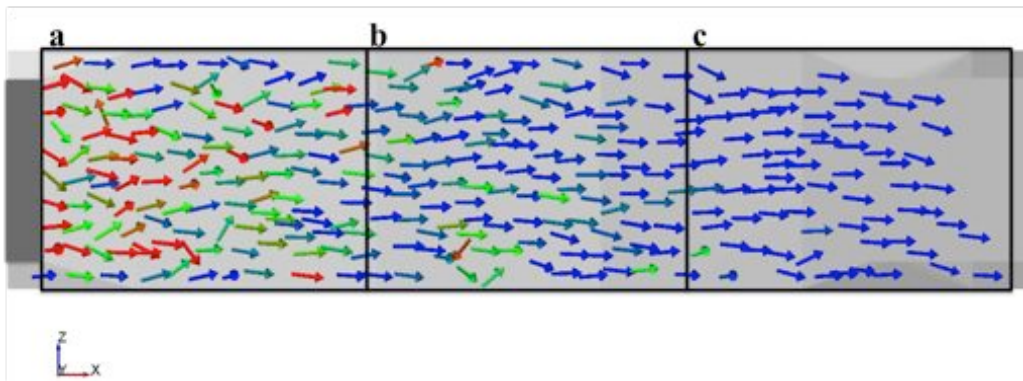


Figure 4.12. Velocity vectors in the vicinity of the paddle.

Besides the force of gravity, powder flow into the dies is also induced by the force applied by paddles, which has a component in the Z direction (upward and downward) as shown in figure 4.13. Increasing the paddle wheel speed from 20 to 60 rpm increases the velocity vectors magnitude by approximately 50%. Therefore, the average mass in each die increases for the simulations at 60 rpm (table 4.2). The maximum mass that can fit in a die is approximately 210 mg but at lower paddle wheel speed the dies are filled with less than 180 mg. It was demonstrated in section 4.4.2 that decreasing the number of paddles increases the

die weight variability. A decrease in the number of paddles represents an increment in distance between paddles. As shown in figure 4.10, as the number of paddles decreases, the difference between the initial force and the force at the end increases. This causes a larger difference between the velocity vectors direction and magnitude in the space between paddles, resulting in an increase in die weight variability.

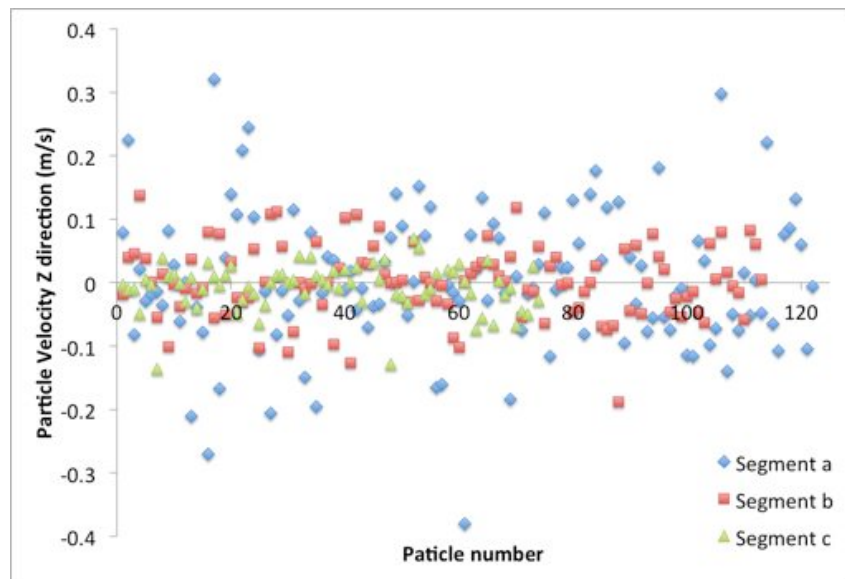


Figure 4.13. Particle Velocity for the Z direction.

4.5 Conclusion

The aim of this study was to provide a fundamental and practical understanding of particle microdynamics in a confined space while external forces are applied. Results show that the faster the paddle wheel speed, the lower the relative standard deviation (RSD) of the die weight. The number of paddles was also demonstrated to be an important factor on decreasing the die weight variability.

The translational motion of particles is controlled mainly by gravity, tangential and normal forces. The total force was examined as a function of the distance from the paddle. It was found that the further the particles are from the paddle, the less the force acting on the

particles. The energy provided by the paddles is dissipated with distance due to particle collisions, particle-particle and particle-wall frictions. As the radial distance increases, the force also increases. The paddle force model was able to predict the total force applied to particles based on the feed frame design (number of paddles and paddle height) and particle bed density. Since the total force is the resultant force and the model only describes the force applied by the paddle, there are some discrepancies between the model and the DEM data. A force balance analysis in a unit volume of powder is needed to take into account all the forces that act on the powder such as gravity and frictional forces. This is needed to model the resultant force properly, which ultimately described how the powder is flowing.

Besides the force of gravity, the force applied by the paddles also induces powder flow into the dies. Therefore the paddle wheel speed increases the amount of particles in each die. As the number of paddles is decreased, the difference between the initial force and the force at the end increases. The vectors analysis shows that as the distance between paddles increases (decreasing number of paddles), it causes a larger difference between velocity vectors direction and magnitude in the space between paddles. This affects negatively the die weight variability.

These results can create awareness in the pharmaceutical industry to avoid problems during the die filling process such as high tablet weight variability. These findings should lead to changes in feed frame design (number of paddles, paddle height, level of confinement and operating conditions) to avoid high die weight variability and improve tablet quality.

4.6 References

- [1] A. Grima, P. Wypych, On Improving the Calibration and Validation of Computer Simulations for Bulk Materials Handling Systems, *Aust. Bulk Handl. Rev.* (2009) 84–91.

- [2] A. Grima, P. Wypych, Discrete element simulation of a conveyor impact-plate transfer: calibration, validation and scale-up, *Aust. Bulk Handl. Rev.* (2010) 64–72.
- [3] Y.C. Zhou, B.D. Wright, R.Y. Yang, B.H. Xu, A.B. Yu, Rolling friction in the dynamic simulation of sandpile formation, *Phys. A Stat. Mech. Its Appl.* 269 (1999) 536–553.
- [4] J.M. Boac, M.E. Casada, R.G. Maghirang, Material and Interaction Properties of Selected Grains and Oilseeds for Modeling Discrete Particles, *Am. Soc. Agric. Biol. Eng.* 53 (2010) 1201–1216.
- [5] Y.C. Zhou, B.H. Xu, A.B. Yu, P. Zulli, An experimental and numerical study of the angle of repose of coarse spheres, *Powder Technol.* 125 (2002) 45–54.
- [6] D. Mateo-Ortiz, F.J. Muzzio, R. Méndez, Particle size segregation promoted by powder flow in confined space: The die filling process case, *Powder Technol.* (2014).
- [7] D.F. Bagster, J. Bridgwater, The measurement of the force needed to move blades through a bed of cohesionless granules, *Powder Technol.* 1 (1967) 189–198.
- [8] D.F. Bagster, J. Bridgwater, The flow of granular material over a moving blade, *Powder Technol.* 3 (1969) 323–338.
- [9] D. Mateo-Ortiz, Y. Colon, R.J. Romañach, R. Méndez, Analysis of powder phenomena inside a Fette 3090 feed frame using in-line NIR spectroscopy, *J. Pharm. Biomed. Anal.* 100 (2014) 40–49.
- [10] Y.C. Zhou, A.B. Yu, R.L. Stewart, J. Bridgwater, Microdynamic analysis of the particle flow in a cylindrical bladed mixer, *Chem. Eng. Sci.* 59 (2004) 1343–1364.

CHAPTER 5

5 ANALYSIS OF POWDER PHENOMENA INSIDE A FETTE 3090 FEED FRAME USING IN-LINE NIR SPECTROSCOPY¹

5.1 Summary

New analytical methods are needed to understand and optimize the processes by which tablets are produced. Fette 3090 tablet presses are commonly used in the pharmaceutical industry. A near-infrared (NIR) probe was installed into a Fette 3090 feed frame to understand and monitor the die filling process. A detailed study was performed to study the effect of feed frame operating conditions on NIR spectra and prediction. A powder wave behavior caused by the paddle motion was observed. This behavior was previously demonstrated using the Discrete Element Method (section 4.4.4). The study also revealed that NIR spectra can help in the understanding of powder flow inside the feed frame. It was demonstrated that NIR spectra baselines can also be used to determine changes in mass inside the feed frame. The new NIR method showed that the paddle wheel speed has a significant impact over the powder dynamics inside the feed frame. The baselines of the NIR spectra depended on the mass hold-up inside the feed frame and paddle wheel speed. Studies using blends were performed to develop a NIR calibration model based on the feed frame system dynamics to determine acetaminophen drug concentration variability during the die filling process. The study demonstrated that the variation in the distance from the powder to the probe due to paddle wheel speed has a significant effect on the NIR prediction. This study found that with NIR spectroscopy, blend uniformity can be assessed with accuracy during the die filling process using the corresponding paddle wheel speed in-line calibration model. NIR

¹ This chapter is based on the publication: D. Mateo-Ortiz, Y. Colon, R.J. Romañach, R. Méndez, Analysis of powder phenomena inside a Fette 3090 feed frame using in-line NIR spectroscopy, J. Pharm. Biomed. Anal. 100 (2014) 40–49.

was demonstrated to be a good development tool for feed frame in-line monitoring and also complements the understanding of powder flow during the die filling process.

5.2 Materials and Methods

5.2.1 Materials

5.2.1.1 Experimental Equipment

The equipment used in this study consists of a tablet press hopper and a standard feed frame taken from a Fette 3090 tablet press (Fig. 5.1). Additional details of the feed frame can be found in a previous study [1]. A die disk was built to simulate a tablet press turret. The die disk consists of a high-density polyethylene disk with 36 holes of 10 mm in diameter, connected to a Dayton DC gear motor to rotate the disk in the counter clockwise direction at controlled speeds.

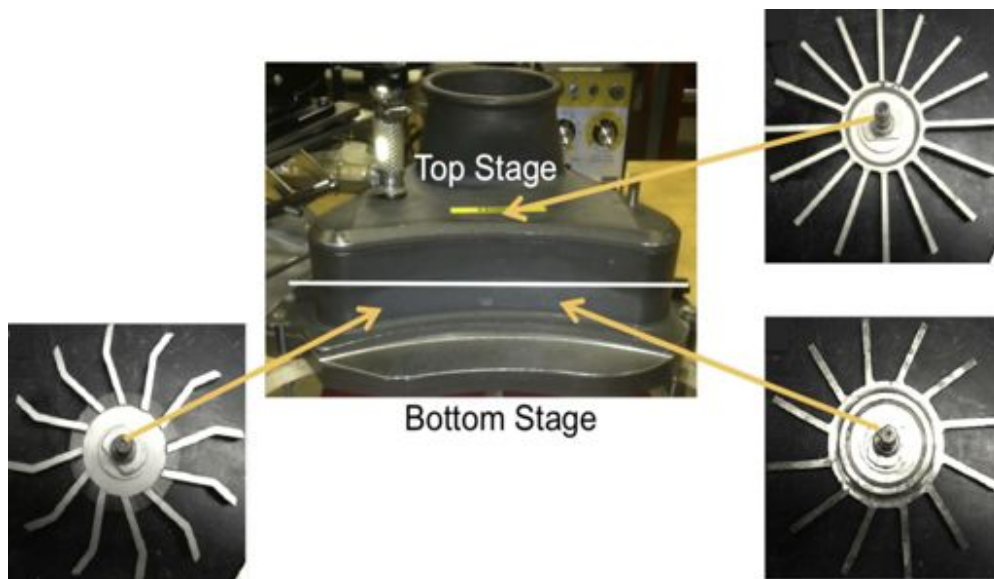


Figure 5.1. Fette 3090 feed frame.

5.2.1.2 *Materials*

The materials used for the continuous experiments consist of monohydrate lactose (Tabletose 70 Agglomerated, Ph. EUR/USP-NF/JP, Malkerei Meggle Wasserburg GmbH & Co.) with 125 μm median particle size, magnesium stearate (Ligamed MF-2-K, Peter Greven) with median particle size $< 10 \mu\text{m}$ (MgSt), colloidal silicon dioxide (Aerosil 200 Pharma) and acetaminophen (Hebei Jiheng Pharmaceutical Co.) (APAP).

5.2.2 Experimental Set-up

5.2.2.1 *Experimental Set-up for Preliminary Experiments*

The experimental set up consisted of a tablet press turret consisting of a Fette 3090 feed frame and a high-density polyethylene die disk (Fig. 5.2). The die disk was stationary with the exits closed to have control of the mass hold-up inside the feed frame. The Fette 3090 has two inspection windows in each side of the feed frame, as shown in figure 5.3. The inspection windows were replaced with sapphire windows (Guild Optical Associates, Inc. Amherst, NH). The window prevented probe fouling since the NIR probe was installed over the window to evaluate and monitor in-line the die filling process (Fig. 5.3). The position of the probe was adjusted to reach the minimum distance possible between the NIR probe and the powder inside the feed frame. The total distance from the bottom of the window to the probe was 12.5 mm. Experiments were performed on both sides of the feed frame to evaluate any differences in powder dynamics between the probe locations.

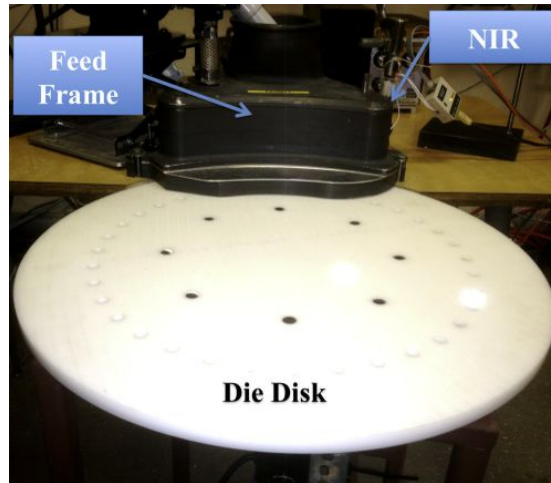


Figure 5.2. Experimental setup.

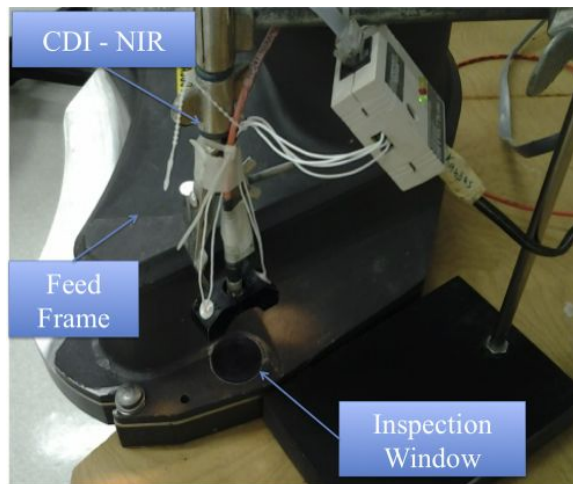


Figure 5.3. NIR probe position.

5.2.2.2 Preliminary Experiments

The effect of the mass hold-up variation inside the feed frame on the NIR spectra was evaluated. Using a paddle wheel speed of 33.0 rpm, NIR spectra were taken from an initial mass of 300g of pure lactose 70 monohydrated to 500g by steps of 50g.

5.2.2.3 NIR Prediction as a Function of Probe Distance

To evaluate the effect of the distance between the probe and the powder, the probe was at a stationary distance and with a lab jack, the sample distance was changed in 1 mm

intervals. 10% (w/w) APAP samples were used and the process was repeated 3 times.

5.2.2.4 Experimental Set-up for Experiments

The experimental set-up for the experiments was similar to the preliminary experiments set-up, with the only difference that the die disk (Fig. 5.2) was operated at 18.0 rpm for all the experiments. The experiments were conducted with three different paddle wheel speeds at each probe location: 16.5, 33.0 and 49.5rpm, for a total of six experiments. These paddle wheel speeds were selected based on typical tablet press operation speeds used in the pharmaceutical industry.

5.2.3 Near Infrared Spectroscopy

5.2.3.1 Instrumentation

A CDI (Control Development Inc, South Bend, IN) NIR spectrometer was used to obtain off-line spectra and in-line spectra for the powders flowing within the feed frame. The CDI system includes an Indium Gallium Arsenide (InGaAs) diode array detector that is thermoelectrically cooled and has 256 elements to cover the 1100-2200 nm spectral area. All spectra in this study correspond to the average of 12 spectra with an integration time of 6.6 milliseconds. This instrument was used because of its fast spectra acquisition time and the small size of the NIR diffuse reflectance probe allowed the measurement of powder spectra within the feed frame.

5.2.3.2 Software Data Processing

Data pre-treatment and NIR calibration model development were performed using

SIMCA-P (Umetrics Multivariate Data Analysis Software). Principal Component Analysis (PCA) and Partial Least Square (PLS) algorithms were used to develop the NIR calibration models. The NIR calibration models were developed after evaluation of different spectral regions, data pretreatments and number of PLS components. These models were first evaluated using the Root Mean Square Errors of Calibration (RMSEC) as a preliminary test of the model. Prediction quality was evaluated in terms of Root Mean Standard Error of Prediction (RMSEP) using the validation sample set. The equations of RMSEC and RMSEP are presented below:

$$RMSEC = \sqrt{\frac{\sum_{i=1}^m (\hat{y}_i - y_i)^2}{N - f - 1}} \quad (5.1)$$

$$RMSEP = \sqrt{\frac{\sum_{i=1}^m (\hat{y}_i - y_i)^2}{N}} \quad (5.2)$$

where, \hat{y}_i is the result predicted by the NIR calibration model, y_i is the API content provided by the analytical weighing, N is the number of samples in the prediction or validation sets and f , the number of factors used in the model.

5.2.3.3 *Off-line NIR Calibration Model*

An off-line PLS NIR calibration model was developed using gravimetric data to monitor drug concentration of powder moving inside the feed frame. A total of 6 calibration blends were prepared. Each blend had a total batch size of 500 g. Each of the blends was prepared in a 5-liter V-Blender following three mixing steps. Step 1, a pre-blend was prepared with 0.5% of silicon dioxide and the corresponding amount of acetaminophen (APAP) and blended for 20 minutes at 15 rpm. Step 2, the pre-blend was mixed with lactose 70 for 20 minutes at 15 rpm. Step 3, the mixture was mixed with 1.0% of MgSt for an

additional 6 minutes at 15 rpm. The APAP target concentrations in these calibration blends were 5, 7, 9, 11, 13 and 15 % (w/w).

After the final mixing, each blend was placed in separate trays. The NIR was mounted at a distance of 10 mm from the blend and 30 spectra were taken on one side of the tray. The tray was flipped over and 30 more spectra were taken for a total of 60 spectra. The locations of the measurements are illustrated in Figure 5.4. All 60 spectra, excluding outliers, were used as representative spectra for each respective calibration mixture.

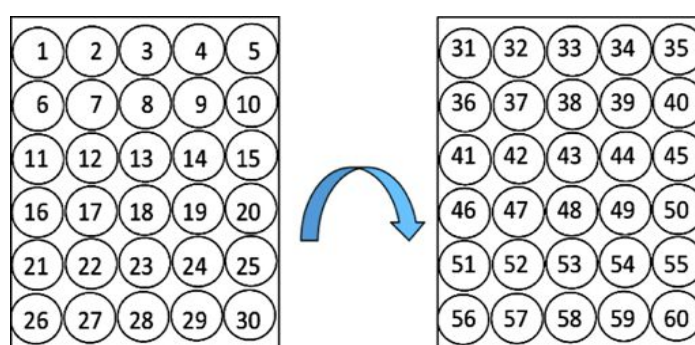


Figure 5.4. Tray sampling procedure.

5.2.3.4 *In-line NIR Calibration Model*

An in-line PLS NIR calibration model was developed using gravimetric data and in-line spectra acquired from moving blends to monitor drug concentration of powder flowing inside the feed frame. A total of 6 calibration blends were prepared. The calibration blends used to develop the in-line NIR calibration model comprise of the same materials (APAP, Lactose 70, colloidal silicon dioxide and MgSt), concentration levels and mixing steps as blends that were used for the off-line model. Each of these calibration blends had a total batch size of 4 kg and were mixed in a 16-quart stainless steel V-blender.

Each blend was added to the hopper, which fed the Fette 3090 feed frame for each corresponding calibration run. The feed frame was fed first while the die disk was stationary

and the paddle wheel was on. The feed frame was completely filled when the material hopper level was stationary. Then, the die disk was turned on at 18.0 rpm and the material run through the feed frame at a paddle wheel speed of 33.0 rpm for approximately 2 minutes before the NIR started collecting spectra of the moving powder. The NIR was placed on both sides of the feed frame and spectra were collected for about 1 minute on each side. Approximately 300 spectra of the moving powder were taken for each of the 6 runs on each side of the feed frame (1 run per calibration blend).

5.2.3.5 Repeatability Study

A repeatability study was performed with a 10% (w/w) APAP target concentration blend to verify the minimum variability of the measurements. Eight spectra were taken in the same location of the blend and the standard deviation of the predictions was calculated.

5.3 Results and Discussion

5.3.1 Preliminary Results

5.3.1.1 Feed Frame Monitory Locations

An accumulation of powder on the right window location was observed (Fig. 5.5) and the blend appeared stagnant at this location. To monitor the powder in this location would represent a false signal since the NIR would be taking spectra of the same material many times. However, this effect was not observed on the left window location (Fig. 5.6). Therefore, the left window location was chosen to develop the inline NIR calibration model and monitor the experiments. The accumulation of powder was mainly due to the paddle height in the Fette 3090 feed frame. The height of the right wheel paddles is 12 mm while the

left wheel paddles have a height of 8 mm. The gaps between the top of the feed frame and the top of the right wheel paddles and left wheel paddles are 1 mm and 5 mm respectively. The gap between the bottom of the feed frame and the bottom of the paddles is 2 mm. The lower paddle height forces the powder to pass above the paddles with more ease and the material does not accumulate at the window location. Similar results were observed in the DEM simulations when analyzing the effect of paddle height on particle flow behavior (sections 4.4.2 and 4.4.4).



Figure 5.5. Stagnant powder observed at the right window location.



Figure 5.6. Left window location where all measurements were obtained.

5.3.1.2 Powder Wave Behavior inside the Feed Frame

Visual inspection revealed a powder wave behavior inside the feed frame due to the movement of the paddles. This behavior was previously explained in detail using the Discrete Element Method in section 4.4.4. Figure 5.7 shows the effect of this wave behavior on the

spectra baselines. At the top of the wave the distance between the powder and the detector is less, more radiation is getting back to the detector and the baseline is lower. At the bottom of the wave the distance is more, less radiation is getting back to the detector resulting in a higher baseline. The paddle wheels were stopped at different times and it was found that the difference between the bottom and the top of the wave was up to 15 mm. Thus, NIR spectra are being affected by powder movement and can be used to understand powder dynamics inside the feed frame. This is an important observation that was not discussed in previous studies [2–5].

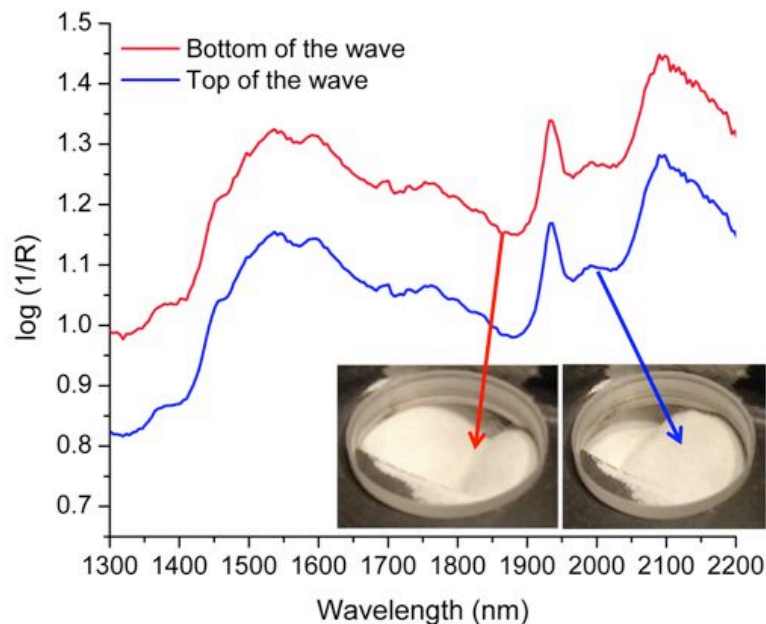


Figure 5.7. Powder wave behavior effect on NIR spectra baseline.

5.3.1.3 Feed Frame Mass Hold-up Effect

When the mass hold-up inside the feed frame was varied, a change in the spectra baselines was observed due to the change of distance between the powder and the NIR probe (Fig. 5.8). At lower mass hold-up the spectra baselines shifts to higher values, while at higher

mass hold-up spectra baselines shifts toward lower values. The higher the mass hold-up the closer the powder is to the NIR probe. This means that NIR data (spectra baselines) can also be used to determine changes in mass inside the feed frame.

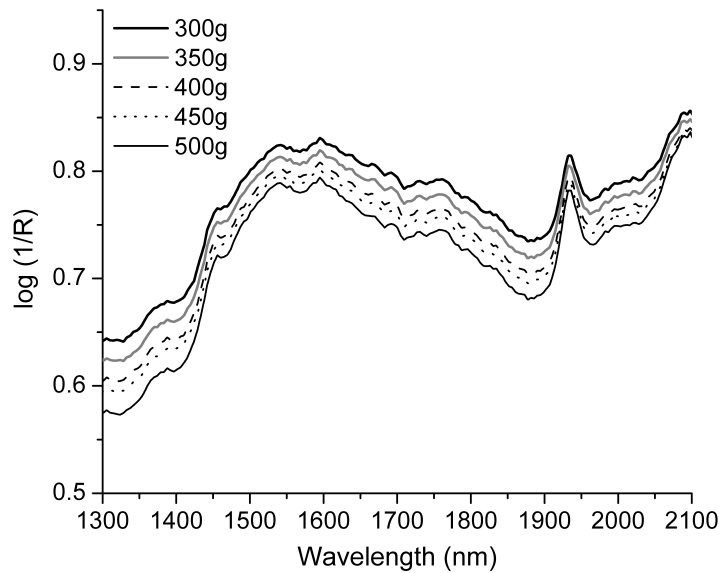


Figure 5.8. Mass hold-up effect on NIR spectra baseline.

5.3.2 Evaluation of Spectra Properties

NIR spectra of the main components of the formulation (APAP and Lactose) were measured off-line as shown in Fig 5.9. Even without pretreatment the APAP (API) raw spectra exhibits characteristic absorption bands around 1600 nm and 2000 nm wavelengths as shown in Fig. 5.9.

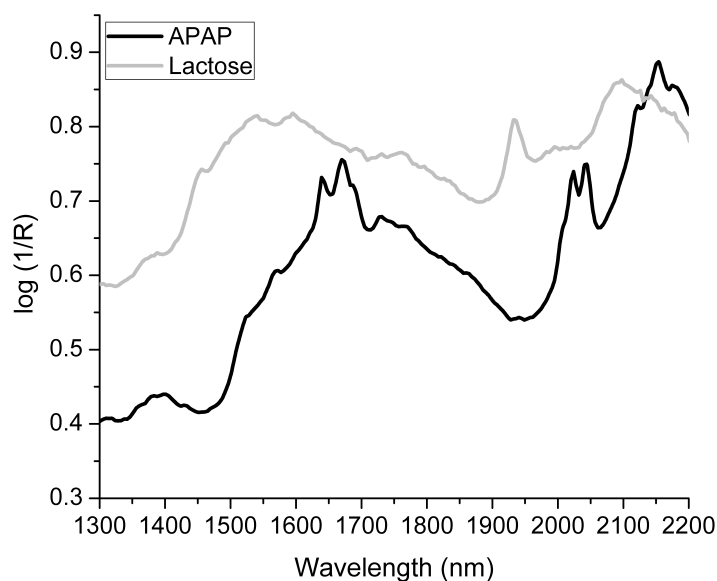


Figure 5.9. Spectra of the two main components in the formulation.

Various spectral regions and number of PLS factors were evaluated to optimize the ability of the NIR calibration model to predict the calibration set. This first assessment was based on the RMSEC (eq. 5.1) and a cross-validation using “leave class out” (RMSECV).

5.3.2.1 *Off-line Calibration Spectra*

The score plot of the off-line calibration spectra did not distinguish among the different levels of concentration. A high variability in the scores of all the blends is observed. This is due to an uneven powder surface with differences in the distance from the probe to the powder during off-line data acquisition (causing baseline differences in the spectra). Therefore, data pretreatment was needed to achieve distinction between the different levels of concentration.

In NIR spectroscopy, the first derivative is used to remove the baseline differences, and the second derivative to remove the slope differences in the spectra. If spectra differ by a multiplicative or additive factor they will be identical after a standard normal variate (SNV) normalization. Figure 5.10 shows the score plot of the pretreated (SNV, 1st derivative) off-line calibration sample set in the 1130-1380 nm, 1697-2135 nm spectral ranges. Each color represents a corresponding blend. The scores corresponding to the 7%, 13% and 15% w/w blends are better grouped than the 5%, 9% and 11% blends. In general, a high variability in the scores is observed. This is due to possible APAP agglomerates in the trays and the fact that the diffuse reflectance probe looks at a small sample volume.

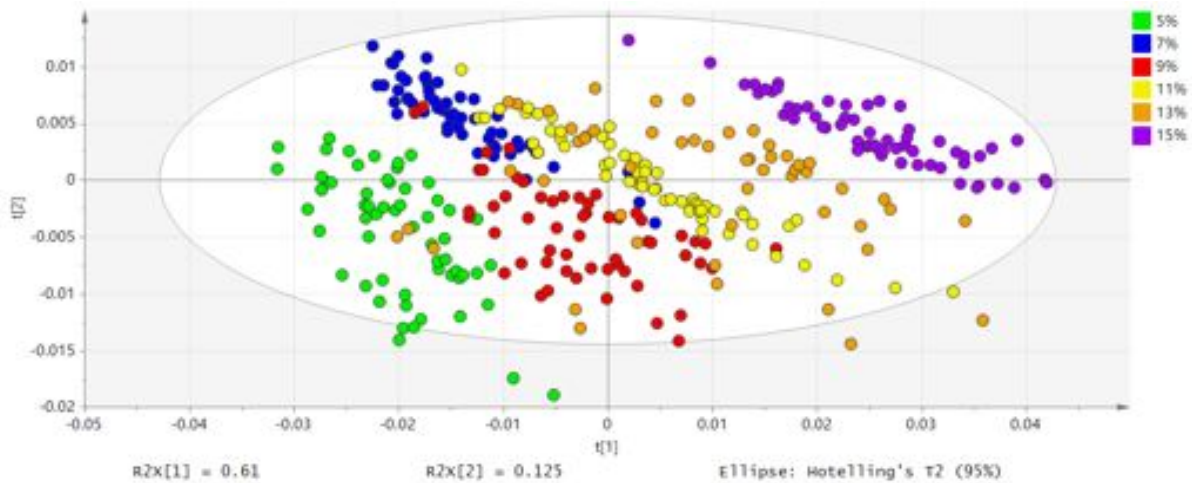


Figure 5.10. PCA score plot of off-line NIR calibration model developed in the 1130–1380, 1697–2135 nm spectral region using SNV+ 1st deriv (17) pre-treatment.

5.3.2.2 In-line Calibration Spectra

Spectra were also acquired in-line with the powder moving inside the feed frame with the fiber optic probe located over the left window. Figure 5.11 shows the score plot of the spectra of the in-line calibration blends. Each color represents a blend concentration. The score plot of in-line spectra (Fig. 5.11) clearly shows a better separation among the different

levels of concentration. It is remarkable that well-defined groups are observed with in-line spectra acquisition even without data pretreatment. Each spectrum corresponds to the average of 12 spectra. Off-line spectra are for a single point, but in-line spectra are obtained with the powder moving, therefore the resultant average spectrum corresponds to a larger sampling area. This could be the reason for obtaining better grouped score clusters with in-line spectra.

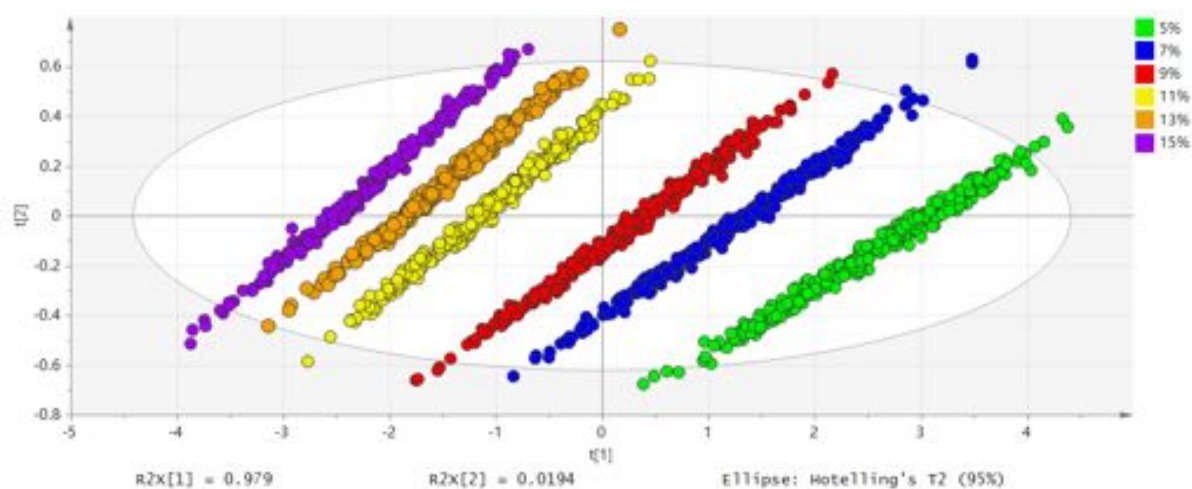


Figure 5.11. PCA score plot for in-line spectra. PCA performed with calibration sample set in the 1130–1380 nm, 1697–2135 nm spectral regions.

5.3.3 NIR Calibration Model Developments

Table 5.1 shows the standard error of calibration and cross-validation results for several of the NIR calibration models evaluated (offline and inline). Table 5.1 does not include all NIR calibration models evaluated for clarity purposes. In addition, an independent off-line set targeting 10% (w/w) APAP was predicted by the off-line calibration models (models 1-3), while another independent in-line set ran at 33.0 rpm targeting 10% (w/w) APAP was predicted by the in-line calibration models (models 4-8). The RMSEP and bias results showed the accuracy of the NIR calibration models.

The NIR calibration models that included lower wavelengths (1130-1380 nm) in their development showed a lower error of calibration and cross-validation for this formulation (models 1 and 4). The standard error of cross-calibration decreased by one-third, from 1.10 to 0.38, when the in-line calibration model was used to predict moving blends, as well as the bias which resulted close to zero. Similar results were also obtained for the RMSEP, where the standard error of prediction decreased by half, from 0.80 to 0.40. Well-defined clusters are observed in Figure 5.12 for each level of concentration in the score plot of the pretreated (SNV, 1st derivative) in-line calibration sample set in the 1130-1380 nm, 1697-2135 nm spectral regions. An increase in band intensity in the 1910-1935 nm spectral region due to a decrease in APAP concentration was observed. Results in Table 5.1 suggest that an in-line NIR calibration model should be developed using spectral region 1030-1380, 1697-2135 nm and 2 PLS factors. This model described the highest percent of variation in the data and the lowest standard errors giving an average RMSECV of 0.38 and lowest RMSEP of 0.40.

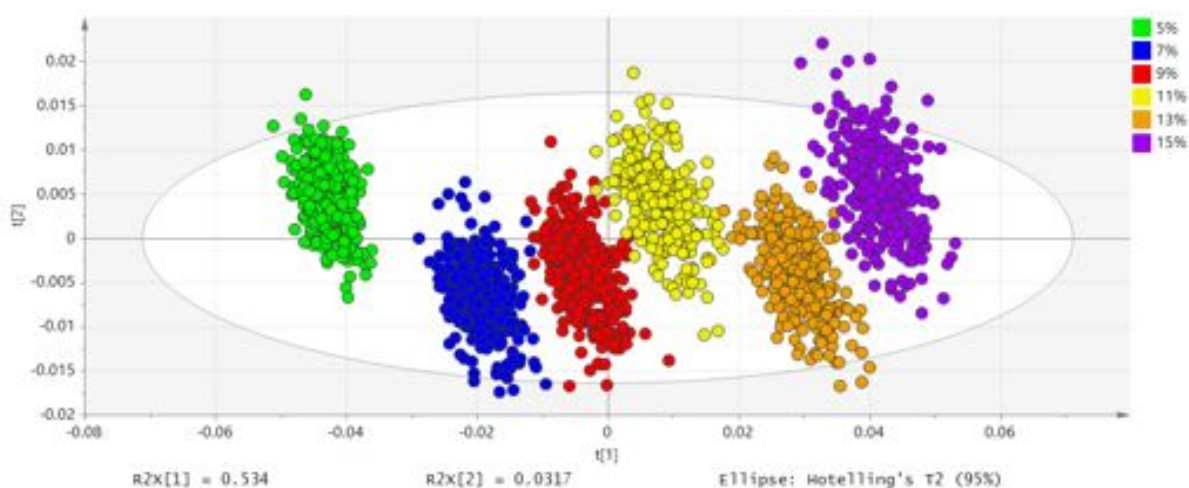


Figure 5.12. PCA score plot of in-line NIR calibration model developed in the 1130–1380, 1697–2135 nm spectral region using SNV+ 1st deriv (17) pre-treatment.

Table 5.1. Summary parameters of the off-line and in-line NIR calibration models constructed and evaluated.

| NIR Calibration Model | Spectral Range (nm) | Data Pretreatment | No. PC | Percent of Variation | RMSEC (% w/w) | RMSECV (% w/w) | RMSEP (% w/w) | Bias |
|--|----------------------|---------------------------|--------|---------------------------------|---------------|----------------|---------------|-------|
| | | | | R ² _{Y cum} | | | | |
| Off-line NIR Calibration Models | | | | | | | | |
| 1 | 1130-1380, 1697-2135 | SNV+1 st deriv | 3 | 0.902 | 1.07 | 1.10 | 0.80 | 0.03 |
| 2 | 1705-2135 | SNV+1 st deriv | 3 | 0.800 | 1.41 | 1.41 | 3.13 | -1.36 |
| 3 | 1479-1714 | SNV+1 st deriv | 3 | 0.808 | 1.51 | 1.58 | 1.52 | -1.14 |
| In-line NIR Calibration Models | | | | | | | | |
| 4 | 1130-1380, 1697-2135 | SNV+1 st deriv | 2 | 0.988 | 0.37 | 0.38 | 0.40 | -0.11 |
| 5 | | SNV+2 nd deriv | 2 | 0.950 | 0.77 | 0.79 | 0.75 | -0.10 |
| 6 | 1479-1714 | SNV+1 st deriv | 2 | 0.982 | 0.46 | 0.47 | 0.51 | 0.27 |
| 7 | | SNV+2 nd deriv | 2 | 0.933 | 0.89 | 0.90 | 0.77 | -0.09 |
| 8 | 1479-1864, 1974-2135 | SNV+1 st deriv | 2 | 0.901 | 0.46 | 0.47 | 0.52 | 0.28 |

5.3.4 Repeatability Study

A repeatability study was performed to assess the precision of the NIR calibration model. Eight consecutive spectra were collected (without moving the blend) at 4 different locations of a blend. The standard deviations average of the NIR predictions at the different locations was 0.19 APAP %. This result represents the minimum variation that was obtained during the monitoring of the powder flow inside the feed frame.

5.3.5 Prediction as a Function of Probe Distance

NIR spectra were collected in the same location of a blend at different probe-to-sample distances. The distance was varied from 12–24 mm. The prediction measurements were started at 12 mm since the thickness of the probe is 10 mm and there was 2 mm of separation between the probe and the window. Table 5.2 shows that the NIR predictions

increased gradually as the probe-to-sample distance increased. The sample volume analyzed at each of these distances is different. The light sources included in the probe provide radiation that penetrates the powder sample. As the diffuse reflectance is moved away the fraction of radiation that returns to the detector changes and also the sample volume analyzed.

Table 5.2. Prediction as function of probe distance.

| Distance (mm) | Prediction Avg. | STDEV |
|---------------|-----------------|-------|
| 12 | 8.97 | 0.18 |
| 14 | 9.47 | 0.23 |
| 16 | 10.29 | 0.16 |
| 18 | 11.11 | 0.19 |
| 20 | 11.53 | 0.39 |
| 22 | 11.69 | 0.16 |
| 24 | 12.59 | 0.30 |

5.3.6 In-line Spectra of Experiments

It was found that the paddle wheel speed has a significant impact on the powder dynamics inside the feed frame. Figure 5.13 depicts the score plots of the spectra obtained from the experiments at 16.5, 33.0 and 49.5 rpm, respectively. No pre-treatment was performed on the spectra to maintain the physical variations caused by the different paddle wheel speeds. The sample order or sequence at which the spectra were taken is represented in the x-axis. The y-axis represents the variation of the scores in the first principal factor, which correspond to changes in spectra baselines caused by the wave behavior. At 16.5 rpm (Figure 5.13a), a high frequency was observed due to a more noticeable wave behavior. To observe the wave behavior more clearly, a moving average trend line (Figure 5.13a, black line) was used with 9 data points. At 33.0 and 49.5 rpm the powder wave behavior is less noticeable based on the wave amplitude, lessening the change in distance from the powder to the NIR probe and a lower wave frequency was obtained. The higher paddle wheel speeds affect the frequency of the wave behavior increased as shown in the comparison of the score plots in

figure 5.13. The passing paddle is directly affecting this behavior, which in turn affects the NIR response. However, it is not the paddle itself that affects the NIR response since it is fully covered with powder at all times.

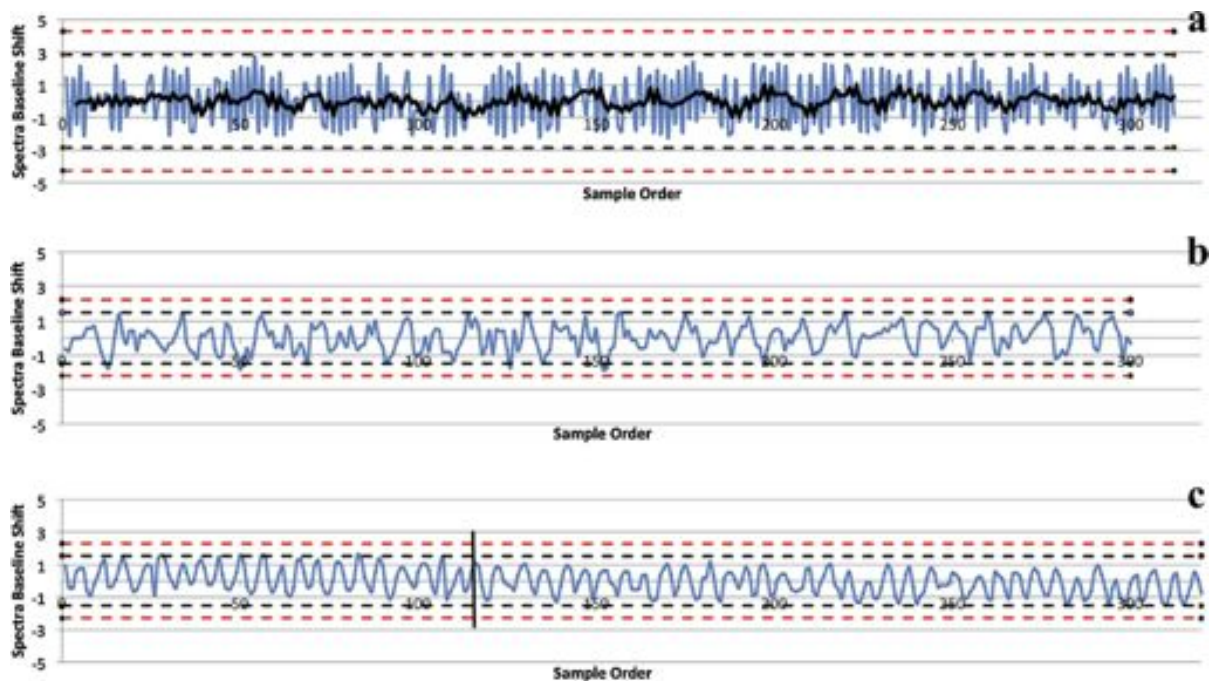


Figure 5.13. Spectra baseline shift vs. Sample order. 16.5 (a), 33.0 (b), 49.5 rpm (c).

Since it was demonstrated in section 5.3.1.3 that NIR spectra could be used to determine changes in mass inside the feed frame, the spectra were also used to verify if the system reached mass steady state. Figure 5.13a and 5.13b show that although the spectra baselines are oscillating due to the wave behavior, it remains constant within a range suggesting the system reached a mass steady state. However, figure 5.13c shows that the oscillations are constant until approximately the first 110 spectra and then begin to move downward. This means the system was in mass steady state and the feed frame began to empty. The spectra of the system in steady state for each experiment were used for the experimental prediction analysis.

The changes in powder wave behavior can be explained using figure 5.14 since the changes in spectra baselines are greater at lower rpm (Fig. 5.14a) and are reduced with increasing paddle wheel speed (Fig. 5.14c). In addition, figure 5.14 shows that the paddles do not have a significant effect on the spectra since the only difference between each spectrum are differences in baseline.

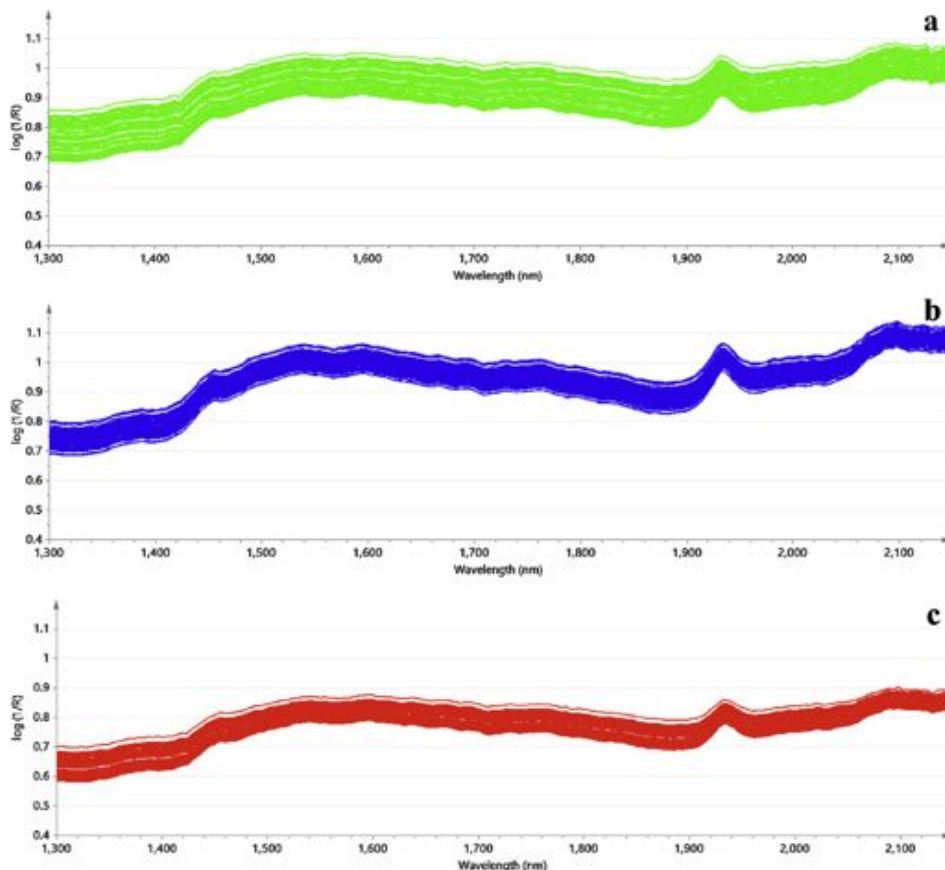


Figure 5.14. Spectra at 16.5 (a), 33.0 (b), 49.5 rpm (c).

As the paddle wheel speed increases, spectra present lower baselines due to the decrease in distance between the powder and the NIR probe (Fig. 5.14). This represents changes in the powder bed volume since a previous study showed that if the die disk speed is kept constant the mass hold-up does not vary significantly (Chapter 2) [6]. Because the mass is constant and the bed volume changes, it can be concluded that at different paddle wheel speeds (increase of frequency of paddle passes) the powder density changes. In addition, a

previous study performed in a flat-bladed stirrer demonstrated that an increase in paddle speed causes an expansion of the bed material [7]. NIR Chemical Imaging measurements also demonstrated that different tablet densities resulted in significant differences in spectra slope [8]. The changes in the spectra slope can be observed even without any spectral preprocessing as shown in Figure 5.15, specifically in the range of 1400 – 1500 nm.

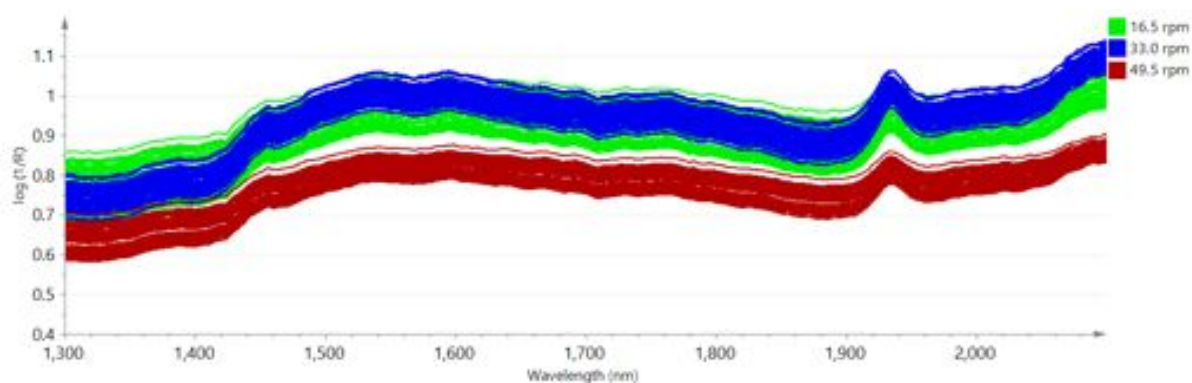


Figure 5.15. Spectra at 16.5, 33.0, 49.5 rpm.

5.3.7 Summary NIR Prediction at Different Paddle Wheel Speeds

Table 5.3 summarizes the impact of paddle wheel speed (16.5, 33.0 and 49.5 rpm) on the average NIR prediction of the different NIR calibration models developed for the 3 independent runs performed. Results demonstrated that the blend uniformity can be assessed with high accuracy during the experiment at 33.0 rpm paddle wheel speed (same paddle wheel speed used to develop the NIR calibration model). The lowest standard deviation for this experiment was achieved using model #4 (developed using in-line spectra in the 1130-1380 nm, 1697-2135 nm spectral range) and the prediction average was close to the 10% w/w target value (10.17%).

Table 5.3. Prediction at different paddle wheel speeds.

| Calibration Model | 16.5 rpm | | 33.0 rpm | | 49.5 rpm | |
|-------------------|------------------|-------|-----------------|-------|-----------------|-------|
| | Off-line Spectra | | | | | |
| | Prediction Avg. | STDEV | Prediction Avg. | STDEV | Prediction Avg. | STDEV |
| 1 | 8.31 | 1.61 | 7.79 | 1.26 | 7.57 | 1.63 |
| 2 | 15.52 | 1.56 | 10.51 | 0.68 | 18.79 | 1.16 |
| 3 | 11.73 | 1.69 | 10.80 | 1.49 | 14.34 | 1.25 |
| Calibration Model | Dynamic Spectra | | | | | |
| | Prediction Avg. | STDEV | Prediction Avg. | STDEV | Prediction Avg. | STDEV |
| | 4 | 14.09 | 1.08 | 10.17 | 0.36 | 16.46 |
| 5 | 12.11 | 1.03 | 10.10 | 0.75 | 13.95 | 0.88 |
| 6 | 13.18 | 0.67 | 9.73 | 0.43 | 14.66 | 0.53 |
| 7 | 12.66 | 1.11 | 10.09 | 0.77 | 13.66 | 0.85 |
| 8 | 14.11 | 1.20 | 9.72 | 0.44 | 17.10 | 1.10 |

For the other experiments at different paddle wheel speeds (16.5 and 49.5 rpm), the NIR calibration model was unable to predict the concentration correctly. It was demonstrated in section 5.3.4 that distance from the powder to the probe affects the NIR calibration model prediction. In addition, in section 5.3.5 it was shown that the powder bed densities change when modifying the paddle wheel speed. Therefore, this difference on the NIR prediction average can be attributed to a combination of the changes in powder densities and distance from the powder to the probe. Furthermore, since the probe is in a stationary position, when paddle wheel velocity changes, the sample size also changes due the differences in powder wave behavior and changes in powder distance from the probe. Regardless of all the data pretreatment and spectral regions evaluated the effects that the different paddle wheel speeds had on the blends made the NIR calibration model development very challenging. Based on results from chapter 4 (section 4.4.4), increasing the number of paddles can decrease the powder wave behavior. This can be one of the solutions for improving the NIR prediction at different paddle wheel speeds.

5.4 Conclusion

The aim of the study was to understand and monitor the die filling process in-line, analyze the different factors that could affect the NIR prediction of the calibration models and understanding of powder flow inside the feed frame. In-line results indicate that the differences in baselines are mainly affected by mass hold-up inside the feed frame and paddle wheel speed. Accumulation in the inspection window was mainly due to the paddle height. This can be avoided by decreasing the paddle height. A powder wave behavior inside the feed frame was visually observed due to the movement of the paddles. These experimental powder behavior observations and data complements those observed using the DEM simulations (Chapter 4). NIR data confirmed this wave behavior based on differences in spectra baseline. It was demonstrated that spectra baselines can also be used to determine changes in mass inside the feed frame. It was found that the paddle wheel speed has a significant impact on the powder dynamics inside the feed frame. As the wheel speed increases, the distance from the powder bed to the probe decreases. This work also suggests that NIR data can be used to determine if a system reached mass steady state.

NIR off-line and in-line PLS calibration models were developed. The 33.0-rpm in-line calibration model resulted in generation of a more accurate model for predicting experiments at the same speed in which the model was developed. A difference on the prediction average was observed due to changes in powder dynamics at different paddle wheel speeds. A change in powder agitation (paddle wheel speed) provokes differences in powder bed density affecting the NIR prediction. In addition, it was demonstrated that differences in distance from the powder to the probe due to paddle wheel speed has a significant effect on the NIR prediction.

This study demonstrated that with NIR spectroscopy, blend uniformity can be assessed

with accuracy during the die filling process using the corresponding paddle wheel speed in-line calibration model. NIR was demonstrated to be a good development tool for the in-line monitoring of powder during die filling.

5.5 References

- [1] R. Mendez, C. Velazquez, F.J. Muzzio, Effect of feed frame design and operating parameters on powder attrition, particle breakage, and powder properties, *Powder Technol.* 229 (2012) 253–260.
- [2] P.R. Wahl, G. Fruhmann, S. Sacher, G. Straka, S. Sowinski, J.G. Khinast, PAT for tableting: Inline monitoring of API and excipients via NIR spectroscopy., *Eur. J. Pharm. Biopharm.* (2014).
- [3] H.W. Ward, D.O. Blackwood, M. Polizzi, H. Clarke, Monitoring blend potency in a tablet press feed frame using near infrared spectroscopy., *J. Pharm. Biomed. Anal.* 80 (2013) 18–23.
- [4] K. Muteki, D.O. Blackwood, B. Maranzano, Y. Zhou, Y.A. Liu, K.R. Leeman, et al., Mixture Component Prediction Using Iterative Optimization Technology (Calibration-Free/Minimum Approach), *Ind. Eng. Chem. Res.* 52 (2013) 12258–12268.
- [5] Y. Liu, D. Blackwood, Sample Presentation in Rotary Tablet Press Feed Frame Monitoring by Near Infrared Spectroscopy, *Am. Pharm. Rev.* (2012) 1–9.
- [6] D. Mateo-Ortiz, F.J. Muzzio, R. Méndez, Particle size segregation promoted by powder flow in confined space: The die filling process case, *Powder Technol.* (2014).
- [7] R.L. Stewart, J. Bridgwater, D.J. Parker, Granular flow over a flat-bladed stirrer, *Chem. Eng. Sci.* 56 (2001) 4257–4271.
- [8] J. Roperio, Y. Colón, B. Johnson-Restrepo, R.J. Romañach, Near-infrared chemical imaging slope as a new method to study tablet compaction and tablet relaxation., *Appl. Spectrosc.* 65 (2011) 459–65.

CHAPTER 6

6 CONCLUDING REMARKS

6.1 General Conclusions

The development of new regulatory initiatives and new technologies such as continuous manufacturing has promoted the need for a better scientific understanding of the pharmaceutical manufacturing processes. The tablet compressing operation is one of the most important processes in the production of tablets. Although several studies have been dedicated to this process, the effect of the feed frame design and operating conditions on the powder flow through the feed frame and the final product (tablets) quality is not fully understood. Also, there is no available knowledge on how to control die weight variability based on *a priori* knowledge of both feed frame design and operating conditions.

For these reasons, the aim of this investigation was to provide a fundamental and practical understanding of particle flow in a confined space while external forces are applied. Results obtained have highlighted the effect of feed frames on powder properties that can ultimately affect the final product. Experimental and DEM studies revealed vertical segregation inside the feed frame, which causes the material to segregate when it enters the dies. However, paddle wheel speed was demonstrated to be the most important factor to control this segregation. It was demonstrated that particle attrition occurs at high paddle wheel speed and over lubrication of the material. Therefore, the optimum paddle wheel speed depends on the particle properties. DEM was proved to be a helpful visualization tool that complemented testing and experimentation and provided detailed information about the die filling process. DEM was helpful in recommending operating conditions for die filling operations. It is also useful for many other pharmaceutical operations and for pharmaceutical process development.

The need for understanding the effect of feed frame design on powder flow through the die filling process led us to develop a simple feed frame design in order to achieve a more controlled environment. A mathematical model based on Newton's 2nd law was developed to describe the force applied by the feed frame paddles as a function of feed frame design (number of paddles and paddle height), operating conditions (paddle wheel rpm) and particle properties (density). The model was able to predict tendencies in die weigh variability based on feed frame design.

As the standards for drug production and quality control are becoming more rigorous, initiatives such as the process analytical technologies (PAT) are gaining importance. Only a small quantity of tablets is analyzed for quality purposes in each batch. This can cause that high potency tablets are overlooked and therefore affect negatively the patients. Therefore, NIR spectroscopy was used to perform in-line monitoring during the die filling process. This work can have a positive and significant impact to society improving the product quality by providing continuous real-time quality assurance. A detailed study was performed to study the effect of feed frame operating conditions on NIR spectra and prediction. NIR spectroscopy was demonstrated to be a useful tool that complements the understanding on powder flow through the feed frame. This work also suggests that NIR data can be used to determine if a system has reached mass steady state. NIR was demonstrated to be a development tool for the in-line monitoring of powder during die filling. Also, NIR results can be helpful in the development and optimization of in-line strategies that can improve process control and the quality of tablets.

These results have created awareness in the pharmaceutical industry to avoid problems during the die filling process such as powder attrition, powder overlubrication and size-induced segregation. The DEM results demonstrating in-die segregation offer an alternative

explanation for tablet quality problems. These findings should lead to changes in feed frame design (number of paddles, paddle height, level of confinement and operating conditions) to avoid segregation, powder attrition and high die weight variability problems. This work also contributes towards the improvement of tablet manufacturing that is integral to an automated continuous manufacturing system.

6.2 Recommendations and Future Perspectives

From this study, some recommendations can be made in order to optimize the die filling process. Additional studies for the DEM modeling with different particle size, particle size distributions, different cohesion models and values and irregular particle shape could provide a more realistic study of the powder flow inside the feed frame. Parallel computing should be considered in order to decrease the computing time and increase the number of particles used in the simulation. Based on the previously presented results, the addition of a paddle shape factor to the paddle force model opens a potential area of further investigation. A force balance analysis in a unit volume of powder is also needed to take into account all the forces that act on the powder such as gravity and frictional forces to model the resultant force properly which ultimately described how the powder is flowing. Experimental validation of the effect of feed frame design on powder flow should also be performed.

Some interesting factors to analyze blend uniformity inside the feed frame include the addition of the paddle wheel speed factor to the in-line NIR model. To make this NIR model more robust, changes such as decreasing the sapphire window thickness, using a different NIR spectrometer and using a different paddle wheel design can be applied. The effect of the NIR analyzing location inside the feed frame should also be studied.